Title
Characterizing the Role of FBXL5 in Intracellular Iron Homeostasis

Author
Powers, David Naoki

Publication Date
2015

Peer reviewed|Thesis/dissertation

UNIVERSITY OF CALIFORNIA
Los Angeles

Characterizing the Role of FBXL5 in Intracellular Iron Homeostasis

A dissertation submitted in partial satisfaction of the
requirements for the degree Doctor of Philosophy
in Biological Chemistry

David Naoki Powers
2015

ABSTRACT OF DISSERTATION

Characterizing the Role of FBXL5 in Intracellular Iron Homeostasis

by

David Naoki Powers

Doctor of Philosophy in Biological Chemistry

University of California, Los Angeles, 2015

Professor James Akira Wohlschlegel, Chair

Iron is an essential trace element found in all forms of life. Despite its critical role in the cell involving redox reactions, many aspects of its intracellular regulation remain unknown. In the following work, we outline extensive research performed on two proteins that were previously uncharacterized with respect to iron homeostatic systems: the iron-binding ubiquitin ligase FBXL5 and the osmotic stress regulatory kinase SPAK. We discovered that FBXL5 controls the protein stability of the mRNA-binding IRP proteins IRP1 and IRP2 in an iron-dependent manner that is controlled by iron bound directly to FBXL5 via a novel hemerythrin-like domain found on the N-terminus. This hemerythrin-like domain is the first mammalian domain of its type to be identified and performs a critical role in iron sensing. When FBXL5

binds iron its structure is stabilized and it assembles into an E3 ubiquitin ligase complex that targets IRP1 and IRP2 for degradation; without iron, FBXL5 is itself destabilized and degraded.

We also studied the osmotic stress regulatory kinase SPAK and its role in iron homeostasis. SPAK has been well-characterized for its role in salt homeostasis: it is activated by an upstream salt-sensing kinase WNK1 and then phosphorylates membrane-bound sodium-potassium-chloride co-transporters to equilibrate changes in osmotic pressure. In addition to this role, we have revealed that SPAK controls the stability of FBXL5 and NCOA4, both important proteins in iron homeostasis. While FBXL5 post-translationally regulates the protein expression of IRP proteins, NCOA4 controls the trafficking of iron-containing ferritin cages to the autophagosome to mediate release of iron.

We discovered that SPAK binding and activity affects the poly-ubiquitination and steady-state abundance of both FBXL5 and NCOA4. SPAK coordinates with HERC2, an E3 ubiquitin ligase, to form a regulatory complex to perform these functions. We believe that it may allow for an additional layer of regulation for these two pathways and can aid in coordinately regulating both ferritin expression and degradation. This complex system has been the subject of our research for years now, and given the role of SPAK in iron regulation and the severity of iron-mediated illnesses SPAK could prove to be an attractive subject for pharmaceutical study.

The dissertation of David Naoki Powers is approved.

Steven G Clarke

Joseph Ambrose Loo

Geraldine A Weinmaster

James Akira Wohlschlegel, Committee Chair

University of California, Los Angeles

2015

TABLE OF CONTENTS

LIST OF FIGURES

LIST OF TABLES

ACKNOWLEDGEMENTS

Without the support of my family, none of this work would have been possible. My parents first helped me greatly with my efforts in getting into a top-rated college at the California Institute of Technology, aided in my applications to both the Fulbright Scholarship in Japan and Harvard School of Public Health and finally played a large part in my time here at UCLA. Without their backing, I do not believe I would have been able to continue working on such a long and difficult project. Additionally, the encouragement provided to me by both my brother, the family dogs (Spud, Dee Dee and Louie) and my extended family assisted my state of mind for the many years it has taken to get this far.

The members of Wohlschlegel lab have also played an essential part in my ability to formulate my body of work. First, the mentorship of James helped me develop into a more insightful and critically minded scientist while also appreciating better other aspects of life. I am now better able to appreciate the different scientific techniques available to prove important points, as well as the need to fully understand all aspects of the experimental work in order to improve as a scientist. I also greatly enjoyed our discussions involving professional sports, even if there is not so much overlap in the teams we support (Go Kings Go). The members of the Wohlschlegel lab (Ajay, Tanu, Khue, Brian, William, Hee Jong, Calvin and Tisha) have aided me greatly through a fun, hospitable research environment that values hard work and dedication without becoming onerous. Through my interactions with my friends and colleagues I have learned a lot not only about science, but of places and cultures all around the world. This played a large part in my motivation to learn more about cooking and my attempts to understand the

different fundamental styles of preparing delicious food. The lab was also a major motivating factor in visiting more countries and continents to expand my breadth of experiences.

My committee members (Steve, Gerry and Joe) have also played an important part in my scientific development with their comments and suggestions for my project. While I may not have pursued every experiment proposed at the committee meetings, each and every one was something I considered for future work.

I would also like to acknowledge the funding here at UCLA that made my Ph.D. and research possible: the Cellular and Molecular Biology Training Grant (Ruth L. Kirschstein National Research Service Award GM007185) and the UCLA Dissertation Year Fellowship. Their funding has allowed me to continue to work on my project and better understand a very complex biological system.

DAVID NAOKI POWERS

Education

MS in Environmental Health, Harvard School of Public Health (2006 – 2008)
BS in Chemistry, California Institute of Technology (2001 – 2005)

Fields of Research

Proteomics, Mass Spectrometry, Iron Regulatory Pathways, Ubiquitin and Proteasome System

Research

University of California, Los Angeles with Dr. James Wohlschlegel (January 2009 – current)

Harvard School of Public Health with Dr. Karl Kelsey (October 2006 – May 2007)

J. William Fulbright Foreign Scholarship Board (FSB) program with Dr. Naotaka Kuroda (September 2005 – August 2006)

Summer Undergraduate Research Fellowship (SURF) at Caltech with Dr. Mitchio Okumura (June 2003 – September 2003)

Awards and Fellowships

Dissertation Year Fellowship (2014 – 2015)
Cellular and Molecular Biology Training Grant (Ruth L. Kirschstein National Research Service Award GM007185) (2010 – 2013)
Horace W. Goldsmith Fellowship (2006 – 2008)
J. William Fulbright Foreign Scholarship Board (FSB) program (2005 – 2006)
Peter A. Lindstrom SURF Fellowship (2003)
Caltech-Japan Internship Program (2002)

Professional Experience

Teaching Assistant, UCLA (September 2010 – December 2010)
- Undergraduate MCDB 165A: Biology of the Cell with Dr. Luisa Iruela-Arispe

Teaching Assistant, UCLA (January 2010 – March 2010)
- Undergraduate LS 3: Introduction to Molecular Biology with Dr. Fuyu Tamanoi

Caltech-Japan Internship Program (June 2002 – September 2002)
- Summer internship at Sumitomo Chemical in Tsukuba, Japan

Presentations

UCLA Biological Chemistry Floor Meeting (UCLA 2010, 2011, 2013)
Oral Presentation: *"Understanding the SPAK-WNK1-FBXL5 Interactions"*
UCLA Biological Chemistry Retreat (UCLA 2011, 2012)
Poster: *"Discovering the Cellular Iron-Regulated Proteome"*
American Society of Mass Spectrometry Conference (Vancouver 2012)
Poster: *"Discovering the Cellular Iron-Regulated Proteome"*
UCLA Molecular Biology Institute Retreat (Lake Arrowhead 2013)
Poster: *"Discovering the Cellular Iron-Regulated Proteome"*
Tri-Campus NIGMS Training Program Symposium (USC 2013)
Poster: *"Discovering the Cellular Iron-Regulated Proteome"*

Publications

1. Vashisht AA, Zumbrennen KB, Huang X, Powers DN, Durazo A, Sun D, Bhaskaran N, Persson A, Uhlen M, Sangfelt O, Spruck C, Leibold EA, Wohlschlegel JA. Control of iron homeostasis by an iron-regulated ubiquitin ligase. Science. 2009 Oct 30;326(5953):718-21.
2. Jonas S, Stieg A, Richardson W, Guo S, Powers DN, Wohlschlegel JA, Dunn B. Protein Adsorption Alters Hydrophobic Surfaces Used for Suspension Culture of Pluripotent Stem Cells. The Journal of Physical Chemistry Letters. J. Phys. Chem. Lett. 2015 Jan 16;6(3):388-93.

Chapter 1: Introduction to the Iron Regulatory Systems and Salt Homeostasis Pathways

Cellular and Systemic Iron Regulation

As an essential cofactor found in almost all living organisms, iron is able to readily accept and donate electrons - it is this redox activity that results in its utilization in numerous biochemical processes such as oxygen delivery and storage, DNA repair and replication, lipid metabolism and chromatin modification[1]. Abnormalities in iron metabolism result in numerous human diseases such as anemia, hereditary hemochromatosis and aceruloplasminemia[2]. Due to the importance of proper iron maintenance at both the cellular and organismal level, the mechanisms of iron acquisition, distribution and regulation are important areas of investigation.

A key regulatory mechanism for cellular iron homeostasis in mammalian systems involves the post-transcriptional regulation activity of the mRNA binding iron-regulatory proteins (IRP) IRP1 and IRP2. The IRPs function as RNA-binding proteins during iron-limiting conditions to regulate the stability and translation of target mRNAs encoding iron homeostasis proteins[3]. These orthologous proteins interact with conserved *cis*-regulatory hairpin structures called iron-responsive elements (IREs) found on target mRNAs. Regulation of IRP binding to their targets can be adjusted in several ways. In iron-replete cells IRP1 has reduced binding to the IREs on target mRNA due to assembly of an iron-sulfur (4Fe-4S) cluster that precludes interaction with IREs, while IRP2 is degraded in a proteasome dependent manner[4,5]. IREs are found either on the 5' or 3' untranslated regions (UTRs) of target mRNAs, with the location determining the effect of binding. Binding of an IRP protein to the 5' UTR of an mRNA results in translational repression and downregulation of the target protein while an IRE in the 3' UTR results in mRNA stabilization and increased expression. Examples of mRNAs with 5' UTR IREs are the ferritin light and heavy chains, ferroportin and hypoxia-inducible factor 2α (HIF2α),

while transferrin receptor has a known IRE in the 3' UTR. In low iron conditions where IRPs are active, IRE binding leads to decreased ferritin and ferroportin production and increased transferrin receptor production (Figure 1).

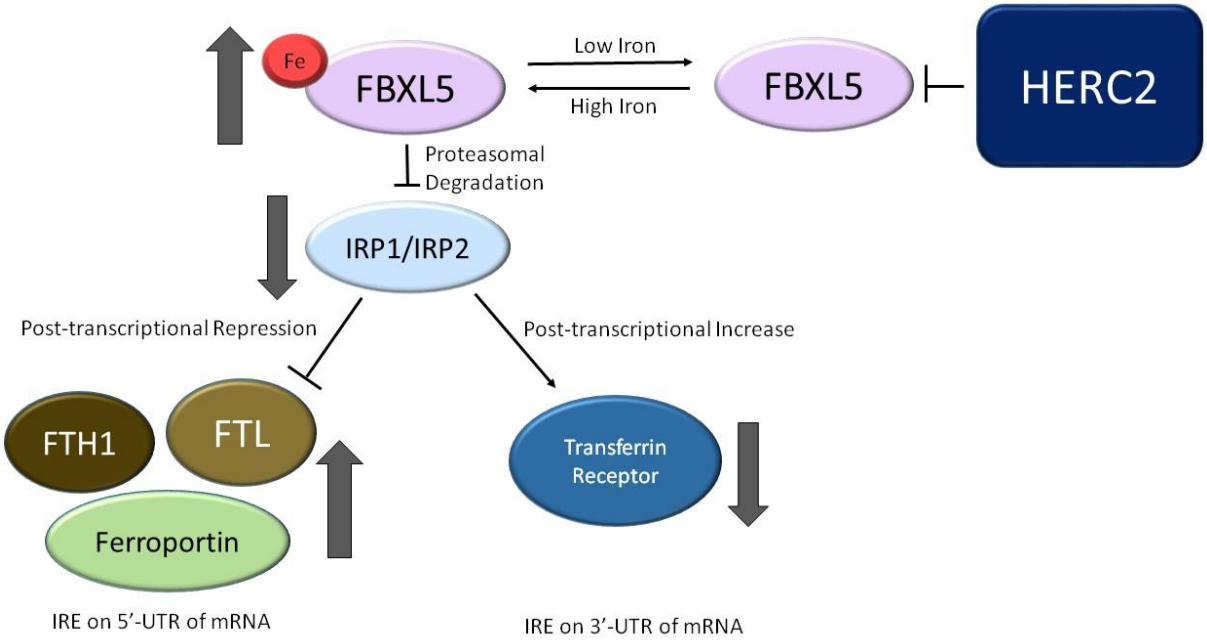

Figure 1. Schematic of intracellular iron homeostasis.

The ability of IRP1 to bind a cubane 4Fe-4S cluster contributes to an additional function of the protein, as iron-sulfur cluster bound IRP1 is able to function as a cytosolic aconitase[4]. Aconitase activity, which requires the iron-sulfur cluster, catalyzes the inter-conversion of citrate to iso-citrate to balance the amount of NADPH generated by isocitrate dehydrogenase and acetyl-CoA generated by citrate lyase. This function is lost in an iron-deficient environment, leading IRP1 to act as an IRE-binding protein.

While IRP2 never interacts with iron directly, it controls the expression of the proteins that do. Iron is not allowed to disuse freely through the cell due to its high reactivity; rather, it is commonly sequestered intracellularly into heteropolymeric ferritin cages that contain ferrous (Fe^{2+}) iron. These ferritin cages are comprised of 24 subunits that exist in both light and heavy forms. The light ferritin chain (FTL) is 19 kilodaltons (kDa) and the heavy ferritin chain (FTH1) is 21 kDa, while the complete ferritin cage is around 450 kDa. Both ferritin chains are ubiquitously expressed, but the ratios between them depend on cell type and changes in response to external conditions such as inflammation[6]. These ferritin complexes can accommodate around 4500 iron atoms within the nanocavity, and containment of iron in a redox-inactive form prevents iron-mediated cell and tissue damage[7].

Iron movement into and out of the ferritin cages are processes that have only recently been described in detail. As only ferric iron can be stored in ferritin heterocomplexes FTH1 possesses ferroxidase activity that oxidizes ferrous iron to ferric iron, while FTL promotes iron nucleation and ferroxidase turnover for FTH1[8]. One potential candidate for ferritin loading is Poly(rC)-binding protein (PCBP1), which is an iron chaperone believed to bind ferrous iron and deliver it to ferritin[9].

Not long ago the only thing known about the extraction of iron from the ferritin complexes was that it required lysosomal activity[10,11]. Recently however, a protein involved in targeting the ferritin cages for degradation was characterized. Mancias et al. utilized a mass spectrometry based approach involving stable isotope labeling by amino acids in cell culture (SILAC) to study proteins enriched in autophagosomes[12]. This method detected nuclear receptor coactivator 4 (NCOA4), and subsequent examination of NCOA4-associated proteins revealed ferritin heavy and light chains. They discovered that NCOA4 is required to deliver ferritin to the

lysosome where it is degraded by autophagy in order to liberate stored iron (Figure 2). NCOA4-deficient cells exhibited a decrease in intracellular iron levels due to the inability to free ferritin-bound iron. A second study focused on characterizing a new autophagy inhibitor PIK-III also identified NCOA4 as an important mediator of ferritin degradation[13].

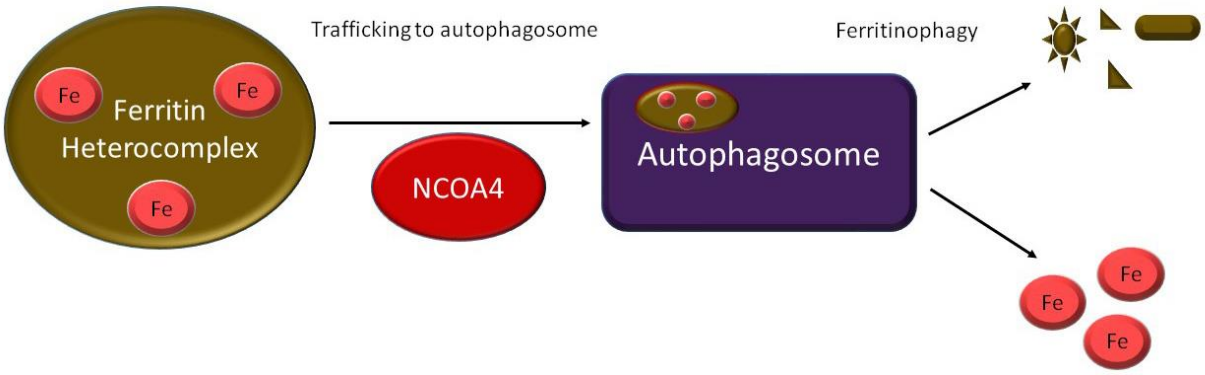

Figure 2. Schematic of NCOA4-mediated ferritinophagy.

While ferritin and the IRP system manage iron homeostasis at the cellular level, different proteins are involved in iron transport and intake at the organismal level. In the extracellular environment iron circulates in the plasma bound to the glycoprotein transferrin which can bind two Fe^{3+} atoms. Transferrin is normally 30% saturated with iron; a saturation of less than 16% indicates iron deficiency while a saturation of greater than 45% indicates iron overload[14]. When saturation of greater than 60% occurs, iron is found in un-bound form in the plasma and can damage parenchymal cells. Iron is delivered into cells by transferrin binding the membrane-expressed transferrin receptor (TfR1) and being internalized via clathrin-dependent endocytosis (Figure 3). The transferrin-TfR1 complex is trafficked to the early endosomes where acidification results in the release of bound iron. The freed iron, being in Fe^{3+} form, must be

then reduced by STEAP metalloreductases to Fe^{2+} in order to be transported into the cytosol by divalent metal transporter 1 (DMT1). After the iron is extracted, apo-transferrin and TfR1 are recycled and sent back to the cell surface.

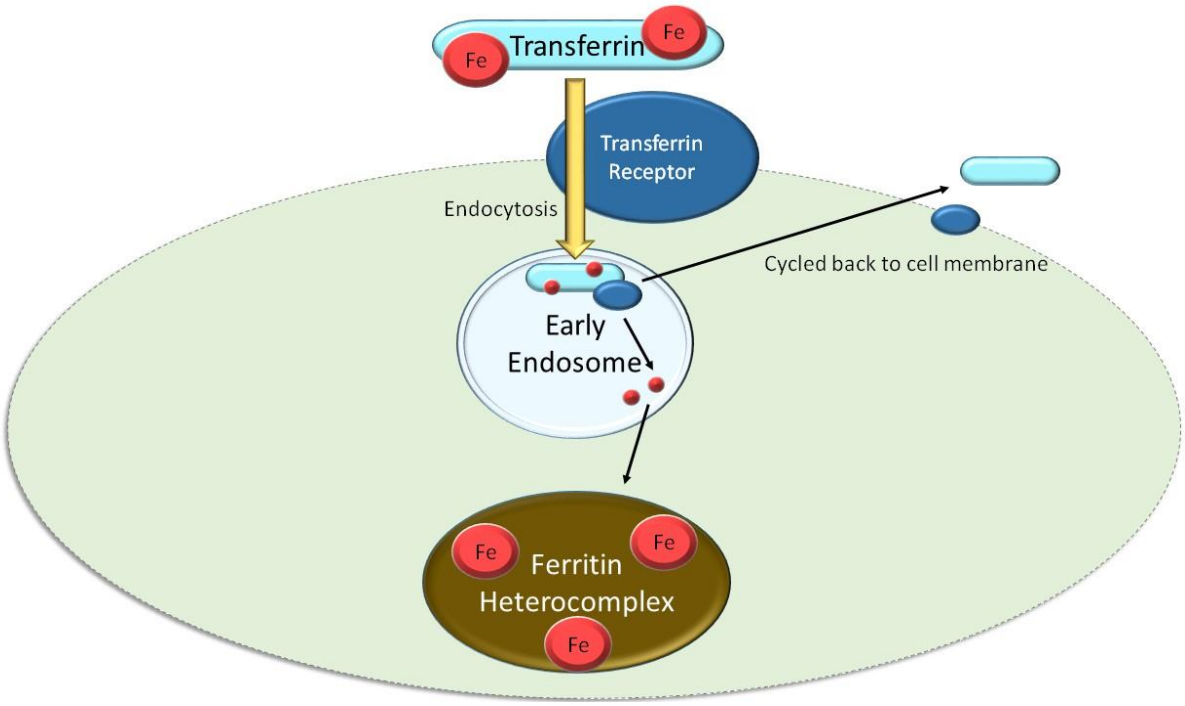

Figure 3. Schematic of cellular iron intake via transferrin receptor.

Although transferrin and transferrin receptor are the proteins that directly bind and result in the internalization of iron into cells, hepcidin is the hormone that controls systemic iron fluxes and plasma iron levels. Hepcidin is a small 2.7 kDa peptide consisting of 25 amino acids in its mature form and is synthesized and secreted by hepatocytes[15]. The mature hepcidin is formed by cleavage of an 84-amino acid pre-propeptide by furin-like prohormone convertases[16]. The mature cleaved hepcidin circulates in the blood in mostly free form and functions by controlling the cell surface concentration of the only known iron exporting transporter, ferroportin[17]. In this

way, hepcidin is able to control of the overall concentration and flux of extracellular iron by controlling the flow of iron from iron stores to iron-consuming tissues.

The target of hepcidin, ferroportin, is only found on the cell surfaces of cells that store or transport iron: enterocytes, hepatocytes, macrophages and adipocytes. The N-terminal end of hepcidin interacts with an extracellular loop of ferroportin, which then stimulates the ubiquitination of lysines on an intracellular region of ferroportin[18]. This event is required for the endocytosis of ferroportin and its degradation in the lysosome. Through this mechanism, iron exit from storage cells can be minimized by increasing the expression of hepdicin, while low levels of hepcidin will result in more cell surface expression of ferroportin and increased export of ferric iron (Fe^{2+}) from the cell.

Hepcidin expression and systemic iron metabolism are regulated transcriptionally and post-translationally as opposed to most proteins involved in intracellular iron homeostasis, which are regulated post-transcriptionally by the IRP proteins. Hepcidin expression occurs primarily in hepatocytes and is regulated at the transcriptional level through several mechanisms, the most well-explored being the bone morphogenic protein (BMP) receptor and the SMAD pathway[19,20]. BMP6 is an essential iron-related signaling protein and its knockout in mice has been shown to cause very low hepcidin levels and extracellular iron overload[21]. BMP6 acts on hepcidin levels through the SMAD pathway and active SMAD4, which can assemble activated transcriptional complexes that drive hepcidin transcription[22]. It has been found that expression of BMP6 increases as iron accumulates in the liver although the cell type that controls BMP6 expression has not been discovered. Furthermore, the exact pathway by which the BMP receptor receives input about the extracellular iron environment is still unknown. Another protein that affects hepcidin levels is transferrin receptor 2 (TfR2), which is thought to have a role by acting as a

sensor for holotransferrin concentration. TfR2 is stabilized by binding holotransferrin and the disruption of this protein results in an increase in iron accumulation brought on by loss of hepcidin production[23]. Hemochromatosis-related membrane protein (HFE) has a similar but independent effect on hepcidin levels, as its knockdown also results in loss of hepcidin and iron accumulation regardless of TfR2 expression[24].

Inflammatory conditions, such as those caused by infection and cancer, are another trigger for hepcidin and ferritin stimulation. In response to these conditions hepcidin is induced in order to minimize the amount of iron available to possible invading microorganisms and ferritin is increased to help in sequestering free iron. The proteins that appear to have significant activity on hepcidin under these conditions are the cytokines interleukin 1 (IL1) and IL6[25]. IL6 activates signaling pathways that control the STAT-binding motif next to the hepcidin transcriptional start site[26]. Hepcidin has been shown to have intrinsic antimicrobial activity[15,16]. Patients with hereditary hemochromatosis have decreased levels of hepcidin and are more susceptible to infections from bacteria such as *Listeria monocytogenes*. However, it is not clear how other factors of the disease such as liver failure, high extracellular iron or lack of hypoferrimic response to infections may affect susceptibility.

Crosstalk between the two iron regulatory systems (systemic and intracellular) appears to center on three proteins: (1) ferroportin (2) HIF2α and (3) TfR1 and TfR2. Ferroportin protein levels are regulated by both hepcidin-binding and by IRP binding to IREs found on its mRNA. Thus, ferroportin is able to be post-translationally regulated during systemic iron regulation by hepcidin while it is also post-transciptionally regulated by the cellular iron homeostasis pathways by IRPs. *HIF2α* mRNA is post-transcriptionally regulated by IRPs, while HIF2α itself is a transcription factor that regulates DMT1 expression. Through this, the IRP proteins are able to

regulate DMT1 and possibly iron import into cells that utilize direct iron uptake. The crosstalk between regulatory systems regarding the transferrin receptor concern the two isoforms and their interactions with the human hemochromatosis protein HFE (HFE for High Fe). HFE protein is a membrane protein that is believed to act as a switch between two sensors of iron-bound transferrin: TfR1 and TfR2. HFE is able to bind at the transferrin binding site in TfR1, thus acting as a competitive inhibitor while TfR2 can bind both HFE and iron-bound transferrin at the same time[27]. Experimental results support a model where iron-bound transferrin can displace HFE from TfR1 to increase HFE binding to TfR2 along with binding of transferrin-Fe_2. Since TfR2 also regulates hepcidin expression through the ERK/MAPK signaling pathway and TfR1 protein levels are IRP-regulated, there is potential for coordination between systemic and cellular iron homeostasis at this junction[28].

These intricate systems of iron regulation are required due to the shortage of soluble oxidized iron available to mammals in the environment, which has resulted in organized structures that aggressively retain iron but have no effective way to rid themselves of excess. Iron found in plant sources exist in forms that cannot be utilized by humans, though iron found in heme from meat sources is readily absorbed[29]. The other types of iron commonly found in the human diet are ferritin and ferric iron (Fe^{3+})[1]. Heme, non-heme iron and ferritin all appear to have different absorption pathways in the intestines which all use different proteins for transport into the body.

Inorganic iron intake in the intestinal enterocytes is performed by the divalent metal transporter 1 (DMT1) that imports ferrous iron as well as other divalent metals, but not ferric iron[30]. DMT1 is expressed on the membrane of duodenal enterocytes and is predicted to have twelve transmembrane domains with both termini in the cytoplasm[31]. The activity of DMT1 is

stimulated by low pH and is accompanied by proton co-transport[32]. Experiments have shown that DMT1 is, in fact, a ferrous iron and proton co-transporter. DMT1 plays an essential role in intestinal iron transport, as conditional intestine-specific knockout in mice develop postnatal anemia and systemic iron deficiency[33]. This phenotype can be rescued by iron administration bypassing the intestines, illustrating the role of DMT1 for systemic iron intake.

Heme import in the intestines is thought to occur via two potential heme transporters: Heme carrier protein 1 (HCP1) and heme responsive gene-1 (HRG1, SLC48A1)[34,35]. While HCP1 exhibits heme transport activity, its essential function appears to be folate transport. When HCP1 function is lost, patients and mice develop folate deficiency anemia that can be rescued with parenteral folate derivatives but not by iron or heme[36]. The second mammalian heme transporter, HRG1, is highly expressed in the brain, kidney, heart and skeletal muscle, while it is moderately expressed in the liver, lung, placenta and small intestine. It localizes to macrophages in the phagolysosomes, suggesting that it is involved in iron recovery from erythrocyte recycling[37].

Despite the importance of iron regulation in normal human function, much is still unknown about the pathways involved. As depicted above, not only are the intracellular and systemic iron regulatory machines highly complex, they also utilize protein systems that are decidedly independent of each other. Underneath this complex interplay of multiple signaling pathways we have discovered a link between the iron regulatory system and the osmotic stress system which could shed light on another aspect of this entity.

F-Box Proteins and Ubiquitin-Regulated Proteolysis

Ubiquitin is a small 76 amino acid long protein that can be conjugated to substrate proteins for either degradation or signaling purposes[38]. Polyubiquitin chains are formed when ubiquitin is conjugated to a lysine in a different ubiquitin molecule via one of seven lysine residues found on ubiquitin itself, with different chains signifying different fates. K11 or K48 chains target the substrate to the proteasome for degradation while monoubiquitination and K63-linked chains are believed to be used for signaling. Ubiquitin chains of four or more are thought to be sufficient for proteasome recognition which directs the ubiquitinated target for degradation[39]. The ubiquitin pathway involves three protein classes: E1 activating enzymes, E2 conjugating enzymes and E3 ubiquitin ligases[40]. E1 enzymes form a covalent thioester bond to the C-terminus of ubiquitin through an ATP-dependent process and then subsequently transfer the ubiquitin to an E2 ubiquitin conjugating enzyme. The next step differs depending on the types of E2 and E3 enzymes involved. For HECT-type E3 ligases the E2 passes the ubiquitin to the HECT-type E3 ligase which then transfers it to the substrate. For RING-type E3 ligases like SCF, the ubiquitin molecule is transferred directly from the E2 to the substrate. The E3 ligase complex signals for substrate degradation by covalently linking a ubiquitin protein via an isopeptide bond to a lysine in the substrate.

F-box proteins are the defining component of a family of multisubunit E3 ligase complexes comprised of the S-phase kinase-associated protein 1 (SKP1), cullin 1 (CUL1), the RING domain-containing protein RBX1 and an F-box subunit (also termed SCF ligases)[41]. The F-box protein is itself a substrate adaptor that contains both a substrate binding domain as well as the F-box domain which mediates its association with SKP1. There are 69 different F-box

proteins in human cells with each F-box protein responsible for targeting a different set of substrates for ubiquitination. F-box proteins are sub-categorized by the presence of recognizable domains other than the F-box, notably the WD40 domain or the leucine-rich repeat domain[42]. The F-box and WD40 domain (FBXW) family consists of twelve proteins in humans while the F-box and leucine-rich repeat (LRR) family contains 21 proteins (of which one is FBXL5). The remaining 36 F-box proteins (FBXO) have domains other than WD40s and LRRs and are termed "O" for "other".

Ubiquitin ligase activity is regulated by various other post-translational modifications, including neddylation and phosphorylation. Neddylation involves the conjugation of NEDD8, a ubiquitin-like protein that is required for normal cullin and CRL ligase activity. Small molecules such as MLN4924 which prevent NEDD8 activation are able to block SCF-dependent poly-ubiquitination and degradation[43].

F-box proteins target their substrates by binding to a defined set of amino acids known as a degron[44]. The best understood degrons are phosphodegrons that entail phosphorylation-dependent substrate binding. While this is not the only mechanism of substrate recruitment, it was the first discovered due to its role in cell cycle regulation and is commonly seen in SCF-substrate interactions.

Once substrate proteins have been modified by poly-ubiquitin chains, their fate is dictated by their recognition by different cellular ubiquitin binding proteins. These factors, which include ubiquitin binding proteins (co-chaperones, multimeric ATPases and ubiquitin like domain (UBL)–ubiquitin associated domain (UBA) shuttle proteins) and ubiquitin receptor proteins, serve to "decode" the complex poly-ubiquitin chain linkages in order to direct them to specific

downstream pathways including proteasome degradation and different intracellular trafficking complexes[45,46].

Proteins that are labeled by K11 or K48 poly-ubiquitin chains are transported to the proteasome for degradation. The 26S proteasome (the S signifies the Svedberg sedimentation coefficient) is a large 2.5 MDa assemblage of over thirty different subunits[47]. The 26S proteasome is shaped like a barrel with the 20S core particle forming the body and capped by one or two 19S regulatory particles[48]. The 20S component provides the protease function of the complex while the 19S caps utilize ATPase activity to regulate degradation by controlling entry of substrates into the central chamber[49]. Proteins are cleaved into small oligopeptides that can then be broken down by peptidases within the cell.

FBXL5 was first identified as an iron-regulated protein in the Wohlschlegel laboratory as part of a study aimed at identifying biological pathways regulated by previously uncharacterized ubiquitin ligases. For this project, our lab studied the F-box family of E3 ubiquitin ligase adaptors primarily due to their poorly defined status. There are 69 known F-box proteins found in human cells, but at the time in 2009 only around ten had proposed substrates[38]. In particular, our lab was interested in F-box proteins implicated in cancer and tumorigenesis. FBXL5 was selected for in-depth characterization based on the observation that high FBXL5 protein expression in primary breast tumors correlated with reduced overall survival for patients with esterogen receptor positive (ER+) but not negative (ER-) tumors.

The initial characterization of F-box proteins such as FBXL5 focused on a proteomic mass spectrometry-based analysis to identify binding partners associated with novel F-box proteins in order to infer pathways they may be regulating. Briefly, stable cell lines over-

expressing a tagged dominant negative F-box protein of interest (i.e. FBXL5-ΔFbox) were generated and used to isolate and identify F-box-associated protein complexes by affinity purification, followed by Multidimensional Protein Identification Technology (MudPIT). Dominant negative F-box proteins are created by deletion of the F-box domain to generate a mutant that can still bind substrates but cannot assemble into a SCF complex and catalyze their ubiquitination. These mutant F-box proteins will trap their substrates when immunoprecipitated, greatly aiding in our ability to detect low abundance potential substrates using mass spectrometry.

MudPIT is a gel-free technique developed for the analysis of highly complex peptide mixtures[50,51]. Peptide digests from a sample of interest are fractionated online using two orthogonal dimensions of separation – C18 reversed phase and strong cation exchange that fractionate peptides based on their hydrophobicity and charge, respectively. When combined online, these two separation approaches enable in-depth fractionation of complex peptide mixtures, ensuring that high complexity, high dynamic range mixtures can still be effectively analyzed.

After tandem mass spectrometry information has been collected, the SEQUEST and the DTASelect algorithms are used to infer the peptide sequence and proteins present in the sample[52,53]. SEQUEST uses a database of protein sequences to determine a candidate set of peptides that could match the experimental data point. For each candidate peptide, a theoretical tandem mass spectrum is created and compared to the original peptide by cross-correlation. DTASelect aids SEQUEST by organizing and filtering identifications and estimating false-positive rates for a given set of filtering criteria.

We utilized bottom-up proteomics with complex peptide mixtures (known as shotgun proteomics) to characterize FBXL5 binding partners. This analysis of FBXL5 and its dominant negative mutant form FBXL5-ΔFbox revealed physical interactions with iron-regulatory proteins IRP1 and IRP2. Although it was known at the time that IRP1 and IRP2 were degraded in a proteasome and iron-dependent manner the ubiquitin ligase responsible for their degradation had not been identified. Our study of FBXL5 and its role in IRP degradation is outlined in chapter 2. Our proteomic analysis of FBXL5 identified the association of WNK1 and SPAK with FBXL5. These proteins had not previously been linked to any known iron-regulatory process prior to our discovery of their binding to FBXL5 - instead, these proteins are well-established osmotic stress regulatory proteins. Work done over the last several years has elucidated the pathway by which these two seemingly unrelated systems would function together and why.

Regulation of Osmotic Stress: The WNK-SPAK/OSR1 pathway

While studying the ubiquitin ligase FBXL5, we discovered that there is overlap between the iron regulatory systems and the osmotic stress management pathways. However, little is known about how and why these two stress networks would interact. The vertebrate salt regulatory pathways involve different proteins compared to iron regulation and are outlined below (Figure 4).

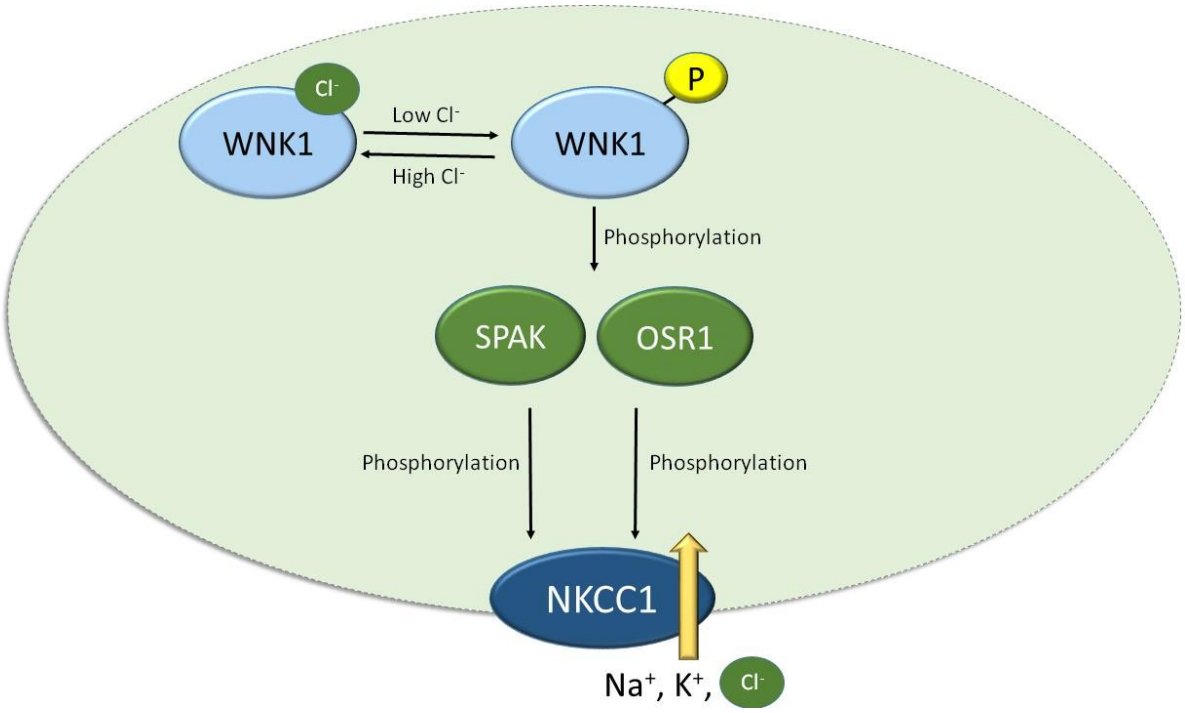

Figure 4. Schematic of intracellular osmotic stress response.

Osmotic stress regulation in vertebrate systems depends on a kinase cascade initiated by WNK (With No K [lysine]) family of kinases. The name of this family of proteins refers to the unusual catalytic site that is used for phosphorylation of substrates, as this site does not have a conserved catalytic lysine in subdomain II used to conjugate ATP[54]. After the crystal structure

of WNK1 was solved, it was determined that a lysine in subdomain I substitutes for the missing lysine residue so that the kinase can function normally[55]. All four mammalian isoforms of WNK lack the conserved lysine residue, yet are catalytically active as demonstrated by their autophosphorylation activity.

The WNK family of proteins has been the subject of much investigation recently due to their potential as drug targets for conditions that are becoming prevalent in the developed world. Loss of control over the WNK signaling pathway has been shown to have downstream effects on blood pressure. Specifically, hypertension (high blood pressure) is a asymptomatic condition that is a major risk factor for stroke, heart disease and kidney failure and affects almost one in four adults in the United States[56]. Due the widespread nature of this illness the financial burden on developed countries is high, estimated to be in the range of billions of dollars per year[57]. Depending on the patient hypertension can be moderated by lifestyle changes, though genetic dispositions can require the use of medications to lower blood pressure. These drugs function in a variety of ways: in the kidneys to reduce the amount of salt retained (thiazide or loop diuretics), to modulate the width of the blood vessels (angiotensin-converting enzyme inhibitors, angiotensin II receptor antagonists, Ca^{2+} channel blockers or alpha-blockers) or to reduce the heart workload (beta-blockers)[58]. Currently, there are no medications that inhibit WNK proteins.

The WNK family of proteins was discovered in 2001 by the Lifton lab when they observed that pseudohypoaldosteronism type II (PHAII) is caused by gain of function mutations in WNK1 and WNK4, the functions of which were unknown at the time[59]. PHAII is an autosomal dominant disorder that results from intronic deletions in WNK1 that elevate expression without altering function. These mutations cause increased salt retention in the kidney and increased serum potassium K^+ (hyperkalemia). In humans, polymorphisms in the

WNK1 have been linked to alterations in blood pressure and heterozygous $WNK1^{-/+}$ mice have lowered blood pressure[60,61].

WNK1 is a large 2,382 amino acid long, 250 kDa protein expressed in many cell types. Cell-type specific expression differences are observed with WNK isoforms with different isoforms showing different expression patterns. For example, while WNK1 is enriched most highly in the kidneys, heart and skeletal muscle WNK4 is mostly found in kidneys, colon and skin. WNK1 also features a kidney-specific splice variant which lacks most of the N-terminal kinase domain[62]. The role of this kidney-specific WNK1 is proposed to be regulatory, although this has yet to be shown definitively.

WNK1 is activated in conditions of osmotic stress – for example, a hyperosmotic treatment such as sorbitol or hypotonic low-Cl^- conditions[63,64]. This activation is likely mediated by autophosphorylation as it depends on a functional kinase domain in WNK1; the activation is also rapid, occurring within one minute of hyperosmotic stress and within five minutes of hypotonic stress. Until recently, it was unknown whether WNK1 was the salt sensor or this ability was possessed by another protein. In 2014, the Cobb and Goldsmith labs at University of Texas Southwestern Medical Center solved the crystal structure of the WNK1 kinase domain and identified the mode of action for salt sensing by WNK1[65]. Their initial observation using differential scanning fluorimetry assays was that the WNK1 kinase domains were stabilized by chloride salts, which indicated that a physical interaction may be occurring. Additionally, this binding was accompanied by an inhibition of WNK1 activity as chloride was found to have a strong inhibitory effect on autophosphorylation of the WNK1 kinase domain. The solved structure of the WNK1 kinase domain revealed that it possesses a chloride-binding site similar to those found in the C1C family of chloride transporters. Chloride binding by WNK1 prevents

substrate binding in the active pocket, thereby preventing downstream phosphorylation. The proximity of the chloride binding region to the active site likely contributes to the speed by which WNK can respond to osmotic shock. While it is now clear how low chloride contributes to WNK activation, it is still uncertain how hyperosmotic conditions result in WNK stimulation. One possible mechanism is that crowding effects from solutes such as other salts or sorbitol could prevent chloride binding by competition, but additional experimental work is necessary to establish this model.

WNK1 and the other WNK proteins exert their activity through their main substrates STE20/SPS1-related proline/alanine-rich kinase (SPAK, also referred to as Serine-Threonine Kinase 39 (STK39)) and oxidative-stress-response kinase-1 (OSR1, OXSR1). These two kinases share very high sequence homology: 96% in the N-terminal catalytic region and 67% in the C-terminal regulatory domain[66]. The region that differs the most between the two proteins is a unique proline-alanine rich 48 amino acid long region in the N-terminus of SPAK from which the protein derives its name. The function of this proline-alanine rich region is still unknown, as the protein can apparently function normally without it[67]. Amino acid sequence alignment has established that OSR1 was the prototypical kinase and SPAK likely evolved from gene duplication[66]. For example, while OSR1 exists in organisms such as *C. elegans* and *Drosophila melanogaster*, SPAK can only be traced back as far as chickens and there are many vertebrate systems where SPAK homologues do not appear to exist at all. Another clue to the evolutionary differences between the two proteins can be found in knockout studies: while disruption of SPAK in knockout mice results in viable animals with no overt phenotype, OSR1 knockout generates no living pups due to embryonic lethality[66].

The interaction between WNK1 and SPAK/OSR1 was discovered in a immunoprecipitation study used to identify WNK1 binding partners[68]. Through these studies the importance of the conserved C-terminal (CCT) domain found on SPAK/OSR1 was discovered, as the majority of the SPAK-WNK1 binding is mediated through this region. The CCT domain interacts with RFx[V/I] motifs found on both upstream effectors such as the WNK proteins and downstream targets such as NKCC1[69,70]. Peptides containing a RFx[V/I] motif can bind the CCT domain of SPAK/OSR1 in the nanomolar affinity range, and structural analysis was used to determine that the CCT domain contains a deep groove that can form interactions with the arginine, phenylalanine and valine residues[71]. All of SPAK's currently known binding partners possess a RFx[V/I] motif: WNK1, WNK2, WNK4, NKCC1, NKCC2, Tumor necrosis factor receptor superfamily member 19L (RELT) and RELT-like Protein 1 (RELL1). Incidentally HERC2, an E3 ubiquitin ligase that we find regulates FBXL5 stability, possesses a RFTV sequence, while FBXL5 does not feature the motif.

Although the CCT domain in SPAK/OSR1 is required to interact with WNK proteins, the actual phosphorylation of SPAK occurs at distal sites. Activation of SPAK happens at two residues: a T-loop threonine residue (T233) and a serine in the S-motif (S373). Of these it seems that the T-loop phosphorylation is more important for activation, as alanine substitution of the S-motif serine has no effect on activity[63,68]. Mutation of the T-loop threonine to alanine inhibits SPAK activity on downstream targets, signifying the importance of this site. Conditions that stimulate WNK1 activation result in SPAK/OSR1 phosphorylation, and WNK1 knockdown using siRNA partially inhibits both the phosphorylation and activity of SPAK/OSR1.

SPAK and OSR1 have at least two classes of substrates, with the best characterized ones being members of the SLC12 family of electroneutral cation-coupled Cl^- co-transporters: the

Na^+/Cl^- co-transporter (NCC) protein and the $Na^+/K^+/2Cl^-$ co-transporters (NKCC) proteins NKCC1 and NKCC2. The NKCC proteins feature twelve transmembrane domains with N-terminal and C-terminal cytoplasmic domains and function by transporting Na^+, K^+ and Cl^- ions into the cell along the sodium gradient to control cell volume and osmotic balance between the intracellular and extracellular spaces[72,73]. While NKCC does not directly require ATP to perform its function, it does rely on the established sodium gradient set by the Na^+-K^+ ATPase and is a form of secondary active transport. *In vitro* studies have revealed that activated SPAK and OSR1 phosphorylate a cluster of conserved threonine residues located on the cytosolic N-terminal end of NKCC1 and this results in NKCC1 activity that transports ions into the cell[74]. This cluster of residues includes Thr203, Thr207, Thr212 and Thr217 on human NKCC1. Activation of NKCC1 by osmotic shock or overexpression of activated SPAK can be lost if Thr212 or Thr217 is mutated[75,76]. For the purposes of assaying SPAK/OSR1 activity, a small synthetic peptide named CATCHtide that contains this cluster of threonine residues can be used as a substrate[70].

The CCT domains of SPAK and OSR1 are required to interact with the two RFxV clusters on the cytosolic N-terminal end of NKCC1. Loss of these motifs through mutation leaves NKCC1 unable to bind SPAK or OSR1 and activation by hyperosmotic stress is lost[77]. Due to SPAK and OSR1 using the same domain to interact with both upstream effectors and downstream substrates, it has been proposed that there must be a mechanism to release binding partners after phosphorylation of the target has occurred. This activity is thought to be steric hindrance brought about by SPAK phosphorylation on either WNK1 or NKCC1[58]. The proposed mechanism includes SPAK-dependent phosphorylation on a threonine or serine near the RFxV motif on the binding partner that promotes the dissociation of the complex. While SPAK/OSR1

phosphorylation of WNK proteins is believed to perform a regulatory function, the details of this remain to be established.

Although drugs that inhibit WNK or SPAK/OSR1 proteins have not been reported, NCC and NKCC1/2 are inhibited by thiazide-diuretic and loop–diuretic drugs. These drugs function in the kidney to reduce salt and fluid retention, thereby combating hypertension. The effects of these inhibitory drugs are directly comparable to the phenotype of the loss-of-function mutations. Loss-of-function in kidney-specific NCC and NKCC2 result in low blood pressure conditions known as Gitelman's syndrome and Bartter's type I syndrome, respectively[78,79].

WNK1 and SPAK/OSR1 activity are also believed to be responsible in regulating K^+/Cl^- co-transporters (KCC) in opposing fashion to their regulation of NKCC proteins[80]. The KCC family of proteins contains four members (KCC1 – KCC4) that catalyze K^+ and Cl^- efflux from the cell. Since KCC proteins operate in the opposite fashion as NKCC family members, they are inhibited in hyperosmotic stress conditions. WNK1 regulates KCC members through phosphorylation, which inhibits KCC proteins. The balance between NKCC-driven intake and KCC-driven efflux is preserved in conditions that de-activate NKCC proteins: hypotonic high K^+ conditions have been shown to induce a rapid dephosphorylation of the two threonine residues found on the C-terminal cytoplasmic domain of the KCC proteins[81]. Of these two threonine sites, one is directly modified by WNK1 while phosphorylation of the second is dependent on SPAK/OSR1 activity. Thus, WNK1 is believed to regulate KCC activity via both a SPAK/OSR1-dependent and independent set of mechanisms[82]. The method of phosphatase activity for activating KCC is poorly characterized, with the protein responsible for action unknown.

Recent structural work on NKCC1 has revealed some insights on how dimerization and conformational changes may influence protein activity. Monette and Forbush used Förster resonance energy transfer (FRET) to examine conformational changes that occur during dimerization and activation of NKCC1[83]. By studying both double-tagged NKCC1 and dimers of singly-tagged NKCC1, they were able to determine that the largest structural changes occurred during activation of NKCC1 dimers. SPAK/OSR1-mediated phosphorylation of NKCC1 could potentially influence these conformational changes, although this has yet to be established.

Like NKCC1, one possible mode for regulation of SPAK/OSR1 activity involves the proteins' ability to hetero- and homo-dimerize. This mode of regulation is attractive since SPAK/OSR1 can only interact with one binding partner at a time through the CCT domain; however, if the proteins form a dimer then regulation by higher-order assemblies is possible[66]. Initial results involving OSR1 showed that the full length protein could be used as a bait to pull down the kinase domain of OSR1 by immunoprecipitation and a domain-swapped dimer involving two OSR1 kinase domains was characterized by x-ray crystallography[84,85]. These experiments verify the existence of the OSR1 homodimer. Based on their high sequence homology, homodimeric SPAK and heterodimeric SPAK/OSR1 forms are likely to exist but there is no current evidence suggesting any regulatory role for these oligomerization states. In fact, when Gagnon et al. tested SPAK phosphorylation activity using an *in vitro* assay, they found that full length wild type SPAK was unable to phosphorylate an inactive form of SPAK[67]. This result appears to signify that SPAK dimerization is not an important regulator of activity, although this might not be the case for OSR1. The ability of SPAK or OSR1 to dimerize could

also play a role in NKCC1 activation and dimerization, as it can be envisioned that a SPAK/OSR1 dimer could bring two NKCC1 proteins together through their CCT domains.

SPAK is implicated in other regulatory systems that do not involve osmotic shock: these include mitogen-activated protein kinases (MAPK) signaling pathways and apoptosis. SPAK has been shown to activate p38 and c-Jun N-terminal kinase (JNK) and this activation is dependent on SPAK's ability to interact with the TNF receptor RELT, as the SPAK-binding deficient mutant version of RELT is defective in MAPK stimulation[86]. In addition, MAPK activation of downstream triggering was blocked by expression of kinase-dead SPAK[86]. While the biological role of SPAK-dependent stimulation of MAPK pathways is unclear, it may be related to its role in apoptotic response.

Apoptosis is another regulatory process influenced by SPAK. This was first suggested by sequence features found in the SPAK protein: it contains a putative nuclear localization signal and caspase-cleavage site (DEMDE), and a truncated version of SPAK localizes in the nucleus. Additional data linking SPAK to apoptosis was discovered when studying its link to cancer. The Teitell lab in 2009 discovered that the gene for SPAK, *stk39*, is hypermethylated in TCL1-tg B-cell lymphomas[87]. Furthermore, SPAK was been found to be downregulated in metastatic prostate and treatment-resistant breast cancers using microarray analysis. Activation of caspase-3, which initiates the apoptotic program, is reduced when SPAK is repressed. In this fashion, SPAK appears to function in stimulating apoptosis and this activity is lost in certain types of cancer in order to promote cell survival. Indeed, SPAK knockdown impairs the induction of apoptosis typically found in response to DNA double strand breaks but not from osmotic or oxidative cell stressors. The SPAK effect on apoptotic activation is mediated by MAPK signaling, as pharmacological inhibition of JNK presented the same phenotype as SPAK

knockdown. This effect is likely dependent on the RELT or the RELL proteins, although no data supporting this connection has been reported. Together, these results indicate that SPAK is involved in activation of apoptosis through its MAPK signaling capabilities and could be important in the context of tumorigenesis. Given that iron has a role in cancer development as well, this could be another link between the two systems attributable to SPAK.

SPAK has been implicated in the regulation of a diverse set of biological pathways, but none of these have been connected to iron homeostasis. In our current work, we have established a basis for SPAK regulation of cellular iron homeostasis by forming a ternary complex with HERC2 to influence the stability of the iron-binding ubiquitin ligase FBXL5 and the ferritin-degrading protein NCOA4.

Chapter 2: Control of Iron Homeostasis by an Iron-Regulated Ubiquitin Ligase

Analysis of FBXL5 N199, the Hemerythin-like Domain

All cells require iron for survival and have developed regulatory mechanisms for maintaining appropriate intracellular iron concentrations. The degradation of iron regulatory protein 2 (IRP2) in iron-replete cells is a key event in this pathway, but the E3 ubiquitin ligase responsible for its proteolysis remained elusive. We found that a SKP1-CUL1-FBXL5 ubiquitin ligase protein complex associates with and promotes the iron-dependent ubiquitination and degradation of IRP2[88]. The F-box substrate adaptor protein FBXL5 was degraded upon iron and oxygen depletion in a process that featured an iron-binding hemerythrin-like domain in its N terminus. Thus, iron homeostasis is regulated by a proteolytic pathway that couples IRP2 degradation to intracellular iron levels through the stability and activity of FBXL5.

My contribution in discovering the function of FBXL5 in iron regulation is found in Figure 8A and Figure 8B of the published manuscript and focused on characterizing the role of the hemerythrin-like domain in the N-terminal end of FBXL5 in iron and oxygen sensing. This involved cloning the hemerythrin-like domain (the N-terminal 199 amino acids) and purifying the 6-His tagged recombinant protein from *E. Coli* for use in inductively coupled plasma mass spectrometry (ICP-MS) experiments to demonstrate that FBXL5's hemerythrin-like domain co-purifies with iron (Figure 8A). I also conducted domain mapping experiments that showed that the hemerythrin-domain of FBXL5 is both necessary and sufficient to confer iron-regulated changes in FBXL5 stability (Figure 8B).

Control of Iron Homeostasis by an Iron-Regulated Ubiquitin Ligase[88]

Ajay A. Vashisht, Kimberly B. Zumbrennen, Xinhua Huang, David N. Powers, Armando Durazo, Dahui Sun, Nimesh Bhaskaran, Anja Persson, Mathias Uhlen, Olle Sangfelt, Charles Spruck, Elizabeth A. Leibold, James A. Wohlschlegel

Iron regulatory proteins 1 and 2 (IRP1 and IRP2) function as RNA-binding proteins during iron-limiting conditions in order to regulate the translation and stability of mRNAs encoding proteins required for iron homeostasis[3,89]. In iron-replete cells, IRP RNA binding is reduced because of the assembly of a 4Fe-4S cluster in IRP1[90] and the proteasomal degradation of IRP2[91-94]. Despite the importance of IRP2 in iron metabolism, the ubiquitin ligase responsible for its degradation remains unclear. Early studies suggested that a unique 73-amino-acid region of IRP2 was a substrate for the haem-oxidized IRP2 ubiquitin ligase (HOIL-1)[95,96]. Other studies, however, showed that deletion of the 73-amino-acid region or HOIL-1 silencing did not affect the iron-dependent degradation of IRP2[97-99].

Human FBXL5 is a member of the F-box family of adaptor proteins that confer substrate specificity to SCF (SKP1-CUL1-F-box) ubiquitin ligases[41,100]. FBXL5 contains a hemerythrin-like domain, a F-box domain that mediates its association with SKP1, and four leucine-rich repeats that probably function in substrate binding (Figure 9). Affinity purification followed by multidimensional protein identification technolology (MudPIT)[50,51] was used to identify proteins that interact with a mutant form of FBXL5 lacking the F-box domain, which cannot assemble into an active SCF complex. Because this mutant retains the ability to interact with substrates but is unable to catalyze their ubiquitination, it functions as a substrate-trapping reagent. IRP1 and

IRP2 were identified as FBXL5-interacting proteins in this analysis. A reciprocal proteomic analysis showed that FBXL5, SKP1, and CUL1 copurify with IRP2 (Table 1).

We confirmed the interaction of FBXL5 with SCF components and IRPs using coimmunoprecipitation analyses. Human embryonic kidney (HEK) 293 cells stably expressing hemagglutinin (HA)–FLAG-FBXL5 were transfected with Myc-CUL1 or Myc-SKP1. HA-FLAG-FBXL5 copurified with immunoprecipitated Myc-CUL1 and Myc-SKP1 (Figure 5A). For the FBXL5-IRP interactions, HA-FLAG-FBXL5 was immunoprecipitated from stable HEK293 cells. Endogenous IRP1 and IRP2 copurified only in extracts containing HA-FLAG-FBXL5 (Figure 5B). We found that the 73-amino-acid region of IRP2 was not required for the interaction with FBXL5 (Figure 10). Thus, FBXL5 is a component of a bona fide SCF complex that interacts with IRP1 and IRP2.

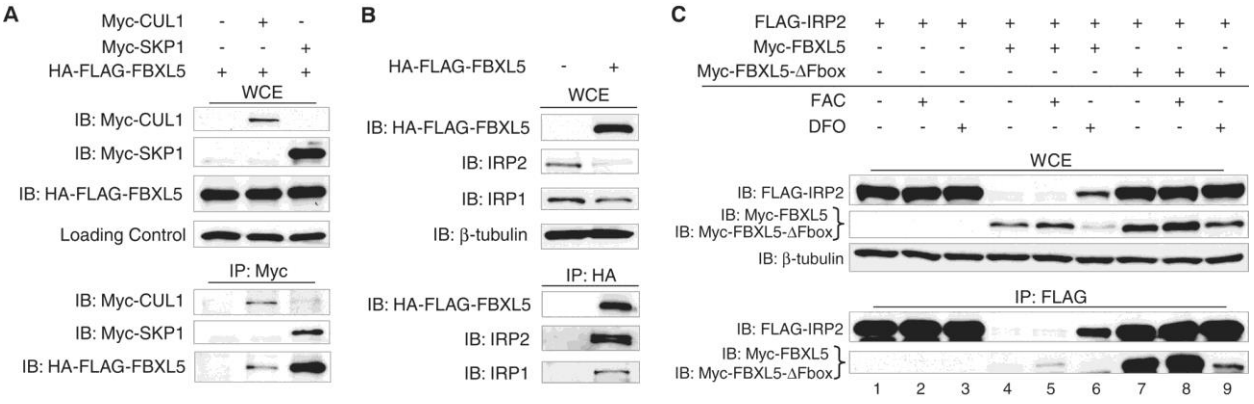

Figure 5. FBXL5 forms a SCF complex that associates with IRP1 and IRP2. (**A**) Flp-In TREx-293 cells (Invitrogen, Carlsbad, CA) stably expressing HA-FLAG-FBXL5 were transfected with Myc-CUL1, Myc-SKP1, or empty vector. Myc-CUL1 and Myc-SKP1 were immunoprecipitated with antibody to c-Myc. Whole-cell extracts (WCEs) and immunoprecipitates (IPs) were immunoblotted with antibodies to FLAG and c-Myc. (**B**) HA-FLAG-FBXL5 was immunoprecipitated from stable Flp-In TREx-293 cells using antibody to HA. WCEs and IPs were immunoblotted with antibodies to FLAG, IRP1, IRP2, and β-tubulin. (**C**) HEK293 cells were cotransfected with FLAG-IRP2 and Myc-FBXL5, Myc-FBXL5-ΔF-box, or empty vector and treated for 8 hours with FAC or DFO. FLAG-IRP2 was immunoprecipitated using antibodies to FLAG. WCEs and IPs were immunoblotted with antibodies to FLAG, c-Myc, and β-tubulin.

To determine whether the FBXL5-IRP2 interaction is regulated by iron, we immunoprecipitated FLAG-IRP2 from HEK293 cells coexpressing either Myc-FBXL5 or Myc-FBXL5-ΔF-box after treatment with ferric ammonium citrate (FAC) or the iron chelator desferrioxamine (DFO). FLAG-IRP2 interacted with Myc-FBXL5 and Myc-FBXL5-ΔF-box more strongly in cells treated with FAC as compared with those treated with DFO, suggesting that the interaction is iron-regulated (Figure 5C). In addition, we found that expression of Myc-FBXL5 but not Myc-FBXL5-ΔF-box strongly reduced the abundance of coexpressed IRP2, which is consistent with a role for FBXL5 in promoting IRP2 degradation and FBXL5-ΔF-box acting as a dominant negative mutant. The interaction of Myc-FBXL5 and Myc-FBXL5-ΔF-box with IRP1 and an IRP1-C3S mutant, which is sensitive to iron-dependent degradation because of its inability to form a 4Fe-4S cluster, was also iron-regulated (Figure 11)[101,102].

Coimmunoprecipitation analyses showed that FBXL5 overexpression reduced the levels of cotransfected IRP2 in an iron-regulated manner (Figure 5C). Stable expression of HA-FLAG-FBXL5 in HEK293 cells also reduced endogenous IRP2 levels in an iron-dependent manner (Figure 6A). Reduced IRP2 was associated with an increase in the iron-storage protein ferritin, indicating that ferritin was translationally derepressed[3,89]. FBXL5 depletion by small interfering RNA (siRNA) in HEK293 cells increased IRP2 and decreased ferritin protein levels independently of iron treatment (Figure 6B). Similar results were found when FBXL5 was depleted from IMR90 human diploid fibroblasts (Figure 12), indicating that IRP2 regulation by FBXL5 is not limited to transformed cells.

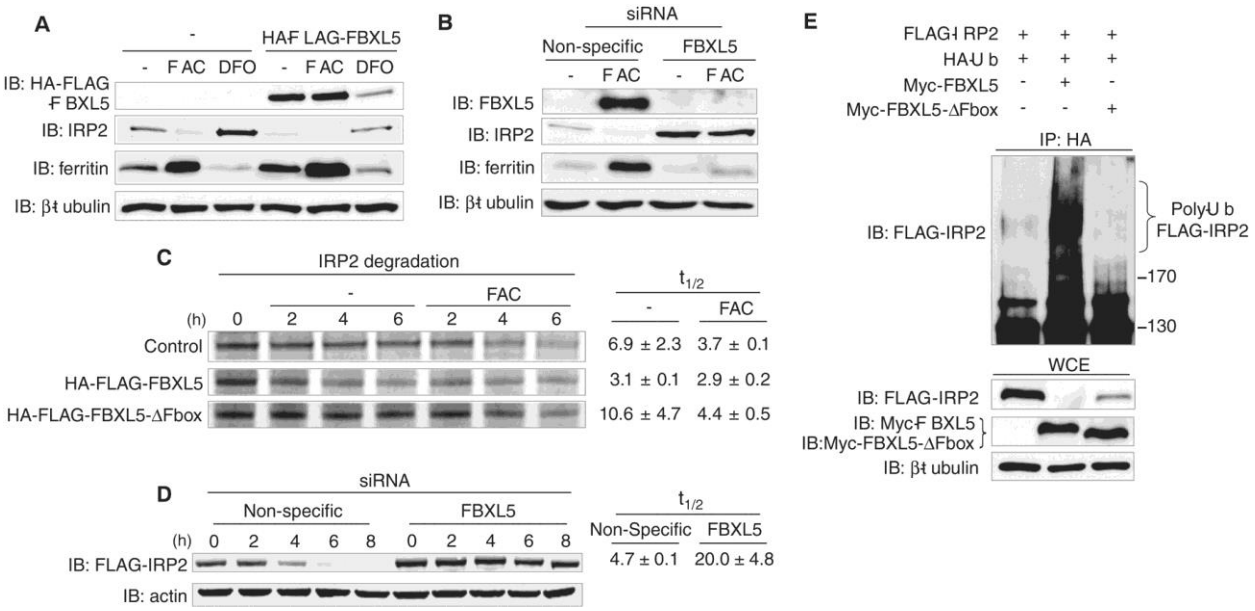

Figure 6. FBXL5 regulates IRP2 ubiquitination and iron-dependent degradation. (**A**) Flp-In TREx-293 cells stably expressing HA-FLAG-FBXL5 or control cells were treated for 8 hours with FAC or DFO. WCEs were probed with antibodies to FLAG, IRP2, ferritin, and β-tubulin. (**B**) HEK293 cells were transfected with nonspecific or FBXL5 siRNAs and then treated with or without FAC for 8 hours. WCEs were immunoblotted with the specified antibodies. (**C**) Flp-In TREx-293 cells stably expressing HA-FLAG-FBXL5 or HA-FLAG-FBXL5-ΔF-box or control cells were pulsed with ^{35}S-met/cys for 1 hour and then chased in medium supplemented with or without additional FAC. ^{35}S-labeled endogenous IRP2 was immunoprecipitated with antibody to IRP2 and half-lives (t 1/2) are shown as average ± SD (*n* = 2 independent experiments). (**D**) Flp-In TREx-293 cells stably expressing FLAG-IRP2 were treated with nonspecific or FBXL5 siRNAs, pulsed with doxycycline overnight so as to induce FLAG-IRP2 expression, and then chased in medium supplemented with FAC. WCEs were probed with antibodies to FLAG and actin. FLAG-IRP2 half-lives (t 1/2) are shown as average ± SEM (*n* = 3 independent experiments). (**E**) HEK293 cells were cotransfected with HA-Ub, FLAG-IRP2 and Myc-FBXL5, Myc-FBXL5-ΔF-box, or empty vector and then treated with FAC and MG132 for 4 hours and ubiquitin conjugates immunoprecipitated by using antibodies to HA. HA-immunoprecipitates (IP: HA) and WCEs were immunoblotted with antibodies to FLAG, c-Myc, and β-tubulin.

To determine whether FBXL5 regulates IRP2 iron-dependent degradation, pulse-chase experiments were performed in order to measure the half-life of endogenous IRP2 in control HEK293 cells or cells expressing HA-FLAG-FBXL5 or HA-FLAG-FBXL5-ΔF-box with or without FAC. Expression of HA-FLAG-FBXL5 reduced the half-life of IRP2 in both untreated

and FAC-treated cells, whereas expression of HA-FLAG-FBXL5-ΔF-box increased IRP2 half-life (Figure 6C). Depletion of FBXL5 by siRNA inhibited FLAG-IRP2 degradation as compared with that of cells treated with nonspecific siRNA (Figure 6D). FBXL5 depletion also prevented the iron-dependent degradation of FLAG-IRP1-C3S (Figure 13).

To determine whether FBXL5 catalyzes IRP2 ubiquitination, we analyzed the abundance of IRP2-ubiquitin conjugates after FBXL5 overexpression. FLAG-IRP2, HA-ubiquitin (HA-Ub), and Myc-FBXL5 or Myc-FBXL5-ΔF-box were coexpressed in HEK293 cells, and Ub-conjugates were immunoprecipitated under denaturing conditions by use of antibodies to HA. Overexpression of Myc-FBXL5, but not Myc-FBXL5-ΔF-box, increased FLAG-IRP2 poly-ubiquitination (Figure 6E). Similarly, Myc-FBXL5, but not Myc-FBXL5-ΔF-box, increased the ubiquitination of FLAG-IRP1 and FLAG-IRP1-C3S (Figure 14).

Our data suggest that FBXL5 protein stability may be iron-regulated (Figure 5C and Figure 7A and B). We hypothesized that oxygen levels may also affect FBXL5 stability because IRP2 is stabilized during hypoxia[97,103]. We tested these hypotheses by analyzing endogenous FBXL5 levels in cells treated with FAC, DFO, or hypoxia (1% O2). FBXL5 levels increased with FAC and decreased with DFO and hypoxia (Figure 7A). Reduction of FBXL5 protein by DFO or hypoxia was blocked by treatment with the proteasome inhibitor MG132, suggesting that FBXL5 is targeted for proteasomal degradation under these conditions (Figure 7B). Pulse-chase experiments at 21% O2 showed that FBXL5 half-lives were increased with FAC treatment (5.8 hours) and decreased by DFO (2.5 hours) as compared with that of untreated cells (4.3 hours) (Figure 7C). The half-life of HA-FLAG-FBXL5 was also decreased in untreated cells exposed to 1% O2 (Figure 7C). Thus, FBXL5 stability is dependent on cellular iron and oxygen concentrations.

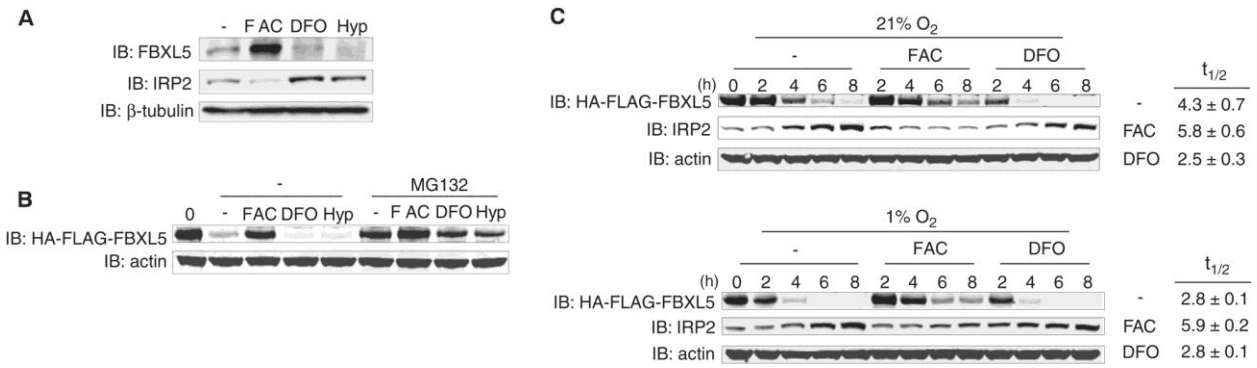

Figure 7. Hypoxia and iron depletion promote the proteasomal degradation of FBXL5. (**A**) Flp-In TREx-293 control cells were treated with FAC, DFO, or 1% O_2 (Hyp) for 8 hours. WCEs were immunoblotted with antibodies to FBXL5, IRP2, and β-tubulin. (**B** and **C**) Flp-In TREx-293 cells stably expressing HA-FLAG-FBXL5 were treated overnight with doxycycline so as to induce HA-FLAG-FBXL5 expression and then chased in control medium (–) in 21% O_2 or 1% O_2 (hypoxia) or in medium supplemented with FAC or DFO. (B) Cells were supplemented with or without MG132 for 6 hours. WCEs were immunoblotted with antibodies to FLAG and actin. (C) WCEs were immunoblotted with antibodies to FLAG, IRP2, and actin. HA-FLAG-FBXL5 half-lives (t 1/2) are shown as average ± SEM (*n* = 3 independent experiments).

We next examined the role of the putative hemerythrin-like binding domain (PFAM01814) in regulating FBXL5 stability and function. Hemerythrins are oxygen carriers that bind to oxygen through a diiron metal center[104]. The hemerythrin-like domain of FBXL5 could therefore function as a cellular iron and oxygen "sensor" by directly binding iron and oxygen. The protein-threading algorithm HHpred[105] revealed that the FBXL5 N terminus is structurally homologous to other hemerythrin family members, with the highest-scoring hit (P = 1.6 × 10–17) belonging to a hemerythrin-like domain protein from Neisseria meningitides (Uniprot, Q9JYL1) (Figure 15). Inductively coupled plasma mass spectrometry (ICP-MS) analysis showed that iron copurified with a recombinant fragment of FBXL5 (FBXL5-N199), which encompasses the hemerythrin-like domain, but not buffer alone or His-Smt3p, an unrelated control protein (Figure 8A). Thus, the N terminus of FBXL5 can function as a hemerythrin domain to coordinate iron and oxygen binding.

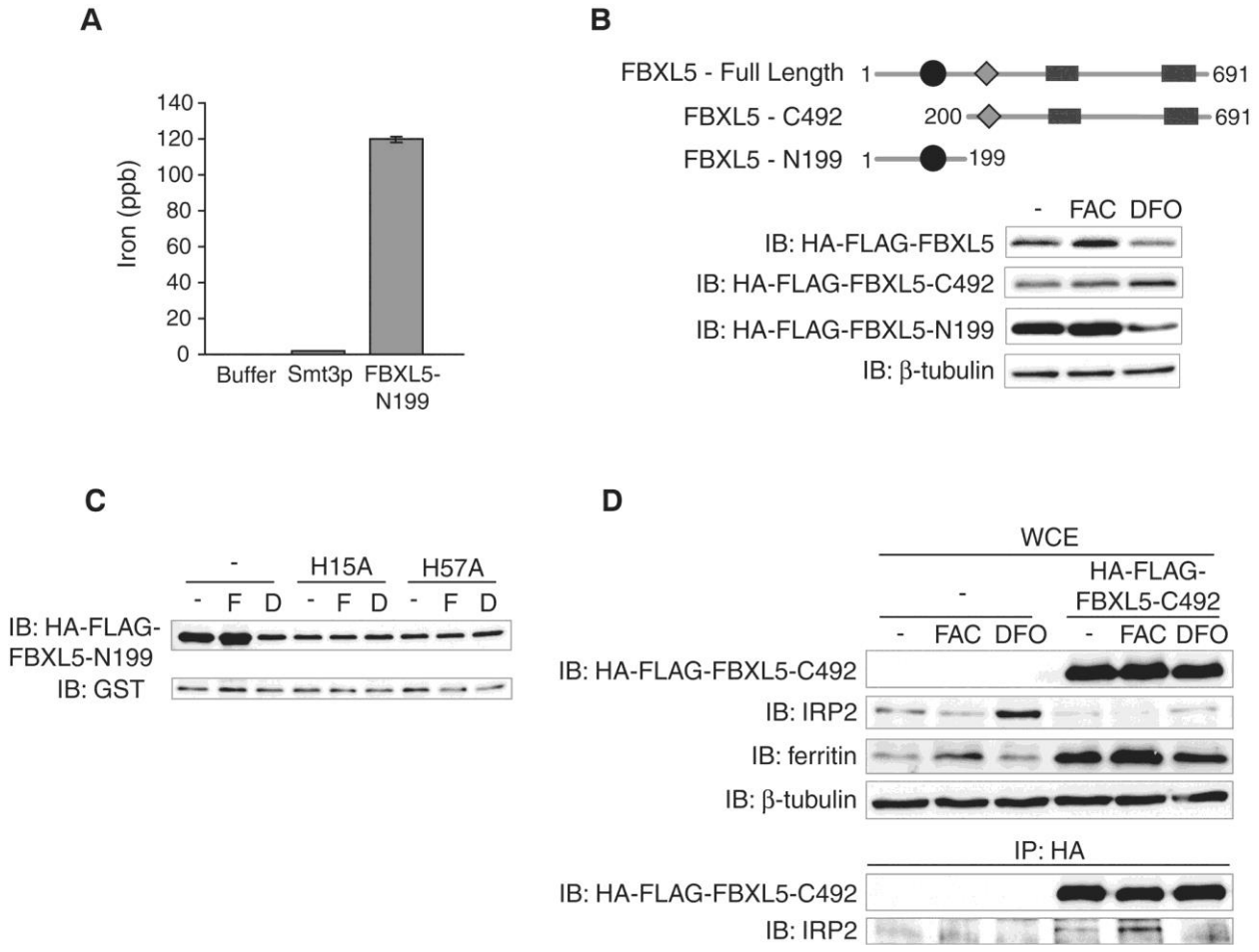

Figure 8. FBXL5 stability is regulated by an iron-binding hemerythrin-like domain. (**A**) An N-terminal fragment of FBXL5 encompassing amino acids 1 to 199 (FBXL5-N199) or Smt3p (negative control) was expressed in *Escherichia coli*, and the amount of copurifying iron was measured by means of ICP-MS. (**B**) HEK293 cells were transfected with HA-FLAG-FBXL5, HA-FLAG-FBXL5-N199, or HA-FLAG-FBXL5-C492 (amino acids 200 to 691) and treated with FAC or DFO for 8 hours. WCEs were immunoblotted with antibodies to FLAG or β-tubulin. (**C**) HEK293 cells were cotransfected with HA-FLAG-FBXL5-N199, HA-FLAG-FBXL5-N199-H15A, or HA-FLAG-FBXL5-N199-H57A, and a plasmid expressing glutathione *S*-transferase (GST) as a marker for transfection efficiency, and treated with FAC (F) or DFO (D) for 8 hours. WCEs were immunoblotted with antibodies to FLAG and GST. (**D**) Flp-In TREx-293 cells stably expressing HA-FLAG-FBXL5-C492 or control cells were treated for 8 hours with FAC or DFO. HA-FLAG-FBXL5-C492 was immunoprecipitated by use of antibodies to HA. WCEs and IPs were probed with antibodies to FLAG, IRP2, ferritin, and β-tubulin.

Based on the FBXL5 domain structure, we hypothesized that the C-terminal 492 amino acids of FBXL5 (FBXL5-C492) containing both the F-box domain and the leucine-rich repeats

function in substrate recognition and ubiquitin conjugation, whereas the N-terminal 199 amino acids regulate FBXL5 stability. We expressed the HA-FLAG-FBXL5-N199 and -C492 fragments in HEK293 cells and analyzed their abundance after FAC and DFO treatments (Figure 8B). HA-FLAG-FBXL5 and HA-FLAG-FBXL5-N199 protein levels were iron-dependent, whereas HA-FLAG-FBXL5-C492 abundance was not iron-regulated. We also found that the mutation of two putative iron-binding residues in the hemerythrin-like domain, H15A and H57A, reduced the abundance and iron-dependent stability of FBXL5 as compared with the wild-type protein (Figure 8C). Collectively, these data indicate the hemerythrin-like domain regulates FBXL5 stability through iron-coordination.

Because FBXL5-C492 is stable in iron-depleted cells but retains the ability to interact with IRP2, we used this C-terminal fragment to determine whether iron regulates the FBXL5-IRP2 interaction beyond controlling FBXL5 stability. Expression of HA-FLAG-FBXL5-C492 in HEK293 cells reduced endogenous IRP2 levels, indicating that this C-terminal fragment can promote IRP2 degradation (Figure 8D). IRP2 levels in the HA-FLAG-FBXL5-C492–expressing cells remain partially iron-regulated (stabilized in DFO compared FAC), suggesting that intracellular iron concentrations are still capable of influencing this pathway. Moreover, HA-FLAG-FBXL5-C492 associates with IRP2 more strongly in FAC-treated cells as compared with DFO-treated cells (Figure 8D). Thus, an iron-dependent mechanism promotes the physical association of FBXL5 with IRP2. By analogy to other F-box proteins in which substrate binding is dependent upon the posttranslational modification of the target, these data could be explained by an iron-regulated modification on IRP2 that stimulates its association with FBXL5.

Our study demonstrates that IRP2 protein levels are controlled by an iron-regulated SKP1-CUL1-FBXL5 complex (Figure 16). In the presence of iron and oxygen, the FBXL5

hemerythrin-like domain binds iron, resulting in the stabilization of a SKP1-CUL1-FBXL5 complex that catalyzes IRP2 ubiquitination and proteasomal degradation. Conversely, loss of iron and/or oxygen binding by the hemerythrin-like domain renders FBXL5 susceptible to proteasomal degradation. These studies identify an iron sensor that functions as a key regulator of iron homeostasis in eukaryotes.

Supplementary Figures and Tables

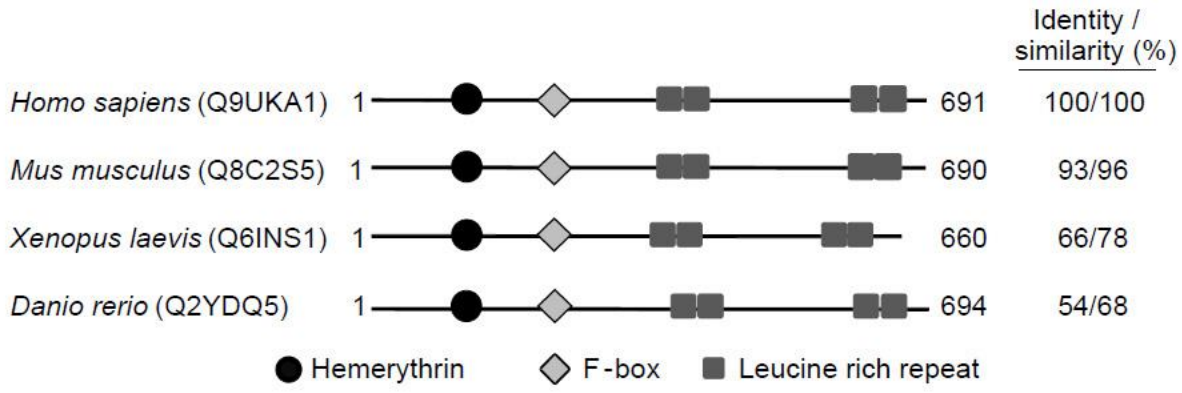

Figure 9. Domain Organization of FBXL5. The primary sequence and domain organization of FBXL5 is strongly conserved among higher eukaryotes and consists of a N-terminal hemerythrin-like domain, a F-box domain, and four C-terminal leucine-rich repeats.

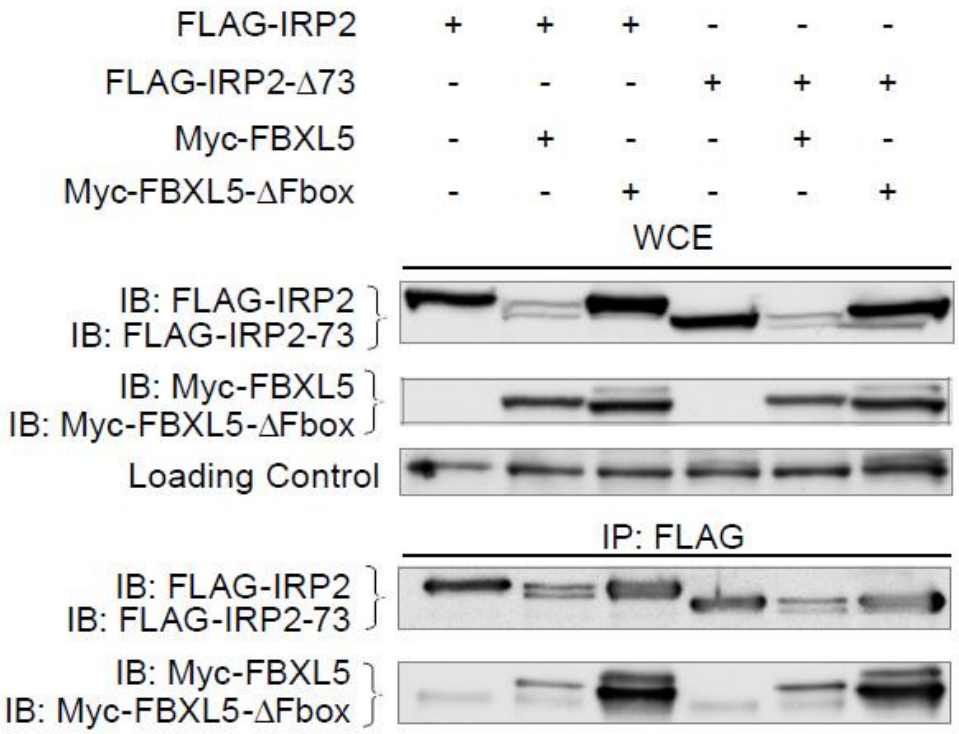

Figure 10. The unique 73-amino acid region of IRP2 is not required for interaction with FBXL5. HEK293 cells were co-transfected with plasmids expressing FLAG-IRP2 or FLAG-IRP2-Δ73 along with Myc-FBXL5, Myc-FBXL5-ΔFbox, or control plasmids. Immunoprecipitations were performed with FLAG antibody. Whole cell extracts (WCE) and immunoprecipitates (IP) were immunoblotted with FLAG and c-Myc antibodies.

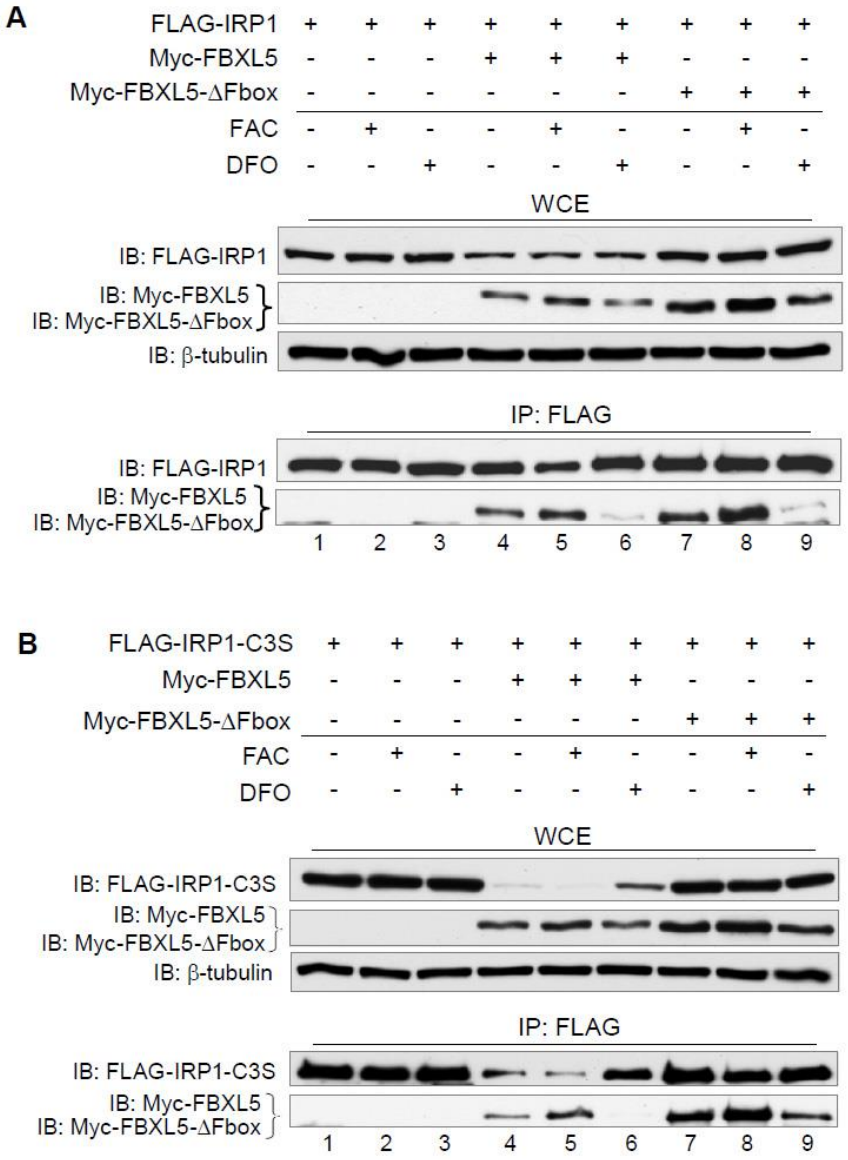

Figure 11. The interaction of IRP1 and IRP1-C3S with FBXL5 is iron-regulated. HEK293 cells were co-transfected with FLAG-IRP1 (A) or FLAG-IRP1-C3S (B) and either Myc-FBXL5, Myc-FBXL5-ΔFbox, or a control plasmid. Transfected cells were treated with 100 μg/mL FAC or 100 μM DFO for 8 hours before harvesting. FLAG antibodies were used to immunoprecipitate FLAG-IRP1 or FLAG-IRP1-C3S. Whole cell extracts (WCE) and immunoprecipitates (IP) were immunoblotted with FLAG, c-Myc, and β-tubulin antibodies.

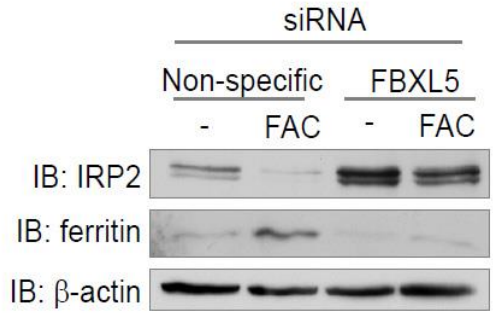

Figure 12. FBXL5 depletion in IMR90 human diploid fibroblasts leads to IRP2 stabilization. IMR90 human diploid fibroblasts were transfected with non-specific or FBXL5 siRNAs and then treated with or without FAC for 8 hours. Whole cell extracts were immunoblotted with IRP2, ferritin, and β-actin antibodies.

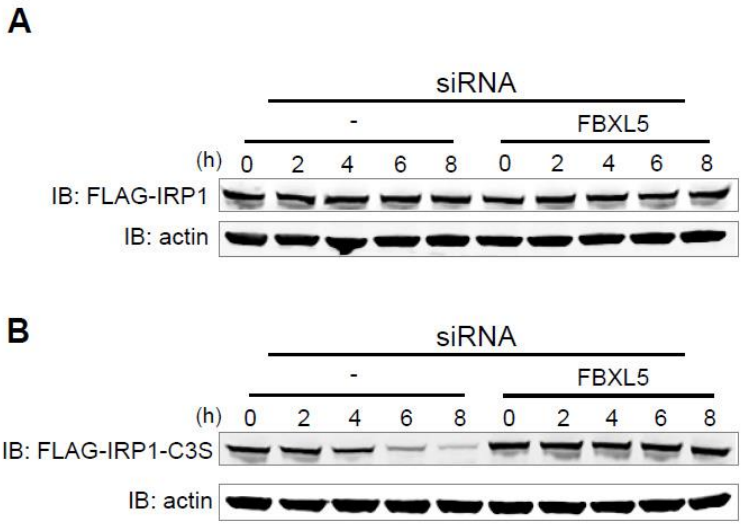

Figure 13. FBXL5 depletion stabilizes an IRP1-3CS mutant. Flp-In TREx-293 cells stably expressing FLAG-IRP1 (A) or FLAG-IRP1-C3S (B) were treated without (-) or with FBXL5 siRNA and then doxycycline overnight. Cells were washed and chased in medium supplemented with 100 μg/mL FAC for the indicated times. Whole cell extracts were immunoblotted with FLAG and actin antibodies.

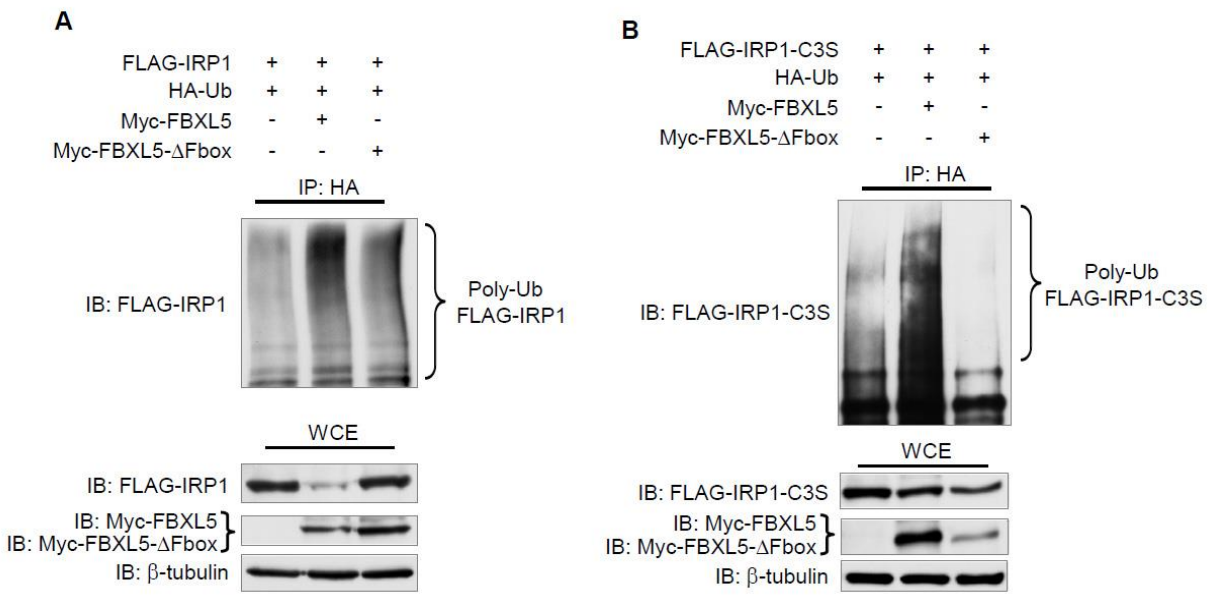

Figure 14. FBXL5 but not FBXL5-ΔFbox overexpression stimulates the ubiquitination of IRP1 and IRP1-C3S. FLAG-IRP1 (A) or FLAG-IRP1-C3S (B) were co-transfected into HEK293 cells with HA-ubiquitin and either Myc-FBXL5, Myc-FBXL5-ΔFbox, or a control plasmid. Transfections were harvested 24 hours later with 100 μg/mL FAC and 25 μM MG132 being added to the media for the final 4 hours. Denaturing immunoprecipitations using HA antibodies were used to purify ubiquitin conjugates that were then probed with FLAG antibodies to detect ubiquitinated forms of FLAG-IRP1 and FLAG-IRP1-C3S. Whole cell extracts (WCE) were immunoblotted with FLAG, c-Myc, and β-tubulin antibodies.

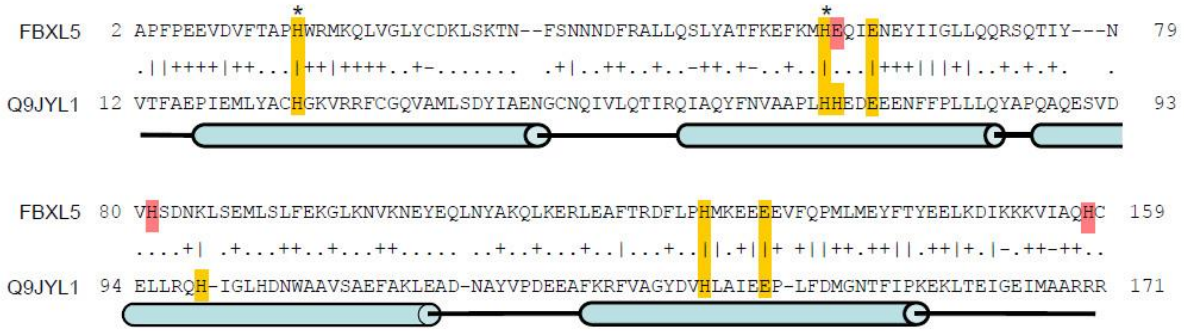

Figure 15. Structural Alignment of the hemerythrin-like domains of FBXL5 and Q9JYL1. Conserved and potential metal-binding residues are in yellow and red, respectively. Predicted FBXL5 helices are in blue; asterisks indicate mutated amino acids.

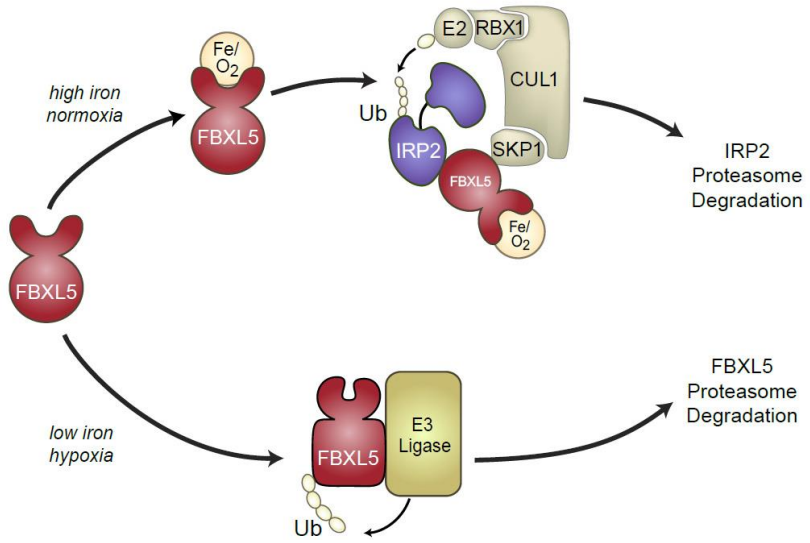

Figure 16. Model for the regulation of FBXL5 and IRP2 by iron and oxygen. When cellular iron and oxygen levels are high, the hemerythrin-like domain of FBXL5 binds iron and oxygen resulting in increased FBXL5 stability. Stabilized FBXL5 associates with SKP1 and CUL1 and catalyzes the ubiquitination and subsequent proteasomal degradation of IRP2. In low iron or hypoxic conditions, FBXL5 is destabilized and targeted for ubiquitin-dependent degradation by proteolytic pathways.

Table 1. Proteomic Identification of FBXL5 and IRP2-associated Factors.

Protein (Acc. Number)	MW (Da)	# Peptides	# Spectra	% Coverage
His-FLAG-FBXL5-ΔFbox				
FBXL5 (Q9UKA1)	78,555	12	384	16.4
IRP1 (P21399)	98,399	5	39	6.1
IRP2 (P48200)	105,012	16	156	11.7
FLAG-IRP2				
IRP2 (P48200)	105,012	135	4691	75.6
FBXL5 (Q9UKA1)	78,555	15	29	23.3
SKP1 (P63208)	18,658	5	39	6.1
CUL1 (Q13616)	89,679	10	11	16.1

The number of unique peptides, number of spectra (reflecting the fact that some peptides are identified more than once in an analysis), and % sequence coverage for each protein are indicated.

Materials and Methods

Plasmids

The full length FBXL5 cDNA (NIH_MGC_97) was obtained from Open Biosystems. The cDNA was amplified using the Advantage-HF2 polymerase (Clontech) and introduced into the pCR8/GW/TOPO vector (Invitrogen). The Quikchange system (Stratagene) was used to generate the FBXL5-ΔFbox mutant lacking amino acids 216-240 using pCR8-FBXL5 as a template. FBXL5 and FBXL5-ΔFbox were subcloned into pcDNA3-6xMyc and pcDNA5-FRT/TO-3xHA-3xFLAG plasmids using pCR8-FBXL5 and DEST plasmids via the Gateway cloning system (Invitrogen). FBXL5-N199 and FBXL5-C492 fragments were generated by PCR using primers containing flanking AttB1 and AttB2 sites and cloned into pDONR221 (Invitrogen). FBXL5-N199-H15A and FBXL5-N199-H57A were generated using the Quickchange system (Stratagene). These fragments were then subcloned into pcDNA5-FRT/TO-3xHA-3xFLAG or pET53-DEST (Novagen) for expression in HEK293 and *E. coli*, respectively. Plasmids expressing 2xFLAG-IRP1, 2xFLAG-IRP1-C3S, 2xFLAG-IRP2, 2xFLAG-IRP2Δ73, HA-Ub, Myc-CUL1, Myc-SKP1, and His_6-Smt3p were previously described[106,107].

Antibodies

Antibodies against human FBXL5 were generated by Swedish Human Proteome Resource as described[108]. Other antibodies used for immunoblotting were as follows: IRP2-7H6 (Santa Cruz Biotechnology), IRP2[92], IRP1[109], FLAG-M2 (Sigma), Myc-9E10 (Covance), HA-HA.11 (Covance), ferritin (Sigma), actin (Calbiochem), β-tubulin (Sigma), and GST (Cell Signaling). Horseradish peroxidase conjugated secondary antibodies were obtained from Jackson

Immunoresearch Laboratories. For quantification of protein half-lives, an immunofluorescent anti-mouse secondary antibody (Rockland) was used. Immunoprecipitation reactions were performed using affinity matrices for anti-FLAG M2, anti-c-Myc, and anti-HA available from Sigma.

Cell Lines

The HEK293 and IMR90 cell lines were obtained from the American Type Culture Collection (ATCC) while Flp-In™ T-REx™-293 was obtained from Invitrogen. Flp-In™ TREx™-293 cells stably expressing 2xFLAG-IRP2, 2xFLAG-IRP1, and 2xFLAGIRP1-C3S were previously described[107]. Flp-In™ T-REx™-293 cells stably expressing 3xHA-3xFLAG-FBXL5, 3xHA-3xFLAG-FBXL5-ΔFbox, 3xHA-3xFLAGFBXL5-N199, and 3xHA-3xFLAG-FBXL5-C492 were generated using the Flp-In system (Invitrogen) according to the manufacturer's directions.

Cell Culture, Plasmid Transfections, and Treatments

Cell culture reagents were obtained from Invitrogen. All cell lines were cultured in complete Dulbecco's Modified Eagles medium (DMEM) containing 10% heat inactivated fetal bovine serum (FBS), 100 units/mL penicillin and streptomycin, and 2 mM glutamine at 37°C in ambient air with 5% CO_2. Hypoxia experiments were performed at 37°C using a Modular Incubator Chamber (Billups-Rothenberg, Inc.) flushed with 1% O_2, 5% CO_2, and balanced N_2 gas and incubated at 37°C. Transient transfections were performed using either BioT (Bioland, Long Beach, CA) according to the manafacturer's protocol or linear PEI as described (*S6*). siRNA transfections were performed according to the manufacturer's protocol (Thermo Fisher)

using Dharmafect I and siGENOME SMARTpool reagents for FBXL5 (Dharmacon #M-012424-01) or a non-targeting siGENOME control siRNA (Dharmacon #D-001210-03-05). Expression of 3xHA-3xFLAG-FBXL5 and 2xFLAG-IRP2 in stable cell lines was induced by treating cells with doxycyline for 24 hours or the times indicated at a final concentration of 100 ng/mL for protein half-life determination experiments and 500 ng/mL for all other experiments. Cells were treated with 100 μg/ml ferric ammonium citrate (FAC) (Thermo Fisher), 100 μM desferrioxamine mesylate (DFO) (Sigma), and/or or 25 μM MG132 (Z-Leu-Leu-Leu-CHO) (BIOMOL) for the times indicated.

Affinity purification of FBXL5-ΔFbox and IRP2-containing Protein Complexes

Twenty-five 15 cm tissue cultures plates each of Flp-In™ TREx™-293 cells stably expressing His_6-3xFLAG-FBXL5-ΔFbox or 2xFLAG-IRP2 were grown, harvested, and lysed in IP buffer (100 mM Tris-HCl pH 8.0, 150 mM NaCl, 5 mM EDTA, 5% glycerol, 0.1% NP-40, 1 mM DTT, 0.5 mM PMSF, 1 μM pepstatin, 1 μM leupeptin and 2 μg/mL aprotinin). 200-300 mg of clarified protein lysate was then incubated at 4°C with 100 μL of equilibrated anti-FLAG M2 agarose (Sigma) for 2 hours. Beads were then washed four times using 1 mL of IP Buffer per wash before eluting with 500 μL of FLAG Elution Buffer (IP buffer lacking NP-40 and supplemented with 250 μg/mL of 3xFLAG peptide (Sigma)). Elutions were precipitated by the addition of trichloroacetic acid (TCA) to a final concentration of 10% followed by incubation on ice for 30 minutes and centrifugation at 16,000g for 10 minutes to collect the precipitate.

Proteomic Characterization of FBXL5 and IRP2 purifications

TCA precipitates from affinity-purified His_6-3xFLAG-FBXL5-ΔFbox and 2x-FLAGIRP2 samples were digested and prepared for proteomic analysis as described[110]. The digested samples were analyzed by MudPIT[50,51]. A 5-step multidimensional chromatographic separation was performed online and fractionated peptides were eluted directly into a LTQ-Orbitrap mass spectrometer (Thermo Fisher) in which tandem mass spectra were collected. Peptide mass spectra were analyzed using the SEQUEST and DTASelect algorithms[52,53]. A decoy database approach was used to estimate peptide and protein level false positive rates which were less than 5% per analysis[111]. Proteins were considered candidate FBXL5 and IRP2 interacting proteins if they were identified in the relevant affinity purification but not in MudPIT analyses of other control purifications. A detailed description of the multidimensional peptide fractionation protocol, mass spectrometer settings, and bioinformatic workflow is described elsewhere[112].

Immunoprecipitation and Immunoblotting

Cell lysates were prepared using IP buffer. Immunoprecipitations were performed using the appropriate affinity matrix equilibrated with IP Buffer and incubated with equal amounts of cell lysates at 4°C for 2 hours. Beads were washed three times with lysis buffer and resuspended in 2x SDS loading buffer. For immunoblotting, whole cell lysates and immunoprecipitates were boiled in SDS-loading buffer, separated using SDS-PAGE, transferred to Immobilon-P PVDF membranes (Millipore), and probed with the appropriate primary and secondary antibodies. Proteins were visualized using Pierce ECL western blotting substrate (Thermo Fisher).

Ubiquitination assay

HEK293 cells were transfected with plasmids expressing HA-Ubiquitin, a 2xFLAG IRP construct (2xFLAG-IRP2, 2x-FLAG-IRP1, or 2x-FLAG-IRP1-C3S), and either 6xMyc-FBXL5, 6xMyc-FBXL5-ΔFbox, or a vector control. Twenty-four hours after transfection, the medium was changed and cells were treated with 100μg/ml FAC and 25 μM MG132 for 4 hours. Cells were harvested and lysed under denaturing conditions as described previously[113]. Ubiquitin conjugates were purified using anti-HA beads and the presence of IRP1 or IRP2 in the purified ubiquitin conjugates was detected by immunoblotting with FLAG M2 antibody.

Pulse – Chase Experiments

For endogenous IRP2 degradation analysis, Flp-In™ TREx™-293 cells stably expressing 3xHA-3xFLAG-FBXL5 or 3xHA-3xFLAG-FBXL5-ΔFbox were treated overnight with doxycycline in complete medium. Cells were then incubated in DMEM lacking methionine and cysteine for 30 minutes prior to a one hour pulse with 100 μCi/ml (3.7 MBq/ml) TRAN^{35}S-LABEL™ (ICN Pharmaceuticals). Cells were washed three times and chased in complete medium supplemented with or without 100 μg/ml FAC for the indicated times. Cells were harvested in Triton Buffer (1% Triton, 150 mM NaCl, 50 mM Tris pH 8.0) and lysates cleared. 200-300 μg of cell extract was immunoprecipitated using IRP2 antibody and Protein A agarose (Invitrogen). Beads were washed three times with Triton Buffer and twice with PBS prior to protein elution by boiling samples in LDS sample buffer (Invitrogen). Proteins were separated on a 4-12% Bis-Tris gel (Invitrogen) using MOPS buffer (Invitrogen) and transferred to nitrocellulose prior to PhosphorImager exposure (Molecular Dynamics, Inc.). Band quantification was performed using a local average background correction with ImageQuaNT 5.0

software (Molecular Dynamics, Inc.). For 2xFLAG-IRP2 degradation analysis with FBXL5 siRNA, Flp-In™ T-REx™-293 cells stably expressing 2xFLAG-IRP2 (3.5×10^5) were plated on a 35 mM dish one day prior to transfection. Cells were transfected with 200 pmol FBXL5 siRNA and 4 µl DharmaFECT1 for 36 hours and then treated with doxycycline overnight. The medium was removed and the plates were washed once with PBS, once with complete medium, and then chased in complete medium supplemented with FAC. For FBXL5 degradation analysis, Flp-In™ T-REx™-293 cells stably expressing 3xHA-3xFLAG-FBXL5 were treated overnight with doxycycline. The medium was removed and the cells were washed as described above, and then chased in complete medium supplemented with or without FAC or DFO in normoxia or hypoxia. Cells were harvested in Triton Buffer, lysates cleared, and proteins separated on a 4-12% Bis-Tris gel using MOPS Buffer. After transferring proteins to nitrocellulose, immunoblotting was performed using FLAGM2 and immunofluorescent secondary antibodies. Band quantification was performed using a local average background correction on an Odyssey (LI-COR) infrared imaging system.

Purification of Recombinant His_6-FBXL5-N199

One liter each of BL21(DE3) cells carrying either pET53-His_6-FBXL5-N199 or pET21-SMT3 was grown at 30°C to OD_{600} ~ 0.5, treated with 1 mM IPTG, and incubated at 30°C for three additional hours. Cells were harvested, resuspended in Nickel Buffer A (50 mM Tris-HCl, pH 8.0, 200 mM KCl, 10% glycerol, 10 mM imidazole), lysed by sonication, and centrifuged at 27,000g for 20 minutes to clarify the lysate. Each lysate was incubated in batch with 0.5 mL of Ni-NTA agarose beads at 4°C for one hour, washed extensively with Nicked Buffer A, and then eluted with Nickel Buffer B (Nickel Buffer A supplemented with 500 mM imidazole). The

eluates were dialyzed exhaustively against Nickel Buffer A lacking imidazole, snap-frozen in liquid N_2, and stored at -80°C.

Inductively-coupled Plasma Mass Spectrometry (ICP-MS)

Aliquots of buffer only, His_6-Smt3p, and His_6-FBXL5-N199 were mixed with an equal volume of concentrated OPTIMA grade nitric acid (Thermo Fisher) followed by digestion at 95 °C for two hours in open vessels in a dust-free environment. The dried contents of the tubes were then extracted with 500 µL of 2% OPTIMA grade nitric acid. The individual extracts were diluted to a total volume of 2 mL with 2% nitric acid. 20 µL of a 5 ppm aqueous scandium ion solution (ICP-MS grade) was then added to each tube as an internal standard and the contents vortexed vigorously. ICP measurements were then conducted on an Agilent 7500 Series ICP-MS in both He and H_2 collision gas modes. Reported measurements of Fe in each sample represent the average of 3 measurements. The individual measurements are typically obtained with a relative standard deviation of approximately 3% or less per sample.

Chapter 3: Early Characterization of FBXL5 and its interaction with SPAK

SPAK as a substrate of FBXL5

After establishing the role of FBXL5 in the degradation of iron-regulatory proteins IRP1 and IRP2, our lab sought to characterize the functional relationships between FBXL5 and the other binding partners (Table 2). We used an HEK293 stable cell line expressing epitope-tagged FBXL5-ΔFbox and immunopurified FBXL5-ΔFbox protein complexes. When these complexes were analyzed by shotgun proteomics, we were able to infer potential FBXL5 binding partners. Peptide count signifies the number of unique peptides from the originating protein that were detected, while spectral count signifies the number of spectra in which peptides from the protein were detected. SPAK is one of the binding partners identified by this strategy, and my earliest work concerns the physical interaction between FBXL5 and the osmotic stress regulatory kinase SPAK. WNK1 is the upstream kinase involved in SPAK activation and was also identified as an FBXL5-associated protein. Due to the preferential binding of SPAK and WNK1 to a substrate-trapping mutant of FBXL5 lacking the F-box domain, FBXL5-ΔFbox, we initially believed that one of these proteins was a possible degradation target.

Table 2. Identification of osmotic stress regulatory proteins in the proteomic analysis of FBXL5-ΔFbox.

Protein (Acc. #)	MW (Da)	Peptide Count	Spectral Count	Sequence Coverage
FXBL5 (Q9UKA1)	76,590	35	301	40.8%
SPAK (Q9UEW8)	59,474	5	8	10.4%
WNK1 (Q9H4A3)	250,794	3	6	1.6%
OSR1 (O95747)	58,022	2	2	4%

We used biochemical approaches to validate the potential interactions identified by mass spectrometry. We transiently transfected Myc-tagged FBXL5 and FBXL5-ΔFbox along with 3HA-FLAG-tagged SPAK into HEK293 cells to detect the interaction using immunoprecipitation with anti-HA beads. The immunoprecipitated proteins were then identified using SDS-PAGE and Western blot analysis against the Myc-tagged FBXL5 variants.

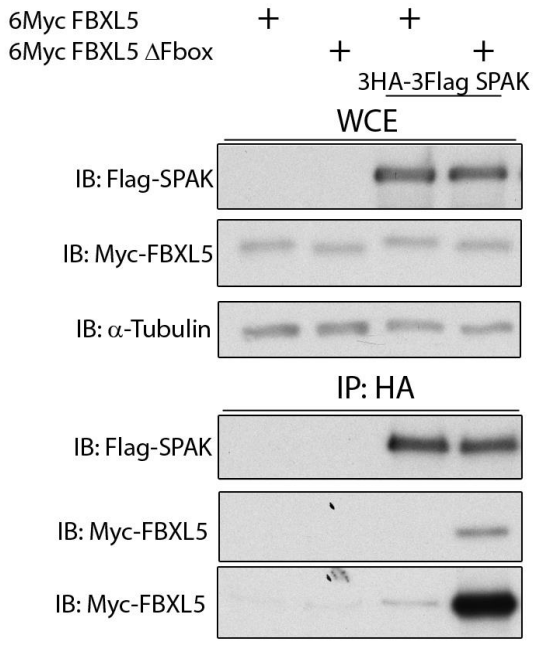

Figure 17. SPAK interaction with FBXL5 and FBXL5-ΔFbox. HEK293 cells were transiently transfected with 3HA-3FLAG SPAK and either 6Myc-tagged FBXL5 WT or FBXL5-ΔFbox. Lysates were immunoprecipitated with FLAG affinity beads to pull down FLAG-SPAK and Western blotting used to determine whether FBXL5 co-purified with SPAK. Whole-cell extracts (WCEs) and immunoprecipitates (IPs) were immunoblotted with antibodies to FLAG, c-Myc and β-Tubulin.

SPAK is able to interact strongly with FBXL5-ΔFbox, but the interaction with FBXL5 wild type (WT) can only be observed with very long exposures (Figure 17). When this experiment is performed with WNK1, we observe only weak binding to FBXL5 and FBXL5-

ΔFbox; we believe this is indirect through their mutual association with SPAK. OSR1 shows preferential binding to FBXL5-ΔFbox over FBXL5, but the binding is much weaker than for SPAK when compared side-by-side (Figure 22).

In other F-box proteins that we have characterized, the ΔFbox mutant acts as a substrate trapping mutant that binds substrates but cannot ubiquitinate them since the interaction with the rest of the E3 ligase complex is lost. Based on the observation that FBXL5-ΔFbox binds preferentially to SPAK we initially believed that this indicated that SPAK was a likely substrate for FBXL5. To definitively establish this, we set out to meet three essential criteria for verifying that SPAK is a substrate of FBXL5: (#1) preferential binding of SPAK to FBXL5-ΔFbox (#2) stabilization of SPAK upon FBXL5 depletion, and (#3) poly-ubiquitination of SPAK in an FBXL5-dependent manner. The first criterion was met in Figure 17.

To examine criteria #2, we evalulated SPAK protein abundance in HeLa cells that had been depleted of FBXL5 using siRNA knockdown.

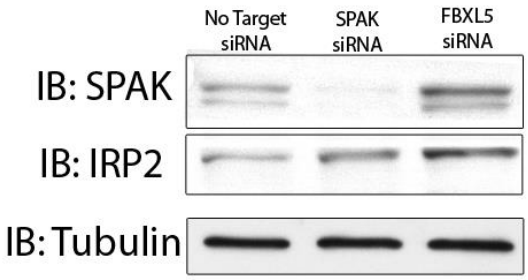

Figure 18. FBXL5 siRNA knockdown stabilizes endogenous SPAK levels. RNAiMAX siRNA transfection was used in Hela cells to knockdown SPAK or FBXL5. WCEs were blotted against with SPAK, IRP2 or β-tubulin antibodies.

FBXL5 siRNA knockdown was able to stabilize SPAK levels relative to the no target control (Figure 18, compare lanes 1 and 3). Endogenous IRP2 levels were also stabilized and are used as a positive control for FBXL5 knockdown in this experiment. Since both proteins behaved in the same fashion when FBXL5 was knocked down, we believe this evidence that SPAK is a substrate of FBXL5.

The last piece of evidence to show that FBXL5 targets SPAK for ubiquitination was to prove that FBXL5 can stimulate poly-ubiquitination of SPAK using either a cell-based or *in vitro* ubiquitination assay. We first performed cell-based ubiquitination assays to measure the amount of SPAK that associates with purified ubiquitin conjugates isolated from cells overexpressing either wild type or the ΔFbox version of FBXL5[113]. These results, however, were inconclusive. Next, we used an *in-vitro* based system to detect SPAK poly-ubiquitination. We employed a baculovirus expression system with *Spodoptera frugiperda* Sf9 cells in order to express and purify recombinant 6xHis-tagged SPAK for use in our *in-vitro* assay. FBXL5 protein was freshly immunopurified for the assay using anti-FLAG M2 agarose and left on the beads for the ubiquitination reaction. The FBXL5-bound beads were washed twice with FLAG buffer and twice with ubiquitination reaction buffer before recombinant 6His-SPAK, E1 enzyme, E2 enzyme and ATP were added for the reaction (30 min at 37^{O}C on Thermoshaker). Recombinant E1 and E2 enzymes were commercially purchased from Boston Biochem and the ATP was from Thermo Fisher.

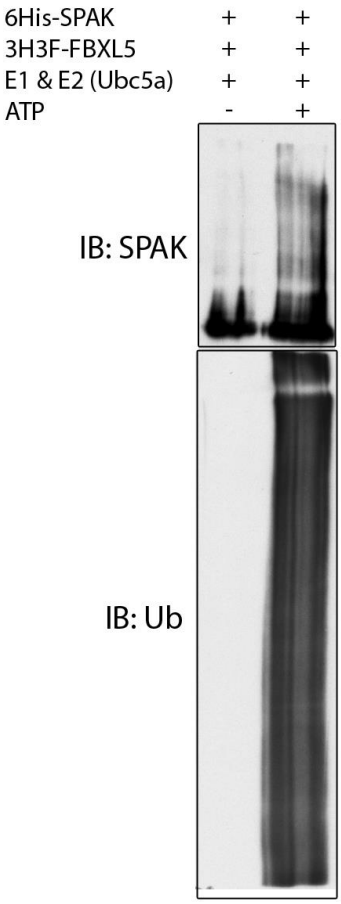

Figure 19. *In-vitro* poly-ubiquitination of SPAK by FBXL5. Recombinant 6His-SPAK, 3HA-3FLAG-FBXL5 bound to FLAG affinity beads and commercial E1, E2 enzymes were combined with or without ATP for 30 minutes at 37^{O}C on a Thermoshaker to perform an *in-vitro* ubiquitination reaction. The reaction products were Western blotted with primary antibodies against SPAK and ubiquitin.

As shown in Figure 19, we were able to detect ATP-dependent FBXL5 poly-ubiquitination activity on SPAK. The mixture is expected be clean of other ubiquitin ligases since only FLAG-bead bound FBXL5 should have been present in significant quantities.

Together, we believed that this data showed that SPAK was an FBXL5 substrate. The next step was to determine the biological significance of FBXL5 degradation of SPAK.

Interaction Domain Mapping of FBXL5 and SPAK

To further characterize the FBXL5-SPAK interaction, we conducted domain mapping experiments to identify the regions in both FBXL5 and SPAK that mediated their interaction. We reasoned that this data would help us establish the biological role of the interactions. For example, if SPAK mapped to the substrate-binding region of FBXL5 we would have additional evidence that SPAK is a target of FBXL5-mediated ubiquitination. To map the binding sites of the two proteins we examined binding between a series of FBXL5 and SPAK truncation constructs that systematically narrowed down the possible interaction region.

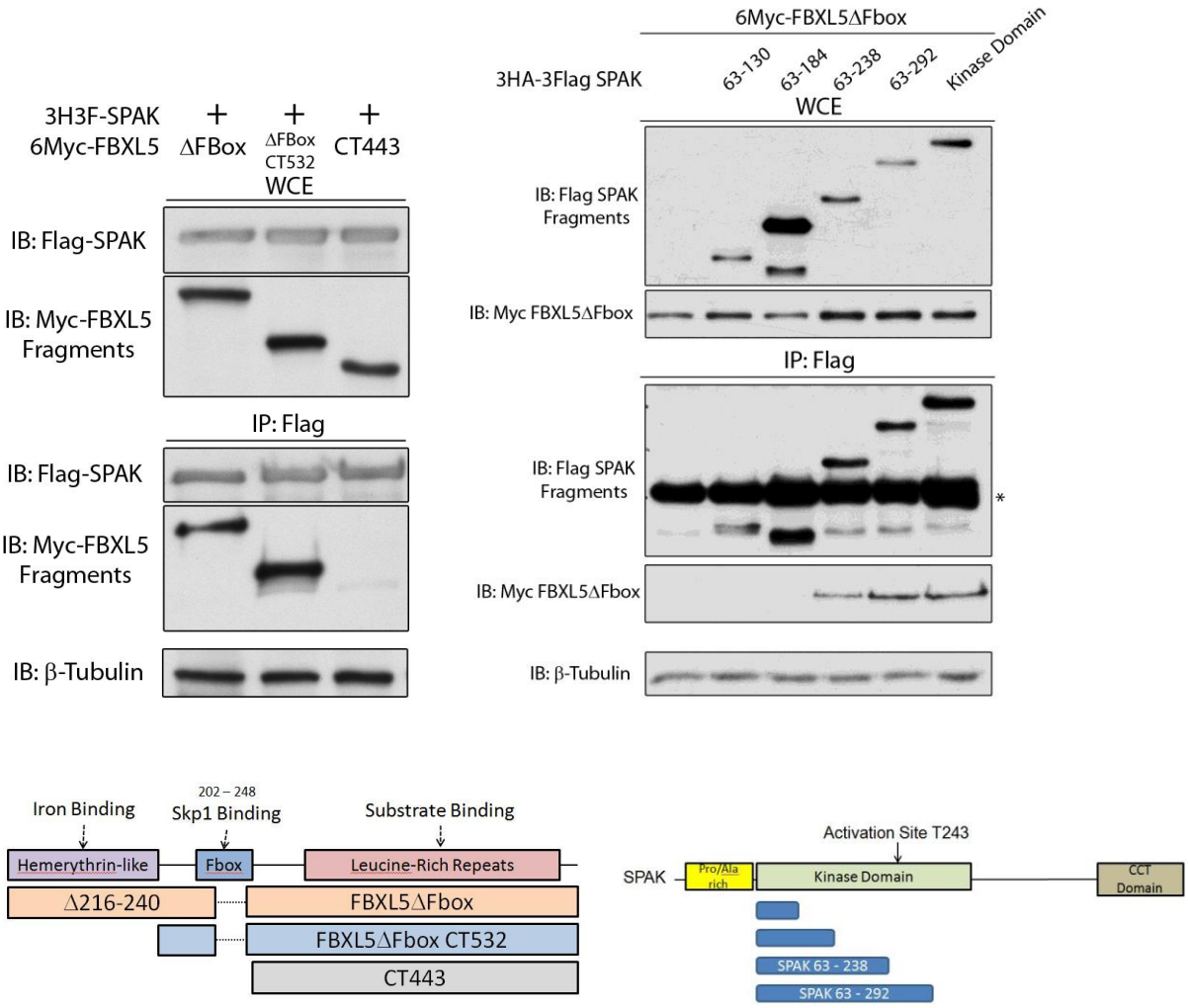

Figure 20. Mapping the SPAK-FBXL5 interaction regions. (**A**) 3HA-3FLAG SPAK was transiently transfected into HEK293 cells with 6Myc-tagged fragments of FBXL5. FLAG affinity purification was used against FLAG-SPAK. WCE and IP were blotted with FLAG and Myc primary antibodies. (**B**) 6Myc-tagged FBXL5-ΔFbox and 3HA-3FLAG tagged SPAK fragments were transiently transfected into HEK293 cells. FLAG purification was used to isolate the SPAK fragments and their binding partners. WCEs and IPs were blotted with FLAG, c-Myc antibodies and β-Tubulin.

SPAK binding to FBXL5 is observed until a critical region between the end of the N-terminal hemerythrin-like domain and the Fbox domain is removed (Figure 20A). FBXL5-ΔFbox-CT532 lacks both the hemerythin-like domain and most of the Fbox domain but retains

high SPAK binding. However, once the region between the two domains is removed in FBXL5-CT443 (which only contains the leucine-rich repeats used to bind substrates) binding is almost completely lost. This is important for two reasons: first, we were able to map the region that SPAK binds FBXL5 to an approximately 40 amino acid long stretch between the hemerythin-like domain and the -Fbox domain and second, since the SPAK interaction does not map to the substrate recognition motif (i.e. the leucine-rich repeats at the C-terminal end of FBXL5), it indicated that SPAK may not be a substrate of FBXL5 and instead the converse might be true (i.e. SPAK regulates FBXL5).

Similarly, we realized that the FBXL5 interaction with SPAK mapped to the kinase domain of the protein (Figure 20B). Specifically, FBXL5 appears to bind to amino acids 185 to 292 in SPAK, which is close to many of the residues known to be critical for SPAK activity. Since FBXL5 does not interact with the CCT domain of SPAK, we did not suspect that it was an SPAK phosphorylation target. In addition to this, since FBXL5 does not feature an RFxV motif typical of SPAK targets, we did not examine how SPAK activity regulated this interaction until our later work with HERC2 (see chapter 4).

The region from amino acids 185 to 292 in SPAK is not only important for FBXL5 binding but it also it includes the putative dimerization domain of SPAK. According to Lee et al., V247 to D255 from the SPAK paralogue OSR1 mediates dimerization of OSR1 through a domain swapping mechanism[85]. Based on the proximity of the FBXL5 binding site to the putative SPAK dimerization site, we next examined whether SPAK dimerization might affect FBXL5 binding. To test this, we mutated the homologous region of SPAK by substituting residues T247 to M256 with four glycine residues (SPAK-G246G5) to see if it would affect dimerization and/or FBXL5 binding.

Initial results showed that while the deletion of the proposed domain swap did not affect dimerization in a co-immunoprecipitation assay, it did have curiously strong effects on FBXL5 stability (Figure 21).

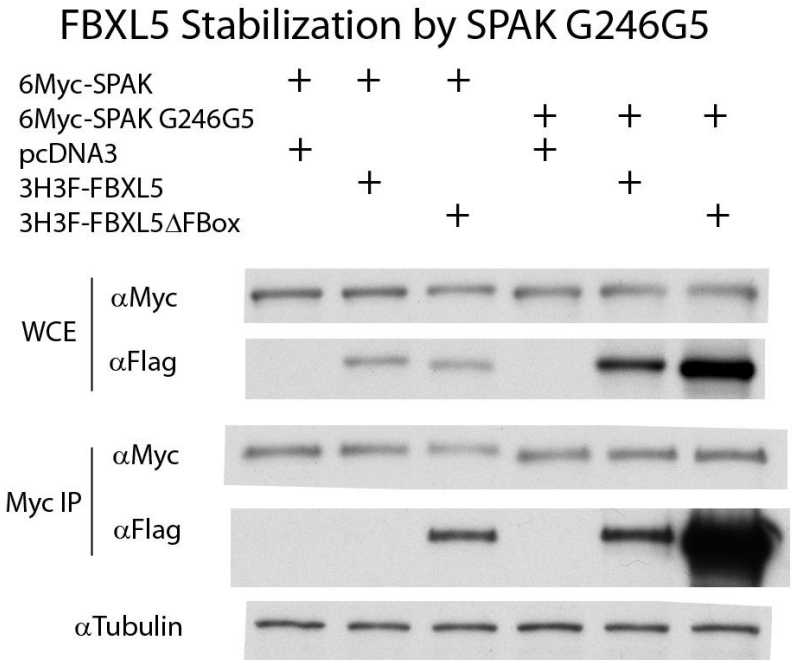

Figure 21. Mutation of the SPAK kinase domain stabilizes FBXL5 and increases binding. 3HA-3FLAG tagged FBXL5 and FBXL5-ΔFbox were co-expressed with 6Myc tagged SPAK WT and a SPAK mutant with a six glycine substitution in the kinase domain (SPAK G246G5). SPAK was affinity-purified with Anti-Myc beads. WCEs and IPs were blotted with FLAG, c-Myc and α-Tubulin.

Overexpression of a SPAK-G264G5 stabilized FBXL5 and FBXL5-ΔFbox protein levels and also greatly increased the ability of the FBXL5 proteins to bind SPAK. When we were unable to show that the mutation altered SPAK dimer formation, we concluded that the mutation likely abolished SPAK kinase activity and caused the phenotype observed.

To further substantiate this observation that SPAK kinase activity altered its ability to bind FBXL5, we generated a kinase-dead version of SPAK in which the lysine residue required for conjugation to ATP was substituted with arginine (SPAK-K104R)[69]. We tested the SPAK-K104R mutant along with a kinase-dead version of the SPAK homologue OSR1 (OSR1 K46R) to determine their effects on FBXL5 stability and binding (Figure 22).

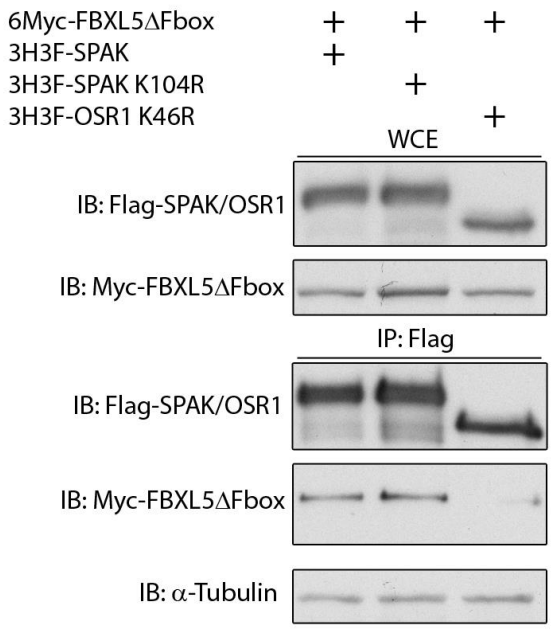

Figure 22. Catalytically inactive SPAK and OSR1 effects on FBXL5. Myc-tagged FBXL5-ΔFbox was co-transfected into HEK293 cells with 3HA-3FLAG tagged SPAK, SPAK K104R or OSR1 K46R. Anti-FLAG beads were used to purify SPAK/OSR1 complexes. WCE and IPs were blotted with antibodies against FLAG, c-Myc and α-Tubulin.

While catalytically inactive SPAK-K104R stabilized FBXL5-ΔFbox, catalytically inactive OSR1-K46R was unable to do so (Figure 22). Additionally, OSR1 exhibits very weak binding to FBXL5-ΔFbox as compared to SPAK. Based on these observations regarding SPAK-

K104R and the effect of SPAK activity on FBXL5 binding, we conclude that SPAK activity may be regulating different aspects of FBXL5 stability rather than the other way around (i.e. FBXL5 regulating SPAK as a ubiquitin ligase). Work in chapter 4 builds on these results and is focused on understanding how SPAK regulates FBXL5 (and other iron-homeostasis proteins) and the biological significance of the interaction.

Proteomic Identification of SPAK, WNK1 and OSR1 Interacting Proteins

In our early characterization of SPAK, OSR1 and WNK1, we used proteomic mass spectrometry to determine the interaction partners of each of the proteins to help us understand the biological role of the FBXL5-SPAK interaction. We reasoned that if any of the binding partners were related to iron homeostasis, these proteins could be explored to help us determine protein networks that were regulated by the FBXL5-SPAK complex. We created Flp-In™ TREx™-293 cell lines that stably express 3HA-3FLAG-tagged SPAK (*Mus musculus*), WNK1 (*Rattus norvegicus*) or OSR1 (*Homo sapien*s) from doxycycline-inducible promotors and immunopurified protein complexes using anti-FLAG M2 agarose beads. The protein complexes were eluted from the beads using 3xFLAG peptide, TCA precipitated and sequentially digested using Lys-C and trypsin proteases. The peptide digests were analyzed in a Linear Ion Trap Quadruple (LTQ) Orbitrap XL hybrid mass spectrometer using an online MudPIT setup and the protein composition of the IP was determined by SEQUEST and DTASelect algorithms.

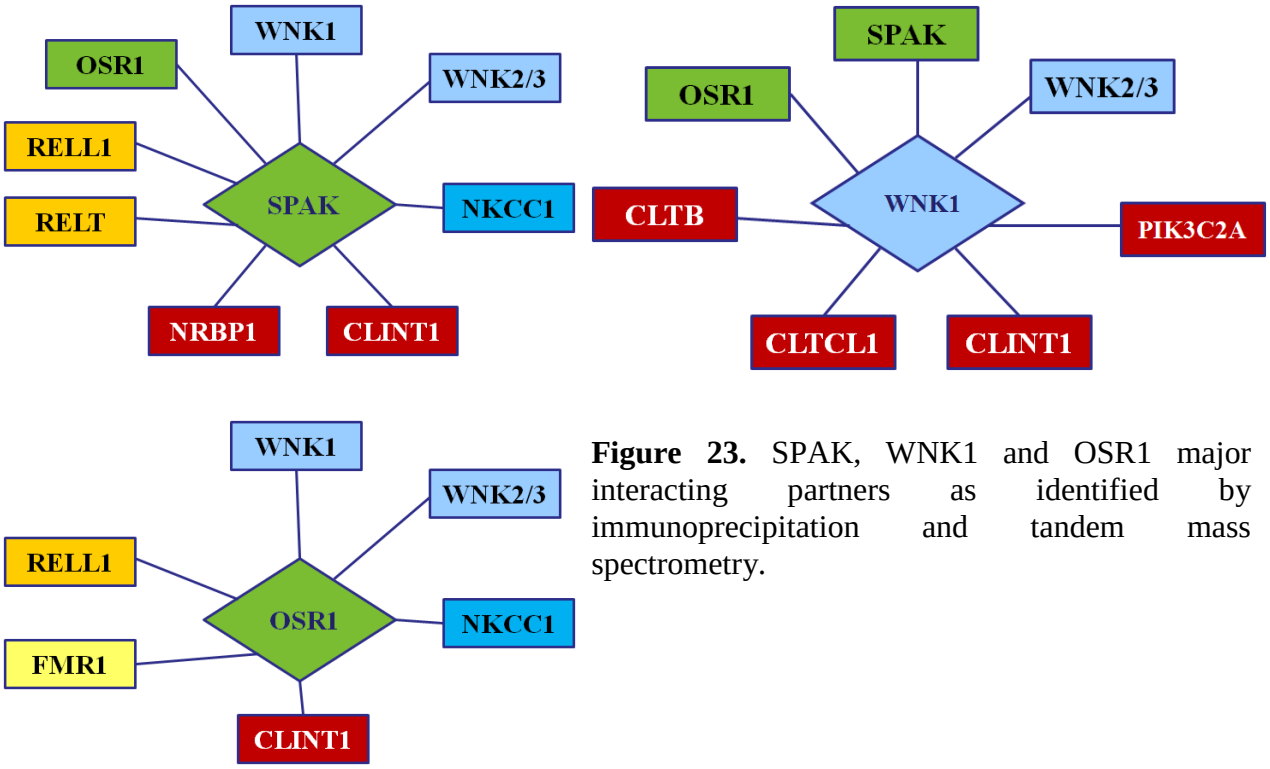

Figure 23. SPAK, WNK1 and OSR1 major interacting partners as identified by immunoprecipitation and tandem mass spectrometry.

Analysis of these proteins did not reveal any obvious iron-related proteins, including FBXL5. The most likely explanation for the absence of FBXL5 is that, as a ubiquitin ligase, its interaction with potential substrates is transient and it may not be sufficiently abundant to identified in these immunoprecipitates. The major SPAK binding partners that we did identify were well established in the literature: the osmotic stress pathway proteins in the WNK family, OSR1 and the NKCC1 co-transporter (Figure 23). The SPAK substrates relevant to MAPK signaling, RELL1 and RELT, were also detected. Previously unidentified proteins included those involved in clathrin-mediated endocytosis such as Clathrin Interactor 1 (CLINT1). CLINT1 was also found in the pulldown for OSR1 and WNK1, while WNK1 had additional endocytosis-related proteins as well (indicated in red in Figure 23). Nuclear Receptor Binding Protein 1 (NRBP1) was an additional protein uniquely identified in complex with SPAK.

NRBP1 is currently classified as a pseudokinase that lacks all of the conserved catalytic residues required for normal ATP hydrolysis and is thought to be involved in cellular homeostasis and protein regulation which supports an additional role in tumor suppression[114]. NRBP1 is also believed to function in intracellular trafficking, as its overexpression causes an impairment of ER to Golgi transport[115]. NRBP1 interacts with two proteins in the TGF-beta-stimulated clone-22 domain (TSC22D) mammalian transcription receptor family (TSC22D2 and TSC22D4), members of which feature a conserved leucine zipper domain and exhibit transcriptional repressor activity[116]. These TSC22D proteins can form homo- and heterodimers using the leucine zipper domain. We observed that SPAK co-purifies with both NRBP1 and TSC22D4 and appears to interact with them in a phosphorylation-dependent manner.

In an effort to better understand how SPAK activity affects its protein interaction partners, we performed additional proteomic experiments with a mutant form of SPAK that is unable to phosphorylate substrates. This mutation, SPAK-K104R, creates a kinase-dead variant of SPAK in which the lysine required to conjugate ATP has been substituted with an arginine[69]. We compared the interaction partners detected between SPAK WT and SPAK-K104R. SPAK wild type (WT) copurifies with TSC22D4 while SPAK-K104R interacts with all four variants. These results suggest that SPAK forms complexes with members of the TSC22D protein family and NRBP1 in a manner that depends on SPAK kinase activity. However, neither NRBP1 nor the TSC22D proteins have any known functions in iron homeostasis, so it seems unlikely that they are relevant to the SPAK-FBXL5 interaction.

A major binding partner for OSR1 that was previously unidentified is Fragile X mental retardation protein 1 (FMR1, FMRP), which is a well-studied protein whose absence results in fragile X syndrome (Figure 23)[117]. This effect is thought to be caused by the loss of regulated

mRNA translation in neuronal dendrites necessary for normal brain development and plasticity. FMR1 is known to form a complex with Cytoplasmic FMRP Interacting Protein (CYFIP1) and Eukaryotic translation initiation factor 4E (EIF4E) that can bind a target mRNA cap and prevent translation[118]. Under normal conditions EIF4E can facilitate ribosome binding and normal translation by unwinding secondary structures in the mRNA. When EIF4E is bound by CYFIP1 and FMR1, however, the mRNA is thought to be wound up by the dual interactions with EIF4E and FMR1 (which also has mRNA binding capability). While the interaction of OSR1 with FMR1 is of high potential biological interest, it seems unlikely to be related to iron or osmotic stress regulation.

Chapter 4: SPAK Regulates FBXL5 Stability through its activity and interaction with HERC2

SPAK Regulates FBXL5 Stability through its activity and interaction with HERC2

Abstract

This chapter focuses on elucidating the mechanism by which FBXL5 is degraded by the ubiquitin-proteasome dependent system in response to iron deficiency. We have identified two novel FBXL5-associated factors that regulate FBXL5 stability: the HECT-type ubiquitin ligase HERC2 (HECT and RLD domain containing E3 ubiquitin protein ligase 2) and the kinase SPAK (STE20/SPS1-related proline-alanine-rich protein kinase), both of which had not been previously implicated in iron homeostasis. We show that HERC2 and SPAK are able to assemble into a ternary complex with FBXL5 and that activated SPAK is able to promote both FBXL5 ubiquitination and degradation under these conditions. This work opens up new routes for iron regulation and potentially unites the iron and osmotic stress regulatory pathways through new crosstalk possibilities.

Introduction

Iron is an essential metal cofactor due to its ability to accept and donate electrons - it is this reactivity that results in its utilization in numerous biochemical processes such as oxygen delivery and storage, DNA repair and replication, lipid metabolism and chromatin modification[1]. Abnormalities in iron homeostasis result in numerous human diseases such as anemia, hereditary hemochromatosis and aceruloplasminemia[2]. Due to the importance of proper iron maintenance at both the cellular and systemic level, the mechanisms of iron acquisition, distribution and regulation are major avenues of research.

The shotgun proteomic characterization of FBXL5-interacting proteins we performed initially to identify IRP1 and IRP2 as FBXL5 substrates also detected several novel FBXL5-associated proteins that play key roles in osmotic stress[88]. One of these interactors is SPAK, a kinase that plays a central role in the signal transduction cascade that results in the cellular response to changes in osmolarity[66].

SPAK activity is governed by a family of upstream WNK (With No-[K] Lysine) kinases. This family includes four members which share high sequence homology, and of which WNK1 is believed to be the main activator of SPAK[58]. WNK1 is activated in conditions of osmotic stress – for example, a hyperosmotic treatment such as sorbitol or hypotonic low-Cl^- conditions[63,64]. This activation is believed to an autophosphorylation event as it depends on a functional kinase domain in WNK1; the activation is also rapid, occurring within one minute from hyperosmotic stress and within five minutes of hypotonic stress. Subsequent structural studies have lent support to this model and found that activation is coupled to a chloride-sensing mechanism found in WNK1[65]. The direct interaction of chloride with WNK1 prevents substrate binding in the active site, thereby preventing phosphorylation. While this explains how low chloride contributes to WNK activation, it is still uncertain how hyperosmotic conditions result in WNK stimulation. One possible mechanism is that crowding effects from solutes such as sorbitol or other salts could prevent chloride binding by competitive interference, although this has not been shown to be true yet.

WNK1 and the other WNK proteins (WNK2, WNK3, WNK4) exert their activity through the phosphorylation of their main substrates, the kinases SPAK and OSR1. These two kinases share very high sequence homology: 96% in the N-terminal catalytic region and 67% in the C-terminal regulatory domain[66]. The region that differs the most between the two proteins is a

unique proline-alanine rich 48 amino acid long region in the N-terminus of SPAK from which the protein derives its name. The function of this proline-alanine rich region is still unknown, as the protein can function normally without it[67]. Another region in SPAK and OSR1 that is important is the conserved C-Terminal (CCT) domain. This domain mediates all known interactions between SPAK/OSR1 and their upstream kinases and downstream substrates[69]. Despite the similarities in structure between the two proteins a major difference can be found using mouse knockout studies: while disruption of SPAK in knockout mice results in viable animals with no overt phenotype, OSR1 knockout causes embryonic lethality and generates no living pups[66].

In this paper we have identified an iron regulatory function that only SPAK possesses. We find that SPAK forms a ternary degradation complex with HERC2 that is able to regulate FBXL5 stability in an activity dependent manner. Our results open up new connections between cellular stress response pathways that have, until now, been largely separated.

Results

The physical interactions between HERC2, SPAK and FBXL5 were initially identified using a proteomic mass spectrometry-based approach to identify FBXL5-associated proteins (Table 3). Briefly, FBXL5-associated protein complexes were purified from an HEK293 stable cell line expressing HA-FLAG-FBXL5 from a doxycycline-inducible promoter. These FBXL5 immunoprecipitates were digested with trypsin and analyzed by Multidimensional Protein Identification Technology (MudPIT) using an LTQ-Orbitrap XL tandem mass spectrometer[88]. Purifications were also done using FBXL5-ΔFbox as the bait due to its dominant negative nature and ability to trap potential substrate proteins[38]. Shotgun proteomic analysis of proteins bound to

FBXL5-ΔFbox revealed three partners involved in osmotic stress response: WNK1, SPAK and OSR1. Sequence coverage was highest for SPAK, and despite the large size of WNK1 (over 250 kDa) only six spectra were observed as compared to the eight spectra for SPAK. These numbers support a model where FBXL5 directly binds SPAK rather than one of the other two proteins.

Table 3. Selected binding partners identified in the proteomic analysis of FBXL5-ΔFbox.

Protein (Acc. #)	MW (Da)	Peptide Count	Spectral Count	Sequence Coverage
FXBL5 (Q9UKA1)	76,590	35	301	40.8%
HERC2 (O95714)	527,228	46	56	12.2%
SPAK (Q9UEW8)	59,474	5	8	10.4%
WNK1 (Q9H4A3)	250,794	3	6	1.6%
OSR1 (O95747)	58,022	2	2	4%

Based on its identity as a HECT-type E3 ubiquitin ligase, we first examined the possibility that HERC2 was responsible for the ubiquitin-dependent degradation of FBXL5 in low iron conditions. To test this hypothesis, we first validated the FBXL5-HERC2 interaction using co-immunoprecipitation assays with a cell line stably expressing 3HA-3FLAG-tagged FBXL5 and observed that endogenous HERC2 interacts with FBXL5 (Figure 24A). Next, we used siRNA knockdown of HERC2 to show that depletion of HERC2 stabilizes FBXL5 (Figure 24B), consistent with a role for HERC2 in regulating FBXL5 stability. Finally, we performed a cell-based ubiquitination assay in which we looked at how HERC2 silencing affected the poly-

ubiquitination of FBXL5. We find that FBXL5 ubiquitination is significantly impaired in cells depleted of HERC2 by siRNA (Figure 24C, compare lanes 2 and 4). MG132, a chemical inhibitor of the proteasome, is used in these assays to stabilize poly-ubiquitinated forms of FBXL5 which are rapidly degraded.

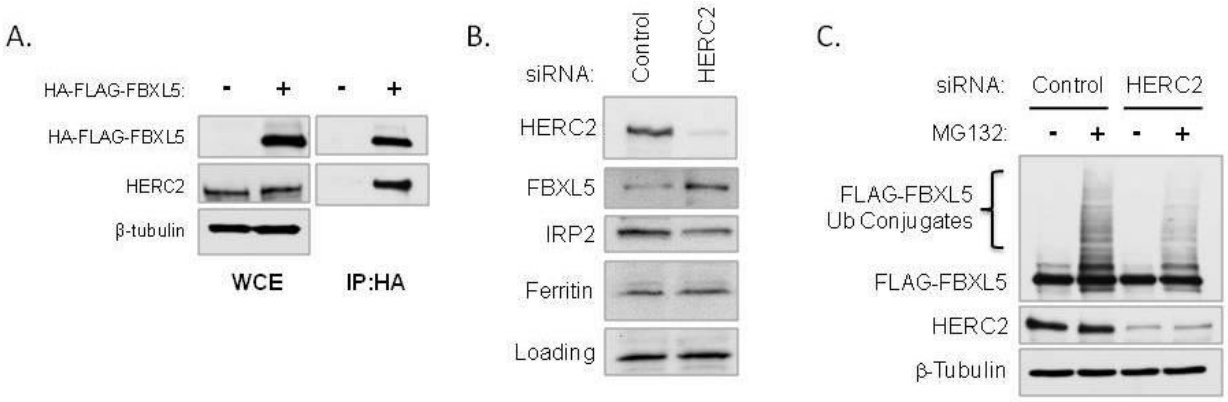

Figure 24. HERC2 interacts with FBXL5 and regulates its stability and ubiquitination. (**A**) An HEK293 stable cell line overexpressing 3HA-3FLAG-tagged FBXL5 was used to immunoprecipitate FBXL5 using anti-HA beads to assess bound endogenous protein. Whole cell extracts (WCE) and immunoprecipitates (IP) were Western blotted with antibodies against FLAG, HERC2 and β-tubulin. (**B**) siRNA transfection was used in HEK293 cells to knockdown HERC2 protein levels. WCEs were blotted with antibodies against HERC2, FBXL5, IRP2 and ferritin. (**C**) A cell-based ubiquitination assay was performed in HEK293 cells by co-transfecting HA-tagged ubiquitin and FLAG-tagged FBXL5 while using siRNA to knockdown HERC2. A 4 hour treatment of MG132 was used to block proteasomal degradation of ubiquitinated proteins. Anti-HA beads were used to immunopurify poly-ubiquitinated conjugates. WCEs and IPs were Western blotted with antibodies against FLAG, HERC2 and β-tubulin.

In addition to HERC2 silencing, we also examined how HERC2 overexpression affected FBXL5 ubiquitination in this cell-based assay. As HERC2 is a >500kD protein, we were unable to create a full-length expression construct. Instead, we have used two C-terminal fragments of HERC2. The first is HERC2-aa2600-3600 (also termed HERC2-F4) which possesses the

FBXL5 binding region but does not contain the HECT domain required for E3 ligase activity. Hence, this mutant can act as a dominant negative and should be able to interact with FBXL5 but not ubiquitinate or degrade it. The second is HERC2-aa-2600-4935 (also termed HECT-HERC2) which contains both the FBXL5-binding and HECT domains and has been demonstrated to have E3 ligase activity[119]. When used in cell-based ubiquitination assays (Figure 25), we find that overexpression of HERC2-aa-2600-4935 but not HERC2-aa-2600-3600 stimulated the poly-ubiquitination of FBXL5. Together, these results indicate that HERC2 is an E3 ubiquitin ligase capable of binding FBXL5 and regulating its ubiquitination and degradation.

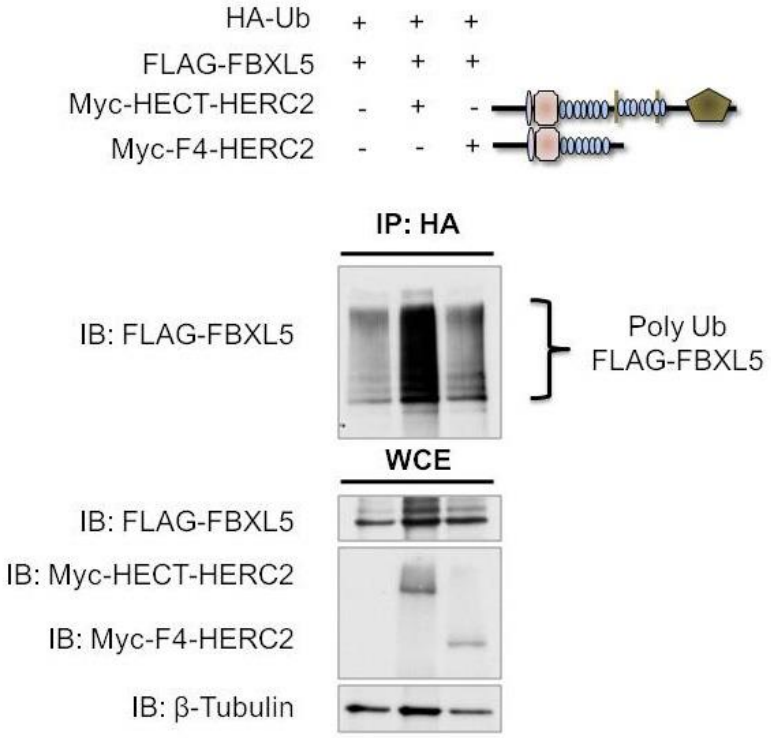

Figure 25. FBXL5 is poly-ubiquitinated in a HERC2-activity dependent manner. HEK293 cells were co-transfected with HA-ubiquitin, FLAG-tagged FBXL5 and Myc-tagged variants of HERC2: HERC2-aa-2600-3600 (denoted here as F4-HERC2) and HERC2-aa-2600-4935 (denoted here as HECT-HERC2). Cells were treated with MG132 for 4 hours to accumulate poly-ubiquitinated proteins. Anti-HA beads were used to immunopurify ubiquitinated conjugates. Western blotting was used on WCEs and IPs using antibodies against FLAG, c-Myc and β-tubulin.

Although these results are consistent with a role for HERC2 in ubiquitinating FBXL5 and targeting it for degradation, we were unable to show that this interaction or activity was significantly iron-regulated. Thus, we hypothesized that there may be an additional factor that helped to confer iron-dependent regulation to the FBXL5-HERC2 relationship. Based on our previous observations that overexpression of kinase dead SPAK (SPAK-K104R)[69] partially stabilized FBXL5 (Figure 22), we considered SPAK a potential candidate for this regulatory factor and sought to examine whether it was able to influence the HERC2-dependent degradation of FBXL5. To test this model, we further characterized the SPAK-FBXL5 interaction. We transiently expressed tagged versions of FBXL5 and FBXL5-ΔFbox with tagged SPAK and determined the relative degree of the interaction. We observed that the SPAK interaction with FBXL5 WT is considerably weaker than the interaction seen with FBXL5-ΔFbox (Figure 26A).

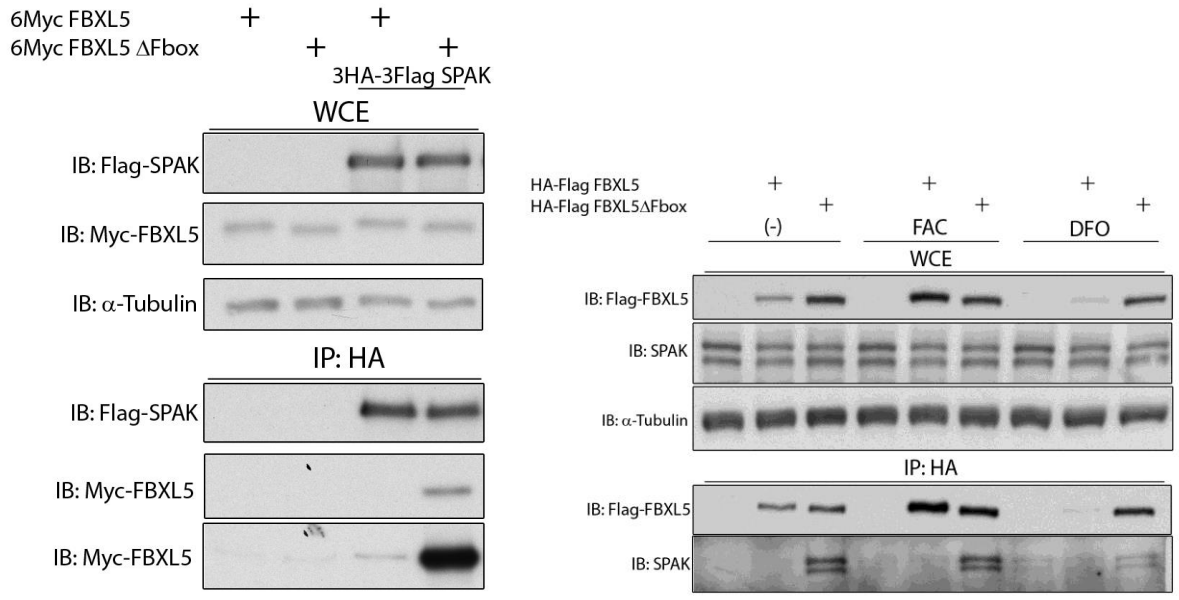

Figure 26. SPAK interacts with FBXL5 and FBXL5-ΔFbox. (**A**) HEK293 cells were transiently transfected with combinations of 6Myc-tagged FBXL5 WT or FBXL5-ΔFbox along with 3HA-

3FLAG-tagged SPAK. SPAK was affinity purified using anti-HA beads and the whole cell extracts (WCE) and immunoprecipitations (IP) were blotted with primary antibodies against FLAG, c-Myc and α-tubulin. (**B**) HEK293 cells stably expressing either 3HA-3FLAG-tagged FBXL5 wild type (WT) or FBXL5-ΔFbox were affinity-purified against HA to co-purify FBLX5 and FBXL5-ΔFbox bound proteins. Cells were treated with 8 hours of FAC or DFO, as indicated. WCEs and IPs were blotted against with FLAG, SPAK and α-tubulin.

We also demonstrated that endogenous SPAK can bind FBXL5-ΔFbox in an iron-dependent manner (Figure 26B). When FBXL5 or FBXL5-ΔFbox is affinity purified from their respective stable cell lines, SPAK can be detected in FBXL5-ΔFbox immunoprecipitates (Figure 26B, lane 3). SPAK binding to FBXL5-ΔFbox is lost in cells treated with the iron chelator desferrioxamine mesylate (DFO) treated cells while treating cells for eight hours with ferric ammonium citrate (FAC) results in high iron conditions that strengthen SPAK-FBXL5 binding. It is worth noting that wild type FBXL5 protein levels are highly sensitive to changes in intracellular iron levels such that it is degraded in low iron conditions, while FBXL5-ΔFbox is stable in low iron conditions. Thus, our results indicate that iron is required to both stabilize FBXL5 protein levels as well as promote its interaction with SPAK.

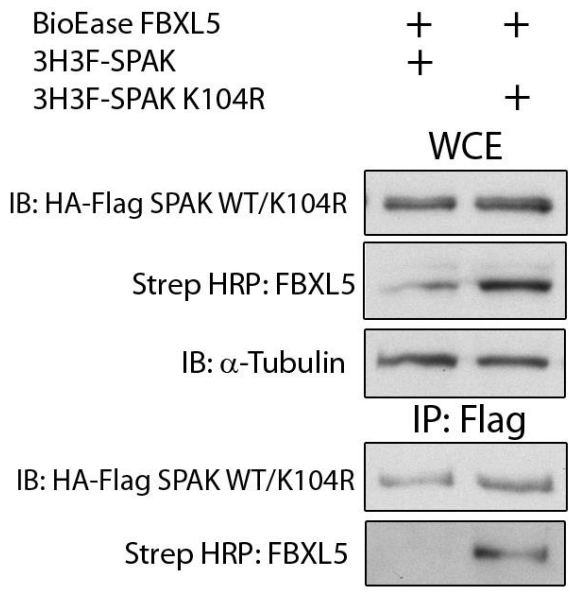

Figure 27. Overexpression of SPAK K104R stabilizes FBXL5 levels relative to conditions with SPAK WT. BioEase-tagged FBXL5 was co-transfected into HEK293 cells with either 3HA-3FLAG-tagged SPAK WT or SPAK-K104R. SPAK was immunoprecipitated using anti-FLAG beads. WCEs and IPs were blotted with streptavidin-HRP and primary antibodies against FLAG and α-tubulin.

In Chapter 3 we showed that SPAK activity, as shown by the results involving inactive SPAK-K104R (Figure 22), plays an important role in regulating FBXL5 stability. Here, we find that SPAK-K104R binds more strongly to FBXL5 as compared to SPAK-WT and SPAK-K104R is able to stabilize protein levels of FBXL5 relative to overexpression of SPAK WT (Figure 27). The observation that kinase dead SPAK stabilizes FBXL5 is also consistent with SPAK silencing results which show that depletion of SPAK by siRNA leads to the accumulation of endogenous FBXL5 (Figure 28A). Together, these results support a model in which SPAK activity is driving degradation of FBXL5 and that is impaired in cells functionally lacking SPAK activity. In addition to FBXL5 stabilization, we also examined whether SPAK depletion or overexpression of SPAK-K104R influenced IRP2 and ferritin levels that are downstream FBXL5-regulated

events. SPAK depletion leads to IRP2 downregulation which is consistent with FBXL5 stabilization under these conditions. Similarly, overexpression of SPAK-K104R in a Tet-On inducible stable cell line is also able to stabilize endogenous levels of FBXL5 leading to downregulation of IRP2 and translation depression of ferritin (Figure 28B). In particular, steady state ferritin levels are considerably higher in SPAK-K104R overexpressing cells as compared to SPAK-T243E/S383D overexpressing conditions (Figure 28B, compare lanes 4 & 5 with lanes 7 & 8). These results corroborate that loss of SPAK activity leads to an increase in FBXL5 protein levels with corresponding effects on downstream regulators.

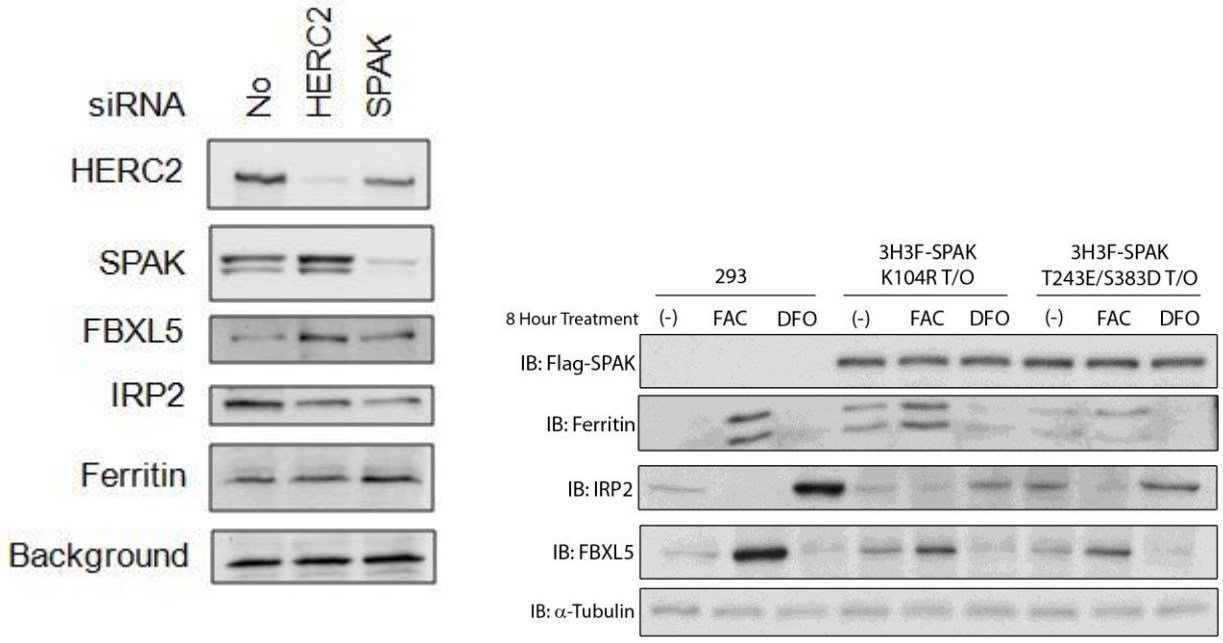

Figure 28. SPAK siRNA-mediated knockdown and overexpression of SPAK K104R both stabilize endogenous FBXL5 levels. (**A**) siRNA transfections using siRNA against HERC2 and SPAK were used to knock down protein expression levels in HEK293 cells. WCEs were run with primary antibodies against HERC2, SPAK, FBXL5, IRP2 and ferritin. (**B**) HEK293 stable cell lines expressing 3HA-3FLAG tagged SPAK-K104R and SPAK-T243E/S383D were treated for 8 hours with FAC or DFO prior to lysis. WCEs were blotted with antibodies against FLAG, ferritin, IRP2, FBXL5 and α-tubulin.

Our results suggest that both HERC2 and SPAK are able to regulate FBXL5 stability. We next determined whether they performed this action via different pathways or as part of the same complex. We hypothesized that they may function as part of the same complex based on the fact that SPAK utilizes its conserved C-terminal (CCT) domain to interact with RFxV motifs found in both its upstream kinases and downstream targets (such as WNK1 and NKCC1)[69,70] and that HERC2 contains this motif at amino acids 3703 to 3706: RFTV. To address whether SPAK can associate with HERC2 and if this interaction is dependent on its CCT domain, we evaluated the ability of HERC2 to bind to either WT SPAK or a SPAK lacking the CCT domain by co-immunoprecipitation assays. We found that full length SPAK is able to bind HERC2-aa-2600-4935, but a SPAK truncation mutant lacking the CCT domain (SPAK-ΔCCT) is defective in this interaction (Figure 29). We conclude that SPAK and HERC2 interact and that the CCT domain of SPAK is critical for the association.

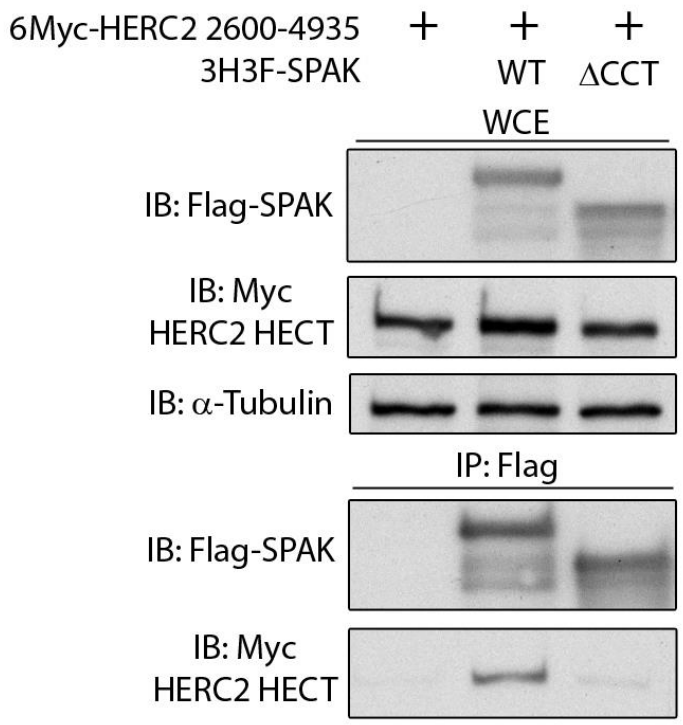

Figure 29. SPAK interacts with HERC2 using its CCT domain. 6Myc-tagged HERC2-aa-2600-4935 was co-transfected in HEK293 cells with two variants of SPAK: full length WT or missing the CCT domain (ΔCCT). SPAK complexes were immunopurified using anti-FLAG beads. WCEs and IPs were Western blotted with primary antibodies against FLAG, c-Myc and α-tubulin.

Our next step was to determine if and how SPAK and HERC2 might work as a cooperative complex to regulate FBXL5 protein levels. Since we recognize that SPAK activity is tied to FBXL5 stability, we reasoned that it might also be linked to the poly-ubiquitination and degradation of FBXL5 as these are essential steps in its proteasome-dependent degradation. To test this, we performed cell-based ubiquitination assays to determine how constitutively active SPAK (SPAK-T243E/S383D) or kinase-dead SPAK (SPAK-K104R) affected FBXL5 ubiquitination in a cell-based ubiquitination assay utilizing the active HERC2 fragment (HERC2-HECT). In Figure 30A, we show that overexpression of SPAK-T243E/S383D strongly

stimulates FBXL5 ubiquitination in comparison to SPAK-K104R suggesting that active SPAK promotes FBXL5 ubiquitination. In addition, we find that co-expression of active SPAK and HERC2 is capable of stimulating FBXL5 degradation/downregulation while co-expression of SPAK-K104R or SPAK-T243E/S383D-ΔCCT (which is defective in interacting with HERC2) are unable to efficiently do so (Figure 30B). Together, these data provide strong evidence that HERC2 and active SPAK cooperatively promote the ubiquitination and degradation of FBXL5.

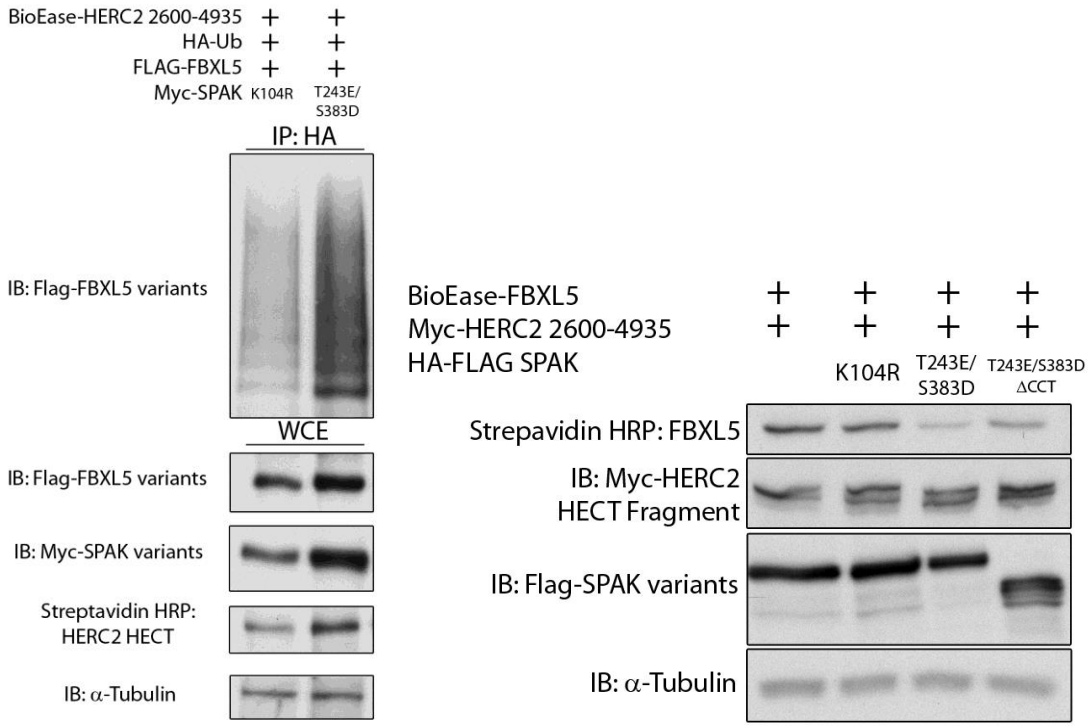

Figure 30. SPAK activity drives poly-ubiquitination and degradation of FBXL5 in an activity and CCT domain dependent manner. (**A**) HEK293 cells were cotransfected with HA-Ub, FLAG-FBXL5 and BioEase-HERC2 2600-4935 with either Myc-SPAK K104R or Myc-SPAK T243E/S383D and treated with MG132 for 4 hours. Ubiquitin conjugates were immunoprecipitated by using anti-HA beads. HA-immunoprecipitates (IP: HA) and WCEs were immunoblotted with antibodies to FLAG, c-Myc, and α-tubulin. (**B**) HEK293 cells were cotransfected with BioEase-FBXL5, Myc-HERC2 2600-4935 and 3HA-3FLAG SPAK WT, K104R, T243E/S383D and T243E/S383D-ΔCCT. WCEs were blotted with streptavidin-HRP and antibodies to FLAG, c-Myc and α-tubulin.

Based on the observation that both SPAK and HERC2 can promote FBXL5 degradation, we propose a model that HERC2 and SPAK cooperate to catalyze the ubiquitin-dependent degradation of FBXL5. Although the molecular basis for this cooperativity is unclear, we propose that it stems from their cooperative assembly into an FBXL5-HERC2-SPAK ternary complex. This model is based on the domains that we have identified that mediate the interactions between these three proteins. None of these interaction regions are mutually exclusive, suggesting that the assembly of a ternary complex is possible (Figure 31). As discussed in chapter 3, the FBXL5-SPAK interaction is mediated by a region adjacent and N-terminal to the F-box domain in FBXL5 and by the kinase domain of SPAK. HERC2 associates with a portion of FBXL5 slightly downstream of its Fbox domain[119]. The SPAK and HERC2 interaction is mediated by the CCT domain of SPAK (Figure 29). Based on the positioning of these interactions, we can hypothesize that SPAK and HERC2 might form a cooperative complex to regulate FBXL5 stability.

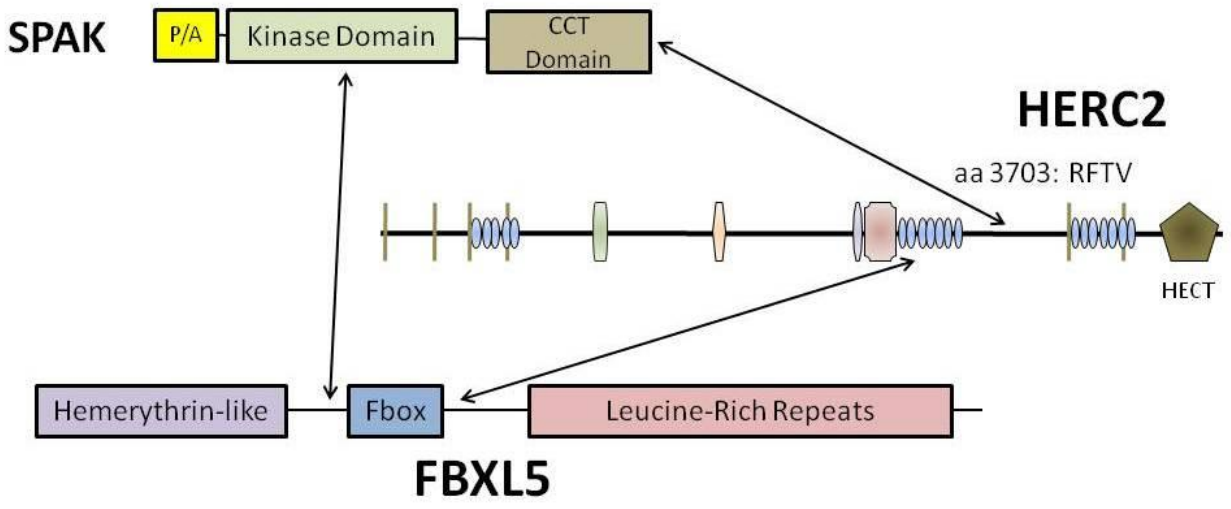

Figure 31. Schematic of the SPAK-HERC-FBXL5 ternary complex. The interaction domains are indicated by the positioning of the arrows between each element of the complex.

To test whether these proteins form a ternary complex and whether the ternary assembly is more stable than any pairwise interactions, we conducted additional binding assays using a combination of mutants. Co-transfection assays using different mutants of FBXL5, HERC2 and SPAK in different combinations were evaluated for their ability to assemble into a complex. In Figure 32A, we find that the ability of SPAK and HERC2 to associate is strongly stimulated upon co-expression of FBXL5-ΔFbox suggesting that the SPAK-HERC2 interaction is strongest when the SPAK-FBXL5 interaction is strongest (Figure 32A, compare lanes 1 and 2 with lanes 3 and 4, 5 and 6 with lanes 7 and 8). Also consistent with this idea, immunoprecipitation of FBXL5 efficiently co-IPs both WT SPAK and HERC2 while introducing the SPAK-ΔCCT mutant into this assay impairs the FBXL5-HERC2 interaction suggesting that the ability of HERC2 to interact with FBXL5 is promoted by forms of SPAK that are able to interact with HERC2 (Figure 32B). Together, these results support a model where SPAK and HERC2 cooperatively assemble into a ternary complex with FBXL5 and that regulates its stability and ubiquitination.

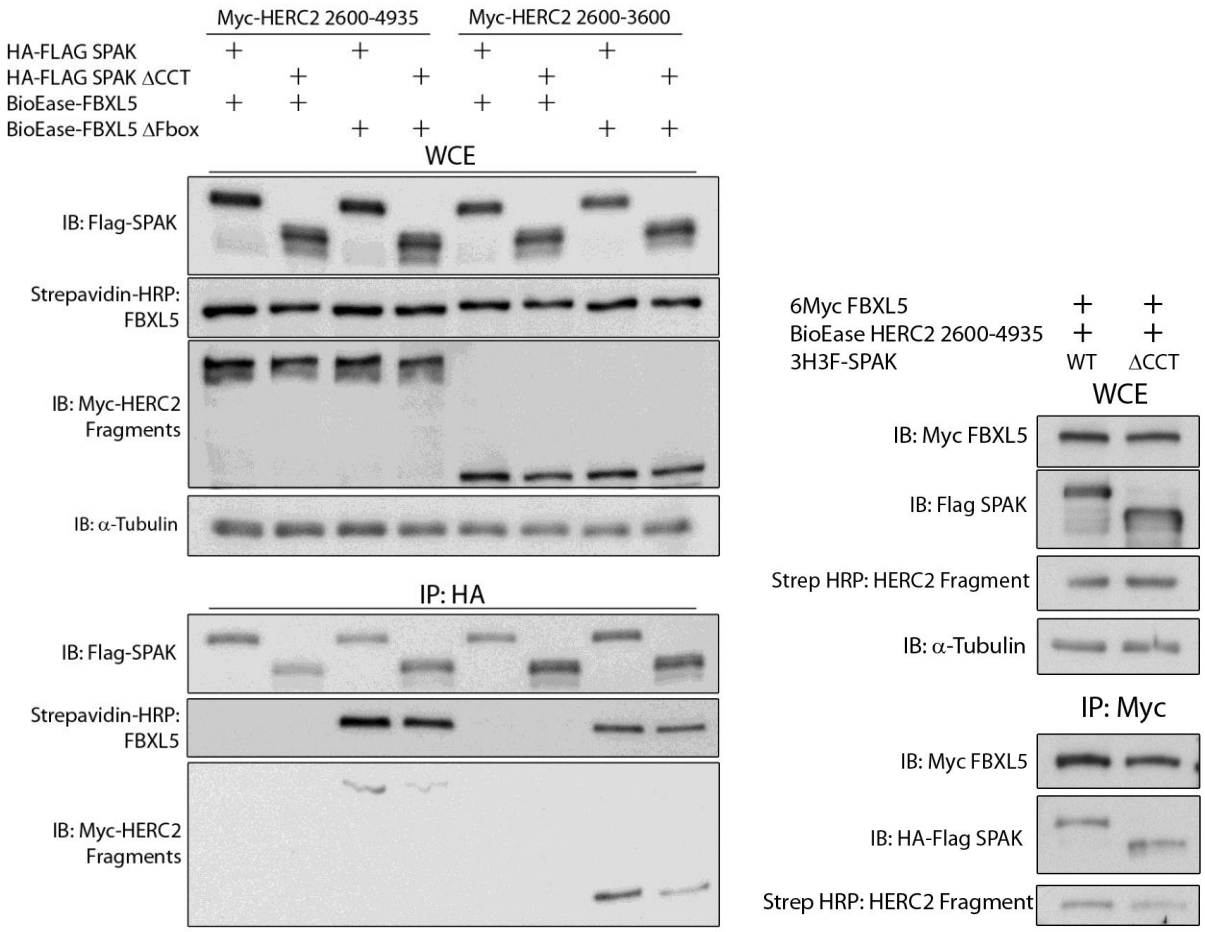

Figure 32. SPAK forms a degradation complex with HERC2 that is dependent on the CCT domain of SPAK. (**A**) HEK293 cells were transfected with combinations of the following: 3HA-3FLAG SPAK WT or SPAK-ΔCCT, BioEase-FBXL5 or FBXL5-ΔFbox, and 6Myc-HERC2 2600-4935 or 2600-3600. SPAK and SPAK-ΔCCT were immunoprecipiated with anti-HA beads. WCEs and IPs blotted with antibodies for FLAG, c-Myc and α-Tubulin as well as blotted with streptavidin-HRP. (**B**) HEK293 cells were transfected with 6Myc-FBXL5, BioEase HERC2 2600-4935 and either 3HA-3FLAG SPAK WT or SPAK-ΔCCT. FBXL5 was immunoprecipitated using anti-Myc beads, WCEs and IPs were blotted with antibodies for c-Myc, FLAG and α-Tubulin and streptavidin-HRP.

To gain additional insight into the mechanism underlying the HERC2- and SPAK-dependent degradation of FBXL5, we re-focused our efforts on understanding the FBXL5-SPAK interaction and why FBXL5-ΔFbox is able to preferentially associate with SPAK. Our previous

data demonstrated that wild type FBXL5 is degraded in low iron while FBXL5-ΔFbox is stable. As SKP1 is known to bind in this region, it is possible that SPAK and SKP1 bind overlapping regions of FBXL5 and that loss of SKP1 binding in the FBXL5-ΔFbox mutant might stimulate SPAK binding by alleviating this competition. A second possibility to explain this data is that the FBXL5-ΔFbox (aa 216-240) deletion that we generated is acting in a SKP1-independent manner, possibly by disrupting some other aspect of FBXL5 structure. To test this, we generated a mutant in FBXL5 in which two highly conserved residues in the F-box region, Leu208 and Pro209 (FBXL5-L208AP209A), were substituted with alanine which we reasoned would disrupt SKP1 binding in a more conservative manner. Substitution of these two amino acids results in an FBXL5 mutant that no longer binds SKP1 (Figure 33). SPAK binds FBXL5 and FBXL5-L208AP209A weakly while SKP1 cannot bind FBXL5-ΔFbox or L208AP209A at the same strength as FBXL5 WT (unpublished data).

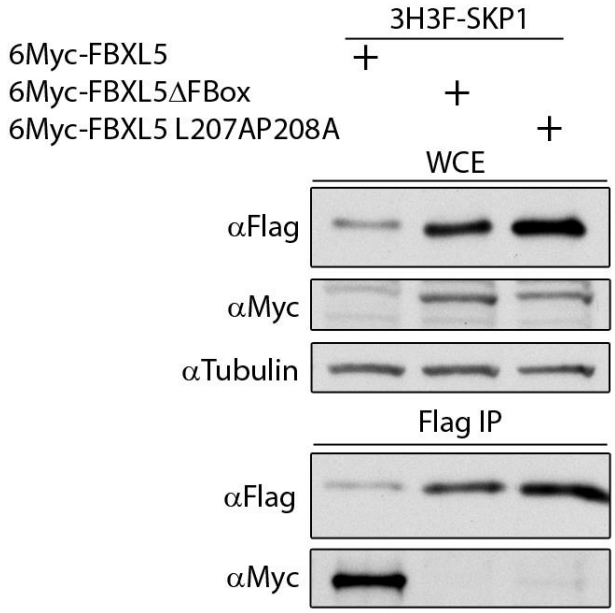

Figure 33. FBXL5 L208AP209A is unable to bind SKP1. HEK293 cells were co-transfected with either 3HA-3FLAG-tagged SKP1 along with 6-Myc-tagged FBXL5 WT, dFbox or

L208AP209A. Flag-tagged proteins were immunoprecipitated using anti-FLAG beads and the WCEs and IPs were Western blotted with antibodies for FLAG, c-Myc and β-tubulin.

These results demonstrate that the SPAK-FBXL5-ΔFbox interaction is not regulated by its competition with SKP1, but instead suggests that the FBXL5-ΔFbox mutant is effectively a gain-of-function mutant that binds SPAK very strongly, potentially acting as a dominant negative that traps SPAK in an FBXL5-SPAK complex. Importantly, we have clearly demonstrated that FBXL5-ΔFbox is not degraded in iron-deficient cells (Figure 26B) suggesting that understanding how this gain-of-function mutant works will have implications for FBXL5 degradation in more physiological contexts.

To further characterize how the FBXL5-ΔFbox deletion functions, we created an FBXL5 mutant in which the entire deleted region (aa 216-240: FBXL5-Fbox AllA,G) or small segments of the deleted region (aa 216-223: 8A-1, aa 224-231: 8A-2, aa 232-240 9A-3) were instead replaced by a stretch of alanines or glycines. None of these new mutants gained the ability to bind FBXL5 more strongly, leading us to believe that the increased binding to SPAK is due to a re-organization of the domain structure of FBXL5 resulting from the 24 amino acid deletion and not specific residues in that region (Figure 34). The FBXL5 constructs used in this experiment feature only the C-terminal 532 amino acids (CT532), lacking the hemerythin-like domain.

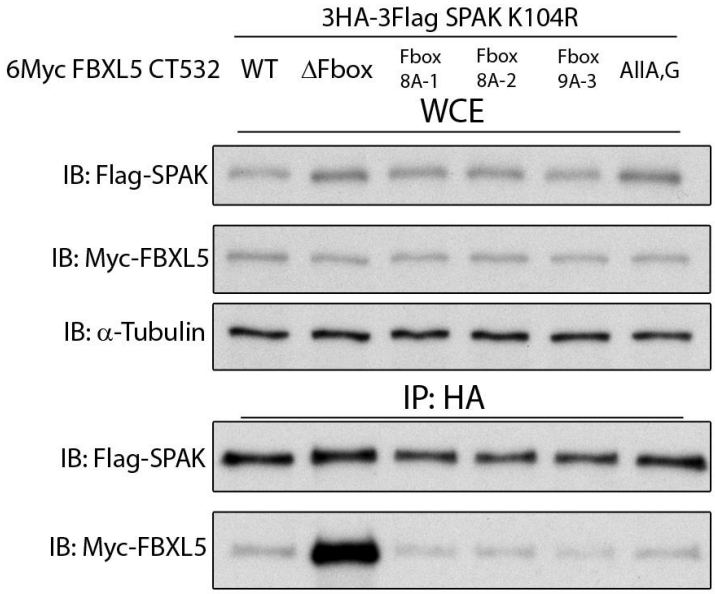

Figure 34. Mutation of the FBXL5 Fbox region to alanines and glycines is not sufficient to promote SPAK binding. HEK293 cells were co-transfected with 3HA-3FLAG-tagged SPAK K104R and 6Myc-tagged variants of FBXL5 CT532 (C-Terminal 532 amino acids): WT, ΔFbox, three mutants with approximately 1/3 of the Fbox region substituted to alanine (Fbox 8A-1,2 Fbox9A-3), and AllA,G which has the entire Fbox region lost in ΔFbox mutated to alanines or glycines. Immunoprecipitation was used with HA beads to purify SPAK-bound complexes. WCEs and IPs were Western blotted with primary antibodies against FLAG, c-Myc and α-tubulin.

Since the FBXL5-ΔFbox is not degraded under low iron conditions, we hypothesized that SPAK and HERC2 would be unable to stimulate ubiquitination of this mutant. We performed a cell-based ubiquitination assay utilizing (1) HA-ubiquitin, (2) catalytically active HERC2, (3) kinase dead or constitutively active SPAK, and (4) either FBXL5 and FBXL5-ΔFbox.

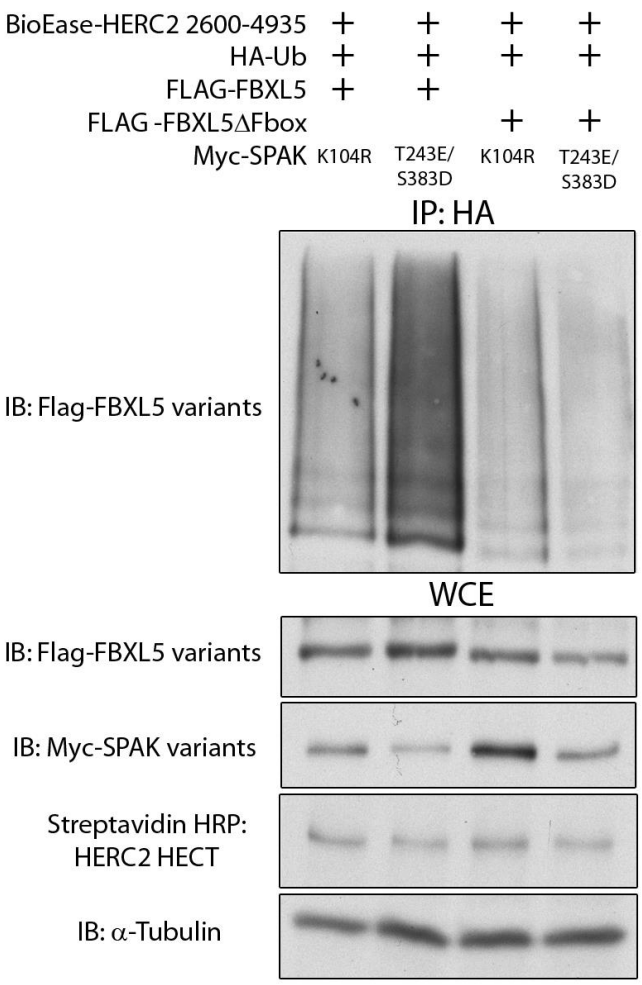

Figure 35. SPAK and HERC2 are unable to drive poly-ubiquitination of FBXL5-ΔFbox. HEK293 cells were co-transfected with HA-tagged ubiquitin, BioEase-tagged HERC2 2600-4935, 6Myc-tagged SPAK K104R or T243E/S383D and 3Flag-tagged FBXL5 or FBXL5-ΔFbox. Lysates were obtained using SDS boiling method and poly-ubiquitin chains were immunoprecipitated using anti-HA beads. WCEs and IPs were Western blotted with streptavidin-HRP and primary antibodies against FLAG, c-Myc and α-Tubulin.

We find that constitutively active SPAK is able to drive poly-ubiquitination of full length FBXL5 but not FBXL5-ΔFbox (Figure 35). This suggests that the increased stability observed for FBXL5-ΔFbox in low iron conditions likely stems from the inability of HERC2 and SPAK to promote its ubiquitin-dependent degradation.

Discussion

SPAK is a kinase that is well-established in salt regulatory processes but has never before been shown to regulate iron homeostasis. Here we have shown that SPAK binding and activity are able to drive FBXL5 poly-ubiquitination and degradation in a HERC2-dependent manner. This presents a major functional difference between SPAK and its close homologue OSR1, as inactive OSR1 is unable to regulate FBXL5 in a similar fashion.

We propose a mechanism where SPAK and HERC2 form a degradation complex that is regulated by the phosphorylation state of SPAK (Figure 36). We believe that the phosphorylation state of SPAK is iron-dependent and regulates the ability of HERC2 to poly-ubiquitinate and degrade FBXL5. SPAK requires the CCT domain to recruit HERC2 to the ternary complex; without it, SPAK alone is unable to drive degradation of FBXL5. Additionally, SPAK-K104R is unable to drive degradation of FBXL5 because it cannot phosphorylate its substrate. In this fashion, FBXL5 is degraded in an SPAK-activity dependent manner, which itself is dependent on iron levels.

Given this new aspect of SPAK function, there are likely other aspects of iron-regulatory systems that have yet to be characterized. For example, it is still not clear why a kinase involved in the osmotic stress signal transduction cascade would be part of an iron homeostatic degradation complex. These new pathways could yield alternative targets for pharmaceuticals and prove useful in combating iron-related illnesses.

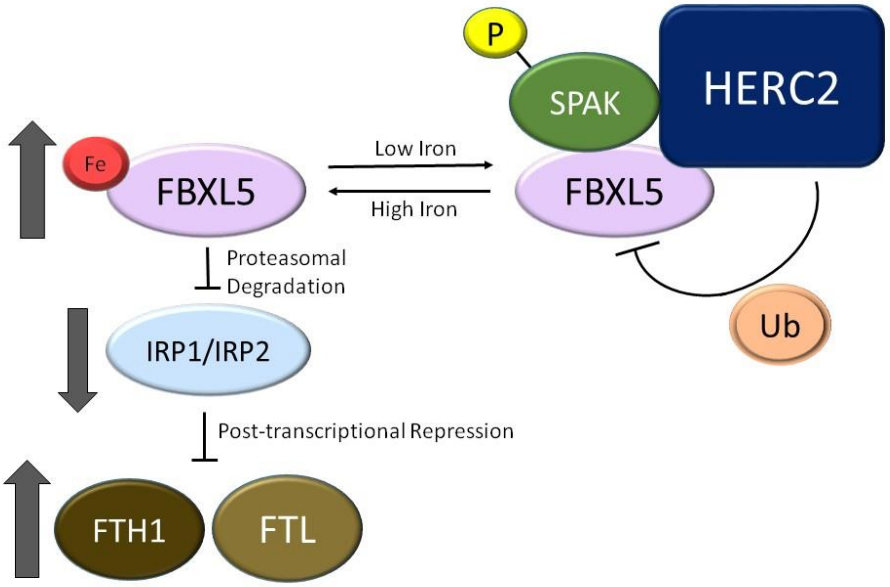

Figure 36. Schematic of SPAK-HERC2-FBXL5 ternary complex and the degradation of FBXL5.

Materials and Methods

Plasmids

The full length FBXL5 cDNA (NIH_MGC_97), full length mouse SPAK cDNA (Clone ID: 5698326) and full length human OSR1 cDNA (Clone ID: 3163379) were obtained from Open Biosystems while full length rat WNK1 was a gift from Melanie Cobb. The cDNA was amplified using the Phusion DNA Polymerase (New England Biolabs) and introduced into the pCR8/GW/TOPO vector (Invitrogen) or the Gateway pDONR221 vector (Life Technologies). The Quikchange system (Stratagene) was used to generate the FBXL5-ΔFbox mutant lacking amino acids 216-240 using pCR8-FBXL5 as a template and was used to create the various mutations in SPAK (K104R, T243E/S383D) using a pDEST SPAK WT vector as a template. FBXL5 and FBXL5-ΔFbox were subcloned into pcDNA3-6xMyc and pcDNA5-FRT/TO-3xHA-3xFLAG plasmids using pCR8-FBXL5 and DEST plasmids via the Gateway cloning system (Life Technologies). SPAK ΔCCT fragments were generated by PCR using primers containing flanking AttB1 and AttB2 sites and cloned into pDONR221. These fragments were then subcloned into pcDNA5-FRT/TO-3xHA-3xFLAG for expression in HEK293 or Hela. Plasmids expressing HA-Ub, Myc-CUL1 and Myc-SKP1 were previously described[106,107].

Antibodies

Antibodies used for immunoblotting were as follows: IRP2-7H6 (Santa Cruz Biotechnology), IRP2[92], IRP1[109], FLAG-M2 (Sigma), c-Myc (Santa Cruz Biotechnology), HA 12CA5 (Roche), ferritin (Sigma), β-tubulin (Sigma), and α-tubulin (Proteintech Group). Horseradish peroxidase conjugated secondary antibodies were obtained from Jackson Immunoresearch Laboratories. For quantification of protein half-lives, an immunofluorescent

anti-mouse secondary antibody (Rockland) was used. Immunoprecipitation reactions were performed using affinity matrices for anti-FLAG M2, anti-c-Myc, and anti-HA available from Sigma. Streptavidin-HRP was purchased from Invitrogen.

Cell Lines

The HEK293 cell line was obtained from the American Type Culture Collection (ATCC) while Flp-In™ T-REx™-293 was obtained from Invitrogen. Flp-In™ T-REx™-293 cells stably expressing 3xHA-3xFLAG-FBXL5, 3xHA-3xFLAG-FBXL5-ΔFbox, 3xHA-3xFLAG-SPAK, 3xHA-3xFLAG-SPAK-K104R and 3xHA-3xFLAG-SPAK-T243E/S383D were generated using the Flp-In system (Invitrogen) according to the manufacturer's directions.

Cell Culture, Plasmid Transfections, and Treatments

Cell culture reagents were obtained from Invitrogen. All cell lines were cultured in complete Dulbecco's Modified Eagles medium (DMEM) containing 10% heat inactivated fetal bovine serum (FBS), 100 units/mL penicillin and streptomycin, and 2 mM glutamine at 37°C in ambient air with 5% CO_2. Transient transfections were performed using either BioT (Bioland, Long Beach, CA) or Lipofectamine 2000 according to the manufacturer's protocol. siRNA transfections were performed according to the manufacturer's protocol (Thermo Fisher) using Dharmafect I and siGENOME SMARTpool reagents for FBXL5 (Dharmacon #M-012424-01), SPAK (Dharmacon #M-004875-02-0005) or a non-targeting siGENOME control siRNA (Dharmacon #D-001210-03-05). Expression of 3xHA-3xFLAG-tagged protein in a stable cell line was induced by treating cells with doxycyline for 24 hours or the times indicated at a final concentration of 100 ng/mL for protein half-life determination experiments and 500 ng/mL for

all other experiments. Cells were treated with 100 μg/ml ferric ammonium citrate (FAC) (Thermo Fisher), 100 μM desferrioxamine mesylate (DFO) (Sigma), and/or or 25 μM MG132 (Z-Leu-Leu-Leu-CHO) (BIOMOL) for the times indicated.

Affinity purification of FBXL5-ΔFbox Protein Complexes

Twenty-five 15 cm tissue cultures plates each of Flp-In™ TREx™-293 cells stably expressing His_6-3xFLAG-FBXL5-ΔFbox were grown, harvested, and lysed in IP buffer (100 mM Tris-HCl pH 8.0, 150 mM NaCl, 5 mM EDTA, 5% glycerol, 0.1% NP-40, 1 mM DTT, 0.5 mM PMSF, 1 μM pepstatin, 1 μM leupeptin and 2 μg/mL aprotinin). 200-300 mg of clarified protein lysate was then incubated at 4°C with 100 μL of equilibrated anti-FLAG M2 agarose (Sigma) for 2 hours. Beads were then washed four times using 1 mL of IP Buffer per wash before eluting with 500 μL of FLAG Elution Buffer (IP buffer lacking NP-40 and supplemented with 250 μg/mL of 3xFLAG peptide (Sigma)). Elutions were precipitated by the addition of trichloroacetic acid (TCA) to a final concentration of 10% followed by incubation on ice for 30 minutes and centrifugation at 16,000g for 10 minutes to collect the precipitate.

Proteomic Characterization of FBXL5 purifications

TCA precipitates from affinity-purified His_6-3xFLAG-FBXL5-ΔFbox cells were digested and prepared for proteomic analysis as described[110]. The digested samples were analyzed by MudPIT[50,51]. A 5-step multidimensional chromatographic separation was performed online and fractionated peptides were eluted directly into a LTQ-Orbitrap XL mass spectrometer (Thermo Fisher) in which tandem mass spectra were collected. Peptide mass spectra were analyzed using the SEQUEST and DTASelect algorithms[52,53]. A decoy database approach was used to estimate

peptide and protein level false positive rates which were less than 5% per analysis[111]. Proteins were considered candidate FBXL5 interacting proteins if they were identified in the relevant affinity purification but not in MudPIT analyses of other control purifications. A detailed description of the multidimensional peptide fractionation protocol, mass spectrometer settings, and bioinformatic workflow is described elsewhere[112].

Immunoprecipitation and Immunoblotting

Cell lysates were prepared using IP buffer. Immunoprecipitations were performed using the appropriate affinity matrix equilibrated with IP Buffer and incubated with equal amounts of cell lysates at 4°C for 2 hours. Beads were washed three times with lysis buffer and resuspended in 2x SDS loading buffer. For immunoblotting, whole cell lysates and immunoprecipitates were boiled in SDS-loading buffer, separated using SDS-PAGE, transferred to Immobilon-P PVDF membranes (Millipore), and probed with the appropriate primary and secondary antibodies. Proteins were visualized using Pierce ECL western blotting substrate (Thermo Fisher).

Ubiquitination assay

HEK293 cells were transfected with plasmids expressing HA-Ubiquitin, a 3xFLAG FBXL5 construct (3xFLAG-FBXL5, 3xFLAG-FBXL5-ΔFbox), and combinations of 6xMyc-SPAK K104R, 6xMyc-SPAK T243E/S383D, 6Myc-HERC2 2600-3600 and 6xMyc-HERC2 2600-4935. Twenty-four hours after transfection, the medium was changed and cells were treated with 100μg/ml FAC and 25 μM MG132 for 4 hours. Cells were harvested and lysed under denaturing conditions as described previously[113]. Ubiquitin conjugates were purified using anti-

HA beads and the presence of FBXL5 in the purified ubiquitin conjugates was detected by immunoblotting with FLAG M2 antibody.

Chapter 5: SPAK Regulation of NCOA4 and Ferritinophagy

SPAK Regulates Ferritin Stability and Ferritinophagy through NCOA4 and HERC2

Abstract

NCOA4 (Nuclear receptor coactivator 4) has been recently linked to iron homeostasis due to its ability to traffic iron-filled ferritin heteropolymer cages to the autophagosome for the release of iron sequestered by the ferritin storage protein. How NCOA4 is regulated during this process, however, is largely unknown. We have determined that the osmotic stress regulatory kinase SPAK can interact with NCOA4, and believe that the SPAK-HERC2 complex we characterized in chapter 3 may also control NCOA4 stability. In this chapter, we provide preliminary evidence that SPAK may also be involved in regulating the NCOA4-dependent degradation of ferritin and represents a novel regulatory system for coupling ferritin degradation through NCOA4 with ferritin expression through the FBXL5-IRP regulatory axis.

Introduction

Due to its high reactivity, iron does not exist at high levels in its free ionic form; rather, it is sequestered intracellularly into heteropolymeric ferritin cages that contain ferric (Fe^{3+}) iron. These ferritin cages are comprised of 24 subunits that include both ferritin light (FTL) and heavy (FTH) chains. FTL and FTH are 19 kDa and 21 kDa, respectively, while the complete ferritin cage is around 450 kDa. Both ferritin chains are ubiquitously expressed, but the ratios between them depend on cell type and changes in response to external conditions such as inflammation[6]. These ferritin complexes can accommodate around 4500 iron atoms within the nanocavity, and containment of iron in a redox-inactive form is critical for preventing iron-mediated cell and tissue damage[7].

Despite its central importance in iron homeostasis and storage, very little is known about how iron is moved into and out of these ferritin cages in response to changes in iron availability. Storage of iron in ferritin cages is thought to require at least FTH1, FTL and Poly(rC)-binding protein (PCBP1). PCBP1 is an iron chaperone which is believed to bind ferrous iron (+2) and deliver it to ferritin[9]. FTH1 possesses ferroxidase activity that oxidizes ferrous iron to ferric iron which is required for storage in the nanocavity of the ferritin cage. FTL promotes iron nucleation and ferroxidase turnover for FTH1[8].

The mechanism by which stored iron is liberated from ferritin has been contested with both proteasome and lysosome-dependent pathways having been reported[10,11]. Recently however, a landmark finding by Mancias et al. has revolutionized our understanding of the process. Utilizing a quantitative mass spectrometry-based approach, they identified nuclear receptor coactivator 4 (NCOA4) as a cellular factor that was highly enriched in autophagosomes[12]. The subsequent characterization of NCOA4 demonstrated that it was physically associated with ferritin heavy and light chains and that it functioned to deliver ferritin to the lysosome during iron deficiency. Consistent with this idea, NCOA4-deficient cells exhibited a decrease in intracellular iron that resulted from the inability to liberate stored iron from ferritin. A second study concerning the characterization of new autophagy inhibitor PIK-III also confirmed the importance of NCOA4 in ferritin degradation[13].

In this chapter, we describe the initial identification in our laboratory of an interaction between NCOA4 and SPAK and raise the possibility that the SPAK-HERC2 complex may regulate multiple facets of iron homeostasis.

Results

We first hypothesized that SPAK might have effects on iron regulation outside of FBXL5 degradation after observing significant increases in ferritin stability in SPAK-overexpressing cell lines.

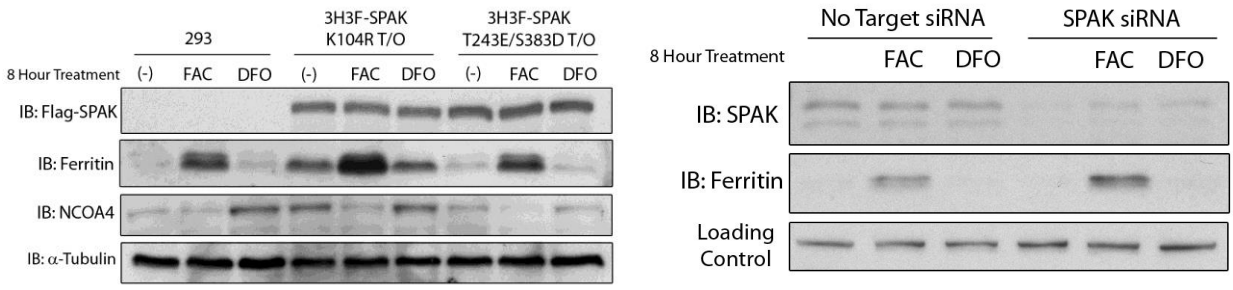

Figure 37. Loss of SPAK activity through overexpression of SPAK K104R or siRNA knockdown stabilizes endogenous ferritin. (**A**) An HEK293 cell line stably expressing 3HA-3FLAG-tagged SPAK K104R or SPAK T243E/S383D and HEK293 WT were treated with FAC or DFO for 8 eight hours prior to harvesting. Cells were lysed to obtain whole cell extract (WCE) and blotted with primary antibodies against FLAG, ferritin, NCOA4 and α-tubulin. (**B**) SPAK knockdown using siRNA in HeLa cells stabilizes ferritin. No Target siRNA and SPAK siRNA were used on Hela cells, along with an 8 hour FAC or DFO treatment. Whole cell extracts were run on Western blot and blotted with antibodies against SPAK and ferritin.

As seen in Figure 37A, overexpression of kinase-dead SPAK (SPAK-K104R) resulted in a stabilization of ferritin protein under all iron treatment conditions tested: ferric ammonium citrate (FAC) was used to induce a high iron environment while desferrioxamine mesylate (DFO) was used to chelate iron. Overexpression of constitutively-active SPAK (SPAK-T243E/S383D) did not affect ferritin levels. Knockdown of SPAK by siRNA also stabilized ferritin levels, with the strongest effects observed in FAC treated cells (Figure 37B). Importantly, the degree of SPAK stabilization seen in these experiments is disproportionately strong with

respect to what would be expected from the stabilization of FBXL5 in these experiments, raising the possibility that SPAK may be capable of influencing ferritin levels independently of FBXL5. Along these lines we tested the ability of SPAK to interact with NCOA4, as NCOA4 is known to regulate ferritin levels. Judging that SPAK-K104R overexpression had strong effects on endogenous ferritin stability, we tested the ability of SPAK-K104R and SPAK-T243E/S383D to bind NCOA4. We determined that NCOA4 can interact with SPAK in a manner independent of the SPAK activation state (Figure 38).

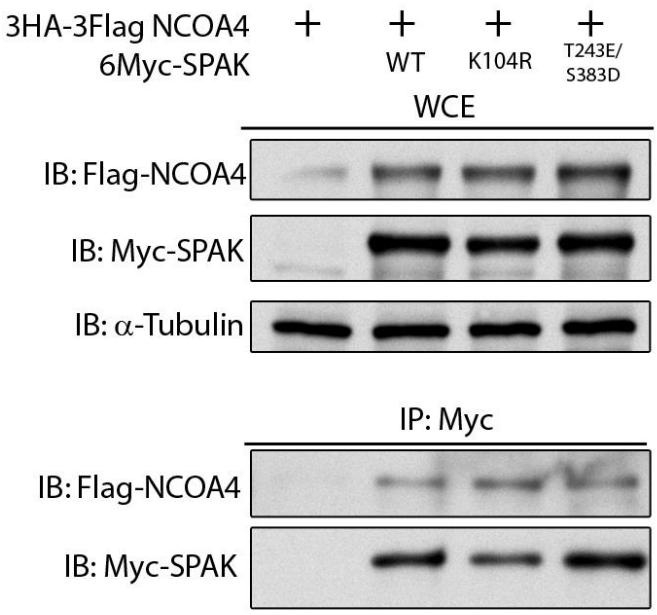

Figure 38. NCOA4 interacts with SPAK in a SPAK activity-independent manner. HEK293 cells were co-transfected with 3HA-3FLAG-tagged NCOA4 and one of three SPAK constructs: SPAK WT, SPAK-K104R or constitutively active SPAK (SPAK-T243E/S383D). Anti-Myc beads were used to immunopurify SPAK-bound proteins. WCEs and IPs were Western blotted with antibodies against FLAG, c-Myc and α-tubulin.

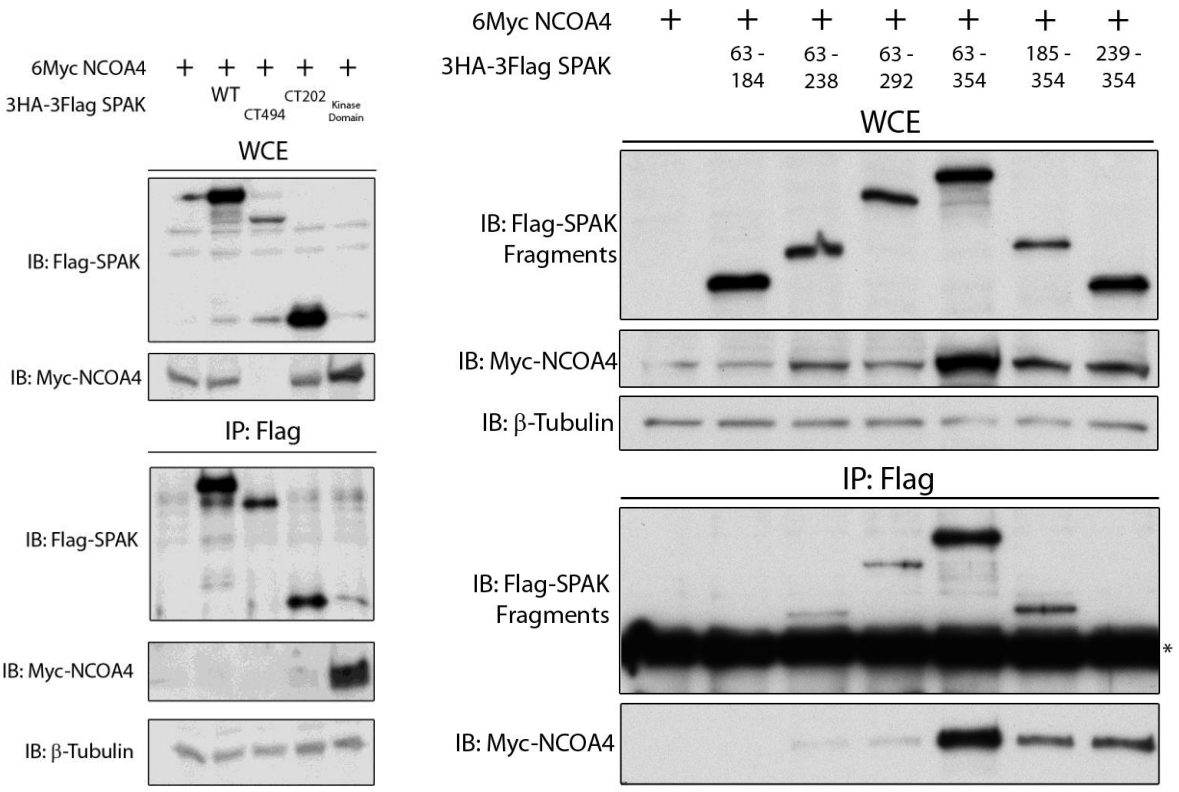

Figure 39. The kinase domain of SPAK interacts with NCOA4. (**A**) 6Myc-tagged NCOA4 was co-transfected into HEK293 cells with 3HA-3FLAG SPAK variants (wild type (WT), C-terminal 494 amino acids (CT494), C-Terminal 202 amino acids (CT202) and the Kinase Domain). The SPAK variants were immunoprecipitated using anti-FLAG beads. The WCEs and immunoprecipitates (IPs) were blotted with primary antibodies against FLAG, c-Myc and β-tubulin. (**B**) 6Myc-tagged NCOA4 was co-transfected into HEK293 cells with fragments of the kinase domain, denoted above as the amino acids contained within the fragment. The SPAK fragments were immunoprecipitated using anti-FLAG beads with the WCEs and IPs blotted with antibodies against FLAG, c-Myc and β-tubulin.

To further characterize the NCOA4-SPAK interaction, we mapped the region of SPAK that mediates its association with NCOA4. We find that NCOA4 binds to the kinase domain of SPAK, specifically amino acids 293 to 354. NCOA4 binds relatively weakly to full-length SPAK but very strongly to the kinase domain expressed alone (Figure 39A, compare lanes 2 and 5). In addition, overexpression of the kinase domain of SPAK has a strong stabilizing effect of

NCOA4 as observed in the WCE (Figure 39A, lane 5). To further refine the binding site within SPAK that associates with NCOA4, we performed additional co-immunoprecipitation experiments with fragments containing different subregions of the SPAK kinase. When we expressed fragments of the kinase domain, we determined that the stabilizing effect is best seen with full length kinase domain (amino acids 63 – 354) (Figure 39B). Only the SPAK kinase domain fragments containing amino acids 293 to 354 were able to interact with NCOA4 and cause a moderate stabilization effect. The SPAK kinase fragments that strongly bind NCOA4 are also shown to stabilize it (Figure 39B, compare lanes 5-7 and lanes 1-4). These results confirm that SPAK interacts with NCOA4 and that it is able to regulate its stability. We propose that the SPAK kinase domain is able to bind NCOA4, but as a small fragment is unable to perform its normal function. Instead, it may act as a dominant negative protein, preventing endogenous full length SPAK from properly maintaining NCOA4 levels.

When we determined that SPAK played a role in NCOA4 expression we reasoned that SPAK may also affect aspects of NCOA4 poly-ubiquitination and degradation. To test this, we performed a cell-based ubiquitination assay to observe any SPAK effects on NCOA4. Since SPAK and HERC2 associate to ubiquitinate and degrade FBXL5, we tested HERC2 and its effect on NCOA4 poly-ubiquitination and degradation. We tested two SPAK forms: kinase-dead SPAK-K104R and constitutively active SPAK-T243E/S383D. For HERC2 we used dominant negative HERC2-aa-2600-3600 which lacks the catalytic HECT domain and the active HECT-HERC2 fragment spanning aa. 2600-4935.

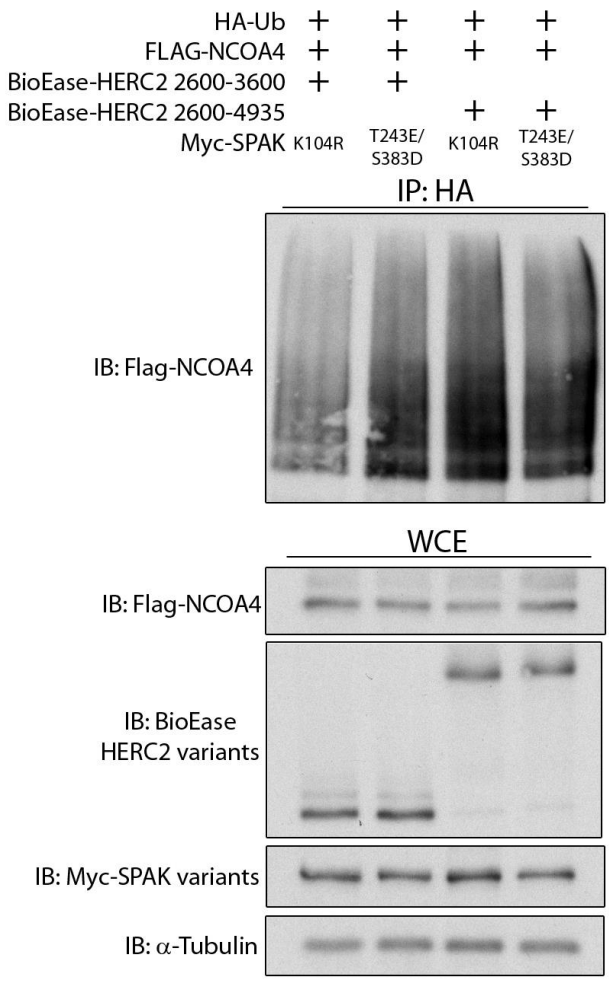

Figure 40. SPAK and HERC2 are both able to drive NCOA4 poly-ubiquitination. HEK293 cells were co-transfected with HA-ubiquitin, FLAG-tagged NCOA4, either BioEase-tagged HERC2 2600-3600 or HERC2 2600-4935 along with either 6Myc-tagged SPAK K104R or SPAK T243E/S383D. Cells were treated with MG132 for 4 hours prior to lysis using SDS boiling method. Anti-HA beads were used to immunoprecipitate ubiquitin-bound proteins. WCEs and IPs were blotted with streptavidin-HRP and antibodies against FLAG, c-Myc and α-tubulin.

Inactive SPAK and dominant negative HERC2 are both unable to drive poly-ubiquitination of NCOA4 (Figure 40). Constitutively active SPAK and active HERC2 fragment are both able to individually drive poly-ubiquitination of NCOA4, but together they create conditions with the highest poly-ubiquitination. This supports that SPAK is able to control

ubiquitination of NCOA4, but whether or not SPAK's activity depends on HERC2 is still unknown.

Discussion

We recently outlined that SPAK is involved in iron homeostasis through its ability to regulate FBXL5 levels – here, we were able to show that SPAK is also involved in NCOA4 stability. Since NCOA4 is able to mediate ferritin degradation and iron release from the autophagosome, it is an important protein in iron homeostasis. Given SPAK's effects on ferritin levels, we believe that this is due to its negative regulation of NCOA4 which results in the accumulation of ferritin.

We have determined earlier that SPAK and HERC2 form a complex that can regulate FBXL5 stability, which then affects IRP proteins and the stability of their downstream targets. SPAK and HERC2 regulation of NCOA4 likely serves to strengthen the downstream effects on ferritin through these two pathways to maximize the cell's ability to respond to changes in iron availability.

Based on what we know about SPAK activity and how it affects FBXL5 and NCOA4 stability, believe that SPAK phosphorylation state serves as an iron-sensitive switch that can dictate the desired degradation target: FBXL5 or NCOA4. These two iron-regulatory proteins serve opposite functions: FBXL5 serves to decrease the amount of intracellular iron while NCOA4 is responsible for increasing intracellular iron. Based on these observations and what we know about HERC2-dependent degradation of FBXL5 and NCOA4, it seems logical that there must be some regulatory protein that controls HERC2 activity.

We propose that in low iron, the SPAK-HERC2 complex targets and degrades FBXL5 while NCOA4 performs its function to break down ferritin complexes (Figure 41). When iron reaches a high level, the SPAK-HERC2 complex instead targets NCOA4 in order to prevent

additional iron from being freed from ferritin complexes (Figure 42). Under these conditions, iron-bound FBXL5 performs its ubiquitin ligase activity on IRP1 and IRP2. Our future work will involve experiments to test the validity of our model.

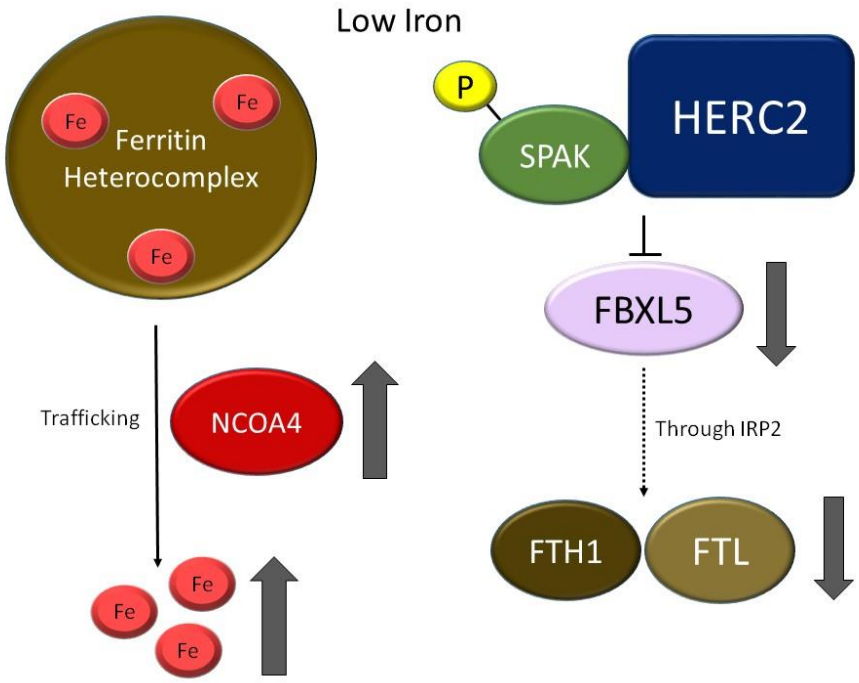

Figure 41. Proposed model of SPAK/HERC2 regulation in low iron conditions.

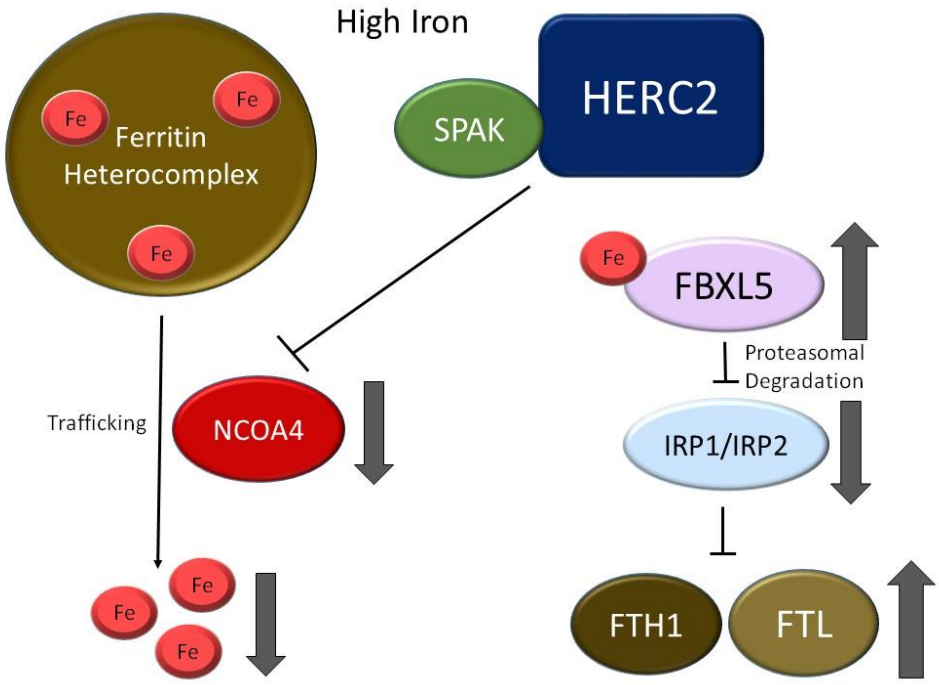

Figure 42. Proposed model of SPAK/HERC2 regulation in high iron conditions.

Summary and Future Directions

By utilizing proteomic mass spectrometry and biochemical assays we were able to identify and characterize two important proteins involved in iron homeostasis: the iron-binding ubiquitin ligase FBXL5 and the osmotic stress kinase SPAK. FBXL5 was a protein that was sought after for years, as IRP proteins were known to be degraded in a proteasome dependent manner but the ligase responsible was unknown. We were able to determine that FBXL5 was not only the ligase responsible for regulating IRP levels, but that it is also an important iron sensor in the cell. FBXL5 possesses the first known mammalian example of a hemerythrin-like domain which is used by the protein to sense iron levels and to manage the protein's own stability.

While its role in osmotic stress regulation has been described extensively we discovered a new role for SPAK in iron regulation. The mechanism for this regulation is still not clear, and we are completing more experimental work to discern the ability of SPAK to regulate both FBXL5 and NCOA4. If SPAK is able to control both arms of this iron homeostasis machinery, it could become an attractive target for managing iron-related illnesses. Additionally, this iron-related role for SPAK could prove as a link between the osmotic stress pathway and the iron regulatory pathway. The reason for this crosstalk is unclear, but there is additional evidence for it to be true.

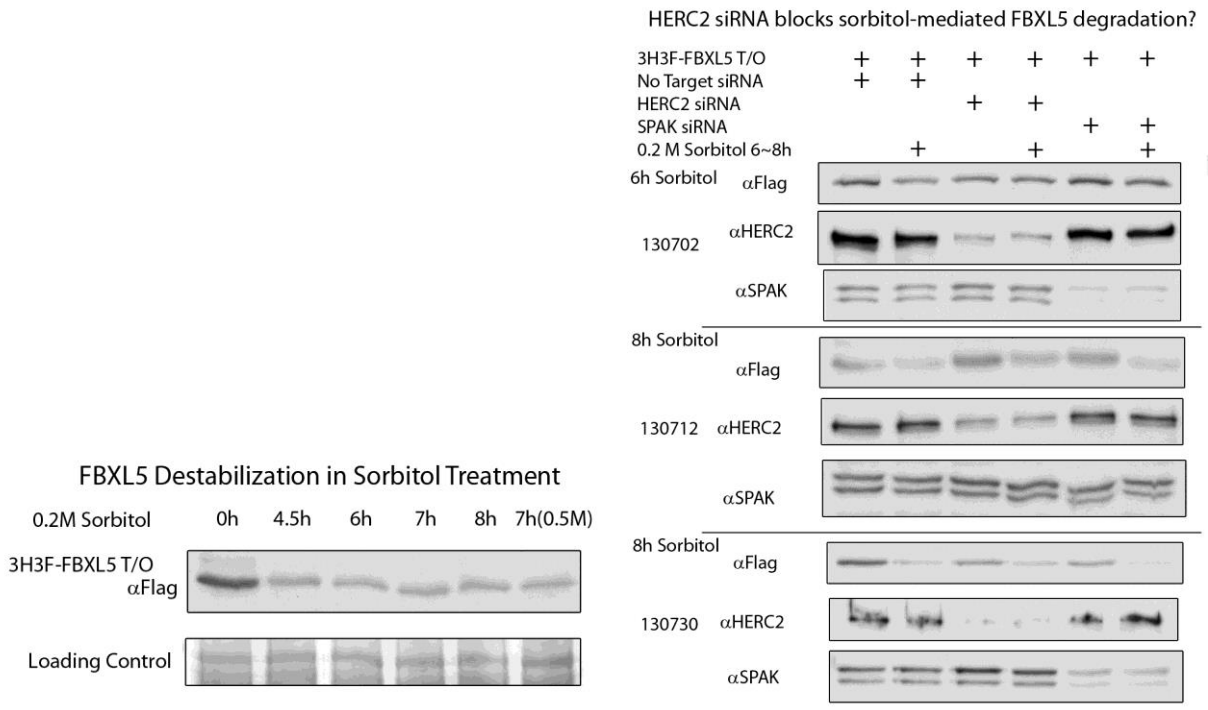

Figure 43. FBXL5 destabilization in sorbitol treatment is independent of SPAK expression. (**A**) An HEK293 cell line stably expressing 3HA-3FLAG-tagged FBXL5 was treated with 0.2M sorbitol for the time durations indicated above. WCE was collected and Western blotted for primary antibodies against FLAG. (**B**) HEK293 cells were transfected with SPAK or HERC2 siRNA to knock down expression of their respective protein and whole cell extracts (WCE) collected. WCEs were Western blotted with primary antibodies against FLAG, HERC2 and SPAK.

We discovered that FBXL5 is destabilized by osmotic stress treatment (Figure 43A). The destabilization of FBXL5 is not dependent on the expression of SPAK or HERC2, however, as siRNA knockdown of SPAK or HERC2 is unable to protect FBXL5 from osmotic stress dependent degradation (Figure 43B).

Despite this, there is considerable evidence that the two pathways are interlinked. SPAK is able to control the stability of FBXL5 and NCOA4 in an activity-dependent manner, and in this fashion is able to regulate a large number of proteins involved in iron homeostasis. My future work in this area will be to discern the physiological role of these interactions.

References

1 Ganz, T. Systemic iron homeostasis. *Physiol Rev* **93**, 1721-1741, doi:10.1152/physrev.00008.2013 (2013).

2 Lawen, A. & Lane, D. J. Mammalian iron homeostasis in health and disease: uptake, storage, transport, and molecular mechanisms of action. *Antioxid Redox Signal* **18**, 2473-2507, doi:10.1089/ars.2011.4271 (2013).

3 Muckenthaler, M. U., Galy, B. & Hentze, M. W. Systemic iron homeostasis and the iron-responsive element/iron-regulatory protein (IRE/IRP) regulatory network. *Annu Rev Nutr* **28**, 197-213, doi:10.1146/annurev.nutr.28.061807.155521 (2008).

4 Walden, W. E. *et al.* Structure of dual function iron regulatory protein 1 complexed with ferritin IRE-RNA. *Science* **314**, 1903-1908, doi:10.1126/science.1133116 (2006).

5 Iwai, K. *et al.* Iron-dependent oxidation, ubiquitination, and degradation of iron regulatory protein 2: implications for degradation of oxidized proteins. *Proc Natl Acad Sci U S A* **95**, 4924-4928 (1998).

6 Arosio, P. & Levi, S. Cytosolic and mitochondrial ferritins in the regulation of cellular iron homeostasis and oxidative damage. *Biochim Biophys Acta* **1800**, 783-792, doi:10.1016/j.bbagen.2010.02.005 (2010).

7 Kurz, T., Gustafsson, B. & Brunk, U. T. Intralysosomal iron chelation protects against oxidative stress-induced cellular damage. *FEBS J* **273**, 3106-3117, doi:10.1111/j.1742-4658.2006.05321.x (2006).

8 Arosio, P., Ingrassia, R. & Cavadini, P. Ferritins: a family of molecules for iron storage, antioxidation and more. *Biochim Biophys Acta* **1790**, 589-599, doi:10.1016/j.bbagen.2008.09.004 (2009).

9 Shi, H., Bencze, K. Z., Stemmler, T. L. & Philpott, C. C. A cytosolic iron chaperone that delivers iron to ferritin. *Science* **320**, 1207-1210, doi:10.1126/science.1157643 (2008).

10 Asano, T. *et al.* Distinct mechanisms of ferritin delivery to lysosomes in iron-depleted and iron-replete cells. *Mol Cell Biol* **31**, 2040-2052, doi:10.1128/mcb.01437-10 (2011).

11 Kidane, T. Z., Sauble, E. & Linder, M. C. Release of iron from ferritin requires lysosomal activity. *Am J Physiol Cell Physiol* **291**, C445-455, doi:10.1152/ajpcell.00505.2005 (2006).

12 Mancias, J. D., Wang, X., Gygi, S. P., Harper, J. W. & Kimmelman, A. C. Quantitative proteomics identifies NCOA4 as the cargo receptor mediating ferritinophagy. *Nature* **509**, 105-109, doi:10.1038/nature13148 (2014).

13 Dowdle, W. E. *et al.* Selective VPS34 inhibitor blocks autophagy and uncovers a role for NCOA4 in ferritin degradation and iron homeostasis in vivo. *Nat Cell Biol* **16**, 1069-1079, doi:10.1038/ncb3053 (2014).

14 Hentze, M. W., Muckenthaler, M. U., Galy, B. & Camaschella, C. Two to tango: regulation of Mammalian iron metabolism. *Cell* **142**, 24-38, doi:10.1016/j.cell.2010.06.028 (2010).

15 Krause, A. *et al.* LEAP-1, a novel highly disulfide-bonded human peptide, exhibits antimicrobial activity. *FEBS Lett* **480**, 147-150 (2000).

16 Park, C. H., Valore, E. V., Waring, A. J. & Ganz, T. Hepcidin, a urinary antimicrobial peptide synthesized in the liver. *J Biol Chem* **276**, 7806-7810, doi:10.1074/jbc.M008922200 (2001).

17 Nemeth, E. *et al.* Hepcidin regulates cellular iron efflux by binding to ferroportin and inducing its internalization. *Science* **306**, 2090-2093, doi:10.1126/science.1104742 (2004).

18 Qiao, B. *et al.* Hepcidin-induced endocytosis of ferroportin is dependent on ferroportin ubiquitination. *Cell Metab* **15**, 918-924, doi:10.1016/j.cmet.2012.03.018 (2012).

19 Babitt, J. L. *et al.* Bone morphogenetic protein signaling by hemojuvelin regulates hepcidin expression. *Nat Genet* **38**, 531-539, doi:10.1038/ng1777 (2006).

20 Babitt, J. L. *et al.* Modulation of bone morphogenetic protein signaling in vivo regulates systemic iron balance. *J Clin Invest* **117**, 1933-1939, doi:10.1172/jci31342 (2007).

21 Andriopoulos, B., Jr. *et al.* BMP6 is a key endogenous regulator of hepcidin expression and iron metabolism. *Nat Genet* **41**, 482-487, doi:10.1038/ng.335 (2009).

22 Casanovas, G., Mleczko-Sanecka, K., Altamura, S., Hentze, M. W. & Muckenthaler, M. U. Bone morphogenetic protein (BMP)-responsive elements located in the proximal and distal hepcidin promoter are critical for its response to HJV/BMP/SMAD. *J Mol Med (Berl)* **87**, 471-480, doi:10.1007/s00109-009-0447-2 (2009).

23 Goswami, T. & Andrews, N. C. Hereditary hemochromatosis protein, HFE, interaction with transferrin receptor 2 suggests a molecular mechanism for mammalian iron sensing. *J Biol Chem* **281**, 28494-28498, doi:10.1074/jbc.C600197200 (2006).

24 Schmidt, P. J., Toran, P. T., Giannetti, A. M., Bjorkman, P. J. & Andrews, N. C. The transferrin receptor modulates Hfe-dependent regulation of hepcidin expression. *Cell Metab* **7**, 205-214, doi:10.1016/j.cmet.2007.11.016 (2008).

25 Nemeth, E. *et al.* IL-6 mediates hypoferremia of inflammation by inducing the synthesis of the iron regulatory hormone hepcidin. *J Clin Invest* **113**, 1271-1276, doi:10.1172/jci20945 (2004).

26 Fleming, R. E. Hepcidin activation during inflammation: make it STAT. *Gastroenterology* **132**, 447-449, doi:10.1053/j.gastro.2006.11.049 (2007).

27 Gao, J. *et al.* Interaction of the hereditary hemochromatosis protein HFE with transferrin receptor 2 is required for transferrin-induced hepcidin expression. *Cell Metab* **9**, 217-227, doi:10.1016/j.cmet.2009.01.010 (2009).

28 Wallace, D. F. *et al.* Combined deletion of Hfe and transferrin receptor 2 in mice leads to marked dysregulation of hepcidin and iron overload. *Hepatology* **50**, 1992-2000, doi:10.1002/hep.23198 (2009).

29 Hurrell, R. & Egli, I. Iron bioavailability and dietary reference values. *Am J Clin Nutr* **91**, 1461S-1467S, doi:10.3945/ajcn.2010.28674F (2010).

30 Illing, A. C., Shawki, A., Cunningham, C. L. & Mackenzie, B. Substrate profile and metal-ion selectivity of human divalent metal-ion transporter-1. *J Biol Chem* **287**, 30485-30496, doi:10.1074/jbc.M112.364208 (2012).

31 Canonne-Hergaux, F., Gruenheid, S., Ponka, P. & Gros, P. Cellular and subcellular localization of the Nramp2 iron transporter in the intestinal brush border and regulation by dietary iron. *Blood* **93**, 4406-4417 (1999).

32 Gunshin, H. *et al.* Cloning and characterization of a mammalian proton-coupled metal-ion transporter. *Nature* **388**, 482-488, doi:10.1038/41343 (1997).

33 Gunshin, H. *et al.* Cybrd1 (duodenal cytochrome b) is not necessary for dietary iron absorption in mice. *Blood* **106**, 2879-2883, doi:10.1182/blood-2005-02-0716 (2005).

34 Rajagopal, A. *et al.* Haem homeostasis is regulated by the conserved and concerted functions of HRG-1 proteins. *Nature* **453**, 1127-1131, doi:10.1038/nature06934 (2008).

35 Shayeghi, M. *et al.* Identification of an intestinal heme transporter. *Cell* **122**, 789-801, doi:10.1016/j.cell.2005.06.025 (2005).

36 Qiu, A. *et al.* Identification of an intestinal folate transporter and the molecular basis for hereditary folate malabsorption. *Cell* **127**, 917-928, doi:10.1016/j.cell.2006.09.041 (2006).

37 Delaby, C. *et al.* Subcellular localization of iron and heme metabolism related proteins at early stages of erythrophagocytosis. *PLoS One* **7**, e42199, doi:10.1371/journal.pone.0042199 (2012).

38 Skaar, J. R., Pagan, J. K. & Pagano, M. Mechanisms and function of substrate recruitment by F-box proteins. *Nature Reviews Molecular Cell Biology* **14**, 369-381, doi:10.1038/nrm3582 (2013).

39 Komander, D. & Rape, M. The ubiquitin code. *Annu Rev Biochem* **81**, 203-229, doi:10.1146/annurev-biochem-060310-170328 (2012).

40 Hershko, A. & Ciechanover, A. The ubiquitin system. *Annu Rev Biochem* **67**, 425-479, doi:10.1146/annurev.biochem.67.1.425 (1998).

41 Petroski, M. D. & Deshaies, R. J. Function and regulation of cullin-RING ubiquitin ligases. *Nat Rev Mol Cell Biol* **6**, 9-20, doi:10.1038/nrm1547 (2005).

42 Jin, J. *et al.* Systematic analysis and nomenclature of mammalian F-box proteins. *Genes Dev* **18**, 2573-2580, doi:10.1101/gad.1255304 (2004).

43 Soucy, T. A. *et al.* An inhibitor of NEDD8-activating enzyme as a new approach to treat cancer. *Nature* **458**, 732-736 (2009).

44 Ravid, T. & Hochstrasser, M. Diversity of degradation signals in the ubiquitin-proteasome system. *Nat Rev Mol Cell Biol* **9**, 679-690, doi:10.1038/nrm2468 (2008).

45 Miller, J. & Gordon, C. The regulation of proteasome degradation by multi-ubiquitin chain binding proteins. *FEBS Lett* **579**, 3224-3230, doi:10.1016/j.febslet.2005.03.042 (2005).

46 Kang, Y. *et al.* UBL/UBA ubiquitin receptor proteins bind a common tetraubiquitin chain. *J Mol Biol* **356**, 1027-1035, doi:10.1016/j.jmb.2005.12.001 (2006).

47 Zwickl, P., Voges, D. & Baumeister, W. The proteasome: a macromolecular assembly designed for controlled proteolysis. *Philos Trans R Soc Lond B Biol Sci* **354**, 1501-1511, doi:10.1098/rstb.1999.0494 (1999).

48 Voges, D., Zwickl, P. & Baumeister, W. The 26S proteasome: a molecular machine designed for controlled proteolysis. *Annu Rev Biochem* **68**, 1015-1068, doi:10.1146/annurev.biochem.68.1.1015 (1999).

49 Kohler, A. *et al.* The axial channel of the proteasome core particle is gated by the Rpt2 ATPase and controls both substrate entry and product release. *Mol Cell* **7**, 1143-1152 (2001).

50 Washburn, M. P., Wolters, D. & Yates, J. R., 3rd. Large-scale analysis of the yeast proteome by multidimensional protein identification technology. *Nat Biotechnol* **19**, 242-247 (2001).

51 Wolters, D. A., Washburn, M. P. & Yates, J. R., 3rd. An automated multidimensional protein identification technology for shotgun proteomics. *Anal Chem* **73**, 5683-5690 (2001).

52 Eng, J. K., McCormack, A. L. & Yates, J. R. An approach to correlate tandem mass spectral data of peptides with amino acid sequences in a protein database. *J Am Soc Mass Spectrom* **5**, 976-989 (1994).

53 Tabb, D. L., McDonald, W. H. & Yates, J. R., 3rd. DTASelect and Contrast: tools for assembling and comparing protein identifications from shotgun proteomics. *J Proteome Res* **1**, 21-26 (2002).

54 Xu, B. *et al.* WNK1, a novel mammalian serine/threonine protein kinase lacking the catalytic lysine in subdomain II. *J Biol Chem* **275**, 16795-16801 (2000).

55 Min, X., Lee, B. H., Cobb, M. H. & Goldsmith, E. J. Crystal structure of the kinase domain of WNK1, a kinase that causes a hereditary form of hypertension. *Structure* **12**, 1303-1311, doi:10.1016/j.str.2004.04.014 (2004).

56 O'Shaughnessy, K. M. & Karet, F. E. Salt handling and hypertension. *Annu Rev Nutr* **26**, 343-365, doi:10.1146/annurev.nutr.26.061505.111316 (2006).

57 Balu, S. & Thomas, J., 3rd. Incremental expenditure of treating hypertension in the United States. *Am J Hypertens* **19**, 810-816; discussion 817, doi:10.1016/j.amjhyper.2005.12.013 (2006).

58 Richardson, C. & Alessi, D. R. The regulation of salt transport and blood pressure by the WNK-SPAK/OSR1 signalling pathway. *Journal of Cell Science* **121**, 3293-3304, doi:10.1242/jcs.029223 (2008).

59 Wilson, F. H. *et al.* Human hypertension caused by mutations in WNK kinases. *Science* **293**, 1107-1112, doi:10.1126/science.1062844 (2001).

60 Zambrowicz, B. P. *et al.* Wnk1 kinase deficiency lowers blood pressure in mice: a gene-trap screen to identify potential targets for therapeutic intervention. *Proc Natl Acad Sci U S A* **100**, 14109-14114, doi:10.1073/pnas.2336103100 (2003).

61 Huang, C. L., Kuo, E. & Toto, R. D. WNK kinases and essential hypertension. *Curr Opin Nephrol Hypertens* **17**, 133-137, doi:10.1097/MNH.0b013e3282f4e4fd (2008).

62 Delaloy, C. *et al.* Multiple promoters in the WNK1 gene: one controls expression of a kidney-specific kinase-defective isoform. *Mol Cell Biol* **23**, 9208-9221 (2003).

63 Zagorska, A. *et al.* Regulation of activity and localization of the WNK1 protein kinase by hyperosmotic stress. *The Journal of Cell Biology* **176**, 89-100, doi:10.1083/jcb.200605093 (2007).

64 Richardson, C. *et al.* Activation of the thiazide-sensitive Na+-Cl- cotransporter by the WNK-regulated kinases SPAK and OSR1. *Journal of Cell Science* **121**, 675-684, doi:10.1242/jcs.025312 (2008).

65 Piala, A. T. *et al.* Chloride sensing by WNK1 involves inhibition of autophosphorylation. *Sci Signal* **7**, ra41, doi:10.1126/scisignal.2005050 (2014).

66 Delpire, E. & Gagnon, Kenneth B. E. SPAK and OSR1: STE20 kinases involved in the regulation of ion homoeostasis and volume control in mammalian cells. *Biochemical Journal* **409**, 321, doi:10.1042/bj20071324 (2008).

67 Gagnon, K. B. E., England, R. & Delpire, E. Characterization of SPAK and OSR1, Regulatory Kinases of the Na-K-2Cl Cotransporter. *Molecular and Cellular Biology* **26**, 689-698, doi:10.1128/mcb.26.2.689-698.2006 (2005).

68 Vitari, A. C., Deak, M., Morrice, N. A. & Alessi, D. R. The WNK1 and WNK4 protein kinases that are mutated in Gordon's hypertension syndrome phosphorylate and activate SPAK and OSR1 protein kinases. *Biochem J* **391**, 17-24 (2005).

69 Gagnon, K. B., England, R. & Delpire, E. Volume sensitivity of cation-Cl- cotransporters is modulated by the interaction of two kinases: Ste20-related proline-alanine-rich kinase and WNK4. *Am J Physiol Cell Physiol* **290**, 1 (2006).

70 Vitari, A. C. *et al.* Functional interactions of the SPAK/OSR1 kinases with their upstream activator WNK1 and downstream substrate NKCC1. *Biochem J* **397**, 223-231 (2006).

71 Villa, F. *et al.* Structural insights into the recognition of substrates and activators by the OSR1 kinase. *EMBO Rep* **8**, 839-845 (2007).

72 Delpire, E., Rauchman, M. I., Beier, D. R., Hebert, S. C. & Gullans, S. R. Molecular cloning and chromosome localization of a putative basolateral Na(+)-K(+)-2Cl- cotransporter from mouse inner medullary collecting duct (mIMCD-3) cells. *J Biol Chem* **269**, 25677-25683 (1994).

73 Gamba, G. Molecular physiology and pathophysiology of electroneutral cation-chloride cotransporters. *Physiol Rev* **85**, 423-493 (2005).

74 Moriguchi, T. *et al.* WNK1 Regulates Phosphorylation of Cation-Chloride-coupled Cotransporters via the STE20-related Kinases, SPAK and OSR1. *Journal of Biological Chemistry* **280**, 42685-42693, doi:10.1074/jbc.M510042200 (2005).

75 Darman, R. B. & Forbush, B. A regulatory locus of phosphorylation in the N terminus of the Na-K-Cl cotransporter, NKCC1. *J Biol Chem* **277**, 37542-37550, doi:10.1074/jbc.M206293200 (2002).

76 Dowd, B. F. & Forbush, B. PASK (proline-alanine-rich STE20-related kinase), a regulatory kinase of the Na-K-Cl cotransporter (NKCC1). *J Biol Chem* **278**, 27347-27353, doi:10.1074/jbc.M301899200 (2003).

77 Gagnon, K. B., England, R. & Delpire, E. A single binding motif is required for SPAK activation of the Na-K-2Cl cotransporter. *Cell Physiol Biochem* **20**, 131-142, doi:10.1159/000104161 (2007).

78 Simon, D. B. *et al.* Bartter's syndrome, hypokalaemic alkalosis with hypercalciuria, is caused by mutations in the Na-K-2Cl cotransporter NKCC2. *Nat Genet* **13**, 183-188, doi:10.1038/ng0696-183 (1996).

79 Simon, D. B. *et al.* Gitelman's variant of Bartter's syndrome, inherited hypokalaemic alkalosis, is caused by mutations in the thiazide-sensitive Na-Cl cotransporter. *Nat Genet* **12**, 24-30, doi:10.1038/ng0196-24 (1996).

80 Kahle, K. T. *et al.* WNK protein kinases modulate cellular Cl- flux by altering the phosphorylation state of the Na-K-Cl and K-Cl cotransporters. *Physiology (Bethesda)* **21**, 326-335, doi:10.1152/physiol.00015.2006 (2006).

81 de Los Heros, P. *et al.* The WNK-regulated SPAK/OSR1 kinases directly phosphorylate and inhibit the K+-Cl- co-transporters. *Biochem J* **458**, 559-573, doi:10.1042/bj20131478 (2014).

82 Alessi, D. R. *et al.* The WNK-SPAK/OSR1 pathway: master regulator of cation-chloride cotransporters. *Sci Signal* **7**, 2005365 (2014).

83 Monette, M. Y. & Forbush, B. Regulatory activation is accompanied by movement in the C terminus of the Na-K-Cl cotransporter (NKCC1). *J Biol Chem* **287**, 2210-2220, doi:10.1074/jbc.M111.309211 (2012).

84 Anselmo, A. N. *et al.* WNK1 and OSR1 regulate the Na+, K+, 2Cl- cotransporter in HeLa cells. *Proc Natl Acad Sci U S A* **103**, 10883-10888, doi:10.1073/pnas.0604607103 (2006).

85 Lee, S. J., Cobb, M. H. & Goldsmith, E. J. Crystal structure of domain-swapped STE20 OSR1 kinase domain. *Protein Sci* **18**, 304-313, doi:10.1002/pro.27 (2009).

86 Polek, T. C., Talpaz, M. & Spivak-Kroizman, T. The TNF receptor, RELT, binds SPAK and uses it to mediate p38 and JNK activation. *Biochem Biophys Res Commun* **343**, 125-134, doi:10.1016/j.bbrc.2006.02.125 (2006).

87 Balatoni, C. E. *et al.* Epigenetic silencing of Stk39 in B-cell lymphoma inhibits apoptosis from genotoxic stress. *Am J Pathol* **175**, 1653-1661, doi:10.2353/ajpath.2009.090091 (2009).

88 Vashisht, A. A. *et al.* Control of iron homeostasis by an iron-regulated ubiquitin ligase. *Science (New York, N.Y.)* **326**, 718-721, doi:10.1126/science.1176333 (2009).

89 Wallander, M. L., Leibold, E. A. & Eisenstein, R. S. Molecular control of vertebrate iron homeostasis by iron regulatory proteins. *Biochim Biophys Acta* **1763**, 668-689, doi:10.1016/j.bbamcr.2006.05.004 (2006).

90 Rouault, T. A. The role of iron regulatory proteins in mammalian iron homeostasis and disease. *Nat Chem Biol* **2**, 406-414, doi:10.1038/nchembio807 (2006).

91 Guo, B., Phillips, J. D., Yu, Y. & Leibold, E. A. Iron regulates the intracellular degradation of iron regulatory protein 2 by the proteasome. *J Biol Chem* **270**, 21645-21651 (1995).

92 Guo, B., Yu, Y. & Leibold, E. A. Iron regulates cytoplasmic levels of a novel iron-responsive element-binding protein without aconitase activity. *J Biol Chem* **269**, 24252-24260 (1994).

93 Iwai, K., Klausner, R. D. & Rouault, T. A. Requirements for iron-regulated degradation of the RNA binding protein, iron regulatory protein 2. *EMBO J* **14**, 5350-5357 (1995).

94 Samaniego, F., Chin, J., Iwai, K., Rouault, T. A. & Klausner, R. D. Molecular characterization of a second iron-responsive element binding protein, iron regulatory protein 2. Structure, function, and post-translational regulation. *J Biol Chem* **269**, 30904-30910 (1994).

95 Ishikawa, H. *et al.* Involvement of heme regulatory motif in heme-mediated ubiquitination and degradation of IRP2. *Mol Cell* **19**, 171-181, doi:10.1016/j.molcel.2005.05.027 (2005).

96 Yamanaka, K. *et al.* Identification of the ubiquitin-protein ligase that recognizes oxidized IRP2. *Nat Cell Biol* **5**, 336-340, doi:10.1038/ncb952 (2003).

97 Hanson, E. S., Rawlins, M. L. & Leibold, E. A. Oxygen and iron regulation of iron regulatory protein 2. *J Biol Chem* **278**, 40337-40342, doi:10.1074/jbc.M302798200 (2003).

98 Wang, J. *et al.* Iron-mediated degradation of IRP2, an unexpected pathway involving a 2-oxoglutarate-dependent oxygenase activity. *Mol Cell Biol* **24**, 954-965 (2004).

99 Zumbrennen, K. B., Hanson, E. S. & Leibold, E. A. HOIL-1 is not required for iron-mediated IRP2 degradation in HEK293 cells. *Biochim Biophys Acta* **2**, 246-252 (2008).

100 Cardozo, T. & Pagano, M. The SCF ubiquitin ligase: insights into a molecular machine. *Nat Rev Mol Cell Biol* **5**, 739-751, doi:10.1038/nrm1471 (2004).

101 Clarke, S. L. *et al.* Iron-responsive degradation of iron-regulatory protein 1 does not require the Fe-S cluster. *EMBO J* **25**, 544-553, doi:10.1038/sj.emboj.7600954 (2006).

102 Wang, J. *et al.* Iron-dependent degradation of apo-IRP1 by the ubiquitin-proteasome pathway. *Mol Cell Biol* **27**, 2423-2430, doi:10.1128/mcb.01111-06 (2007).

103 Meyron-Holtz, E. G., Ghosh, M. C. & Rouault, T. A. Mammalian tissue oxygen levels modulate iron-regulatory protein activities in vivo. *Science* **306**, 2087-2090, doi:10.1126/science.1103786 (2004).

104 Stenkamp, R. E. Dioxygen and hemerythrin. *Chemical reviews* **94**, 715-726 (1994).

105 Soding, J., Biegert, A. & Lupas, A. N. The HHpred interactive server for protein homology detection and structure prediction. *Nucleic Acids Res* **33**, W244-248, doi:10.1093/nar/gki408 (2005).

106 Johnson, E. S. & Blobel, G. Ubc9p is the conjugating enzyme for the ubiquitin-like protein Smt3p. *J Biol Chem* **272**, 26799-26802 (1997).

107 Zumbrennen, K. B., Wallander, M. L., Romney, S. J. & Leibold, E. A. Cysteine oxidation regulates the RNA-binding activity of iron regulatory protein 2. *Mol Cell Biol* **29**, 2219-2229 (2009).

108 Berglund, L. *et al.* A genecentric Human Protein Atlas for expression profiles based on antibodies. *Mol Cell Proteomics* **7**, 2019-2027, doi:10.1074/mcp.R800013-MCP200 (2008).

109 Yu, Y., Radisky, E. & Leibold, E. A. The iron-responsive element binding protein. Purification, cloning, and regulation in rat liver. *J Biol Chem* **267**, 19005-19010 (1992).

110 Florens, L. *et al.* Analyzing chromatin remodeling complexes using shotgun proteomics and normalized spectral abundance factors. *Methods* **40**, 303-311, doi:10.1016/j.ymeth.2006.07.028 (2006).

111 Elias, J. E. & Gygi, S. P. Target-decoy search strategy for increased confidence in large-scale protein identifications by mass spectrometry. *Nat Methods* **4**, 207-214, doi:10.1038/nmeth1019 (2007).

112 Wohlschlegel, J. A. Identification of SUMO-conjugated proteins and their SUMO attachment sites using proteomic mass spectrometry. *Methods Mol Biol* **497**, 33-49, doi:10.1007/978-1-59745-566-4_3 (2009).

113 Bloom, J. & Pagano, M. Experimental tests to definitively determine ubiquitylation of a substrate. *Methods Enzymol* **399**, 249-266 (2005).

114 Kerr, J. S. & Wilson, C. H. Nuclear receptor-binding protein 1: a novel tumour suppressor and pseudokinase. *Biochem Soc Trans* **41**, 1055-1060, doi:10.1042/bst20130069 (2013).

115 De Langhe, S., Haataja, L., Senadheera, D., Groffen, J. & Heisterkamp, N. Interaction of the small GTPase Rac3 with NRBP, a protein with a kinase-homology domain. *Int J Mol Med* **9**, 451-459 (2002).

116 Kester, H. A., Blanchetot, C., den Hertog, J., van der Saag, P. T. & van der Burg, B. Transforming growth factor-beta-stimulated clone-22 is a member of a family of leucine zipper proteins that can homo- and heterodimerize and has transcriptional repressor activity. *J Biol Chem* **274**, 27439-27447 (1999).

117 Kim, M. & Ceman, S. Fragile X mental retardation protein: past, present and future. *Curr Protein Pept Sci* **13**, 358-371 (2012).

118 Napoli, I. *et al.* The fragile X syndrome protein represses activity-dependent translation through CYFIP1, a new 4E-BP. *Cell* **134**, 1042-1054, doi:10.1016/j.cell.2008.07.031 (2008).

119 Moroishi, T., Yamauchi, T., Nishiyama, M. & Nakayama, K. I. HERC2 targets the iron regulator FBXL5 for degradation and modulates iron metabolism. *J Biol Chem* **289**, 16430-16441, doi:10.1074/jbc.M113.541490 (2014).